Deltares

Enabling Delta Life

# Numerical Modelling of Primary and Secondary Erosion in Coarse Sand Barrier Experiments

Deltares

# Numerical Modelling of Primary and Secondary Erosion in Coarse Sand Barrier Experiments

**Small-scale and medium-scale experiments**

E. Rosenbrand
B. Robbins
D.V. Griffiths

11200952-036

© Deltares, 2018, B

Deltares

**Title**
Numerical Modelling of Primary and Secondary Erosion in Coarse Sand Barrier Experiments

| Project | Attribute | Pages |
|---|---|---|
| 11200952-036 | 11200952-036-GEO-0002 | 65 |

**Keywords**
Finite element modelling, coarse sand barrier, primary and secondary erosion, piping, 3D, parameter determination

**Summary**
Piping is one of the most important threats for the safety of Dutch levees, especially for the sections that are located along the main rivers. Based on research conducted in the past years, several piping mitigation measures have been developed that prevent the pipe from progressing towards the river. One of these measures is the coarse sand barrier (CSB). The CSB seems to be a promising measure based on preliminary experiments, but additional research is still required to assess the feasibility of this measure in practice.
A numerical finite element model that allows for modelling piping in three dimensions was developed at the U.S. Army Corps of Engineers Research and Development Center (USACE-ERDC). In the model, pipe progression is controlled by both primary erosion at the pipe tip, and secondary erosion in the pipe. The former is modelled by the critical local gradient at the pipe tip, the latter is modelled as in the Sellmeijer model.
The current report presents the first set of computations in which this preliminary model was used in order to simulate the coarse sand barrier experiments that were performed at the Deltares Laboratories in Delft in 2017 and 2018. These are the small-scale and medium-scale experiments that were performed during the first two experimental phases (phases 2a and 2b) of the coarse sand barrier feasibility study.
The model reproduces key phases of the piping process in the presence of a coarse sand barrier well. The critical head drops that are modelled somewhat overestimate the measured head drops; based on a sensitivity analysis it is expected that this overestimation may be resolved by a reduction of the primary erosion criteria. Additional laboratory experiments to determine these criteria have already been conducted, results should show whether the current criteria are indeed too high. Overall the model shows promising results and can be used to obtain a better insight into the strength of a coarse sand barrier.

| Version | Date | Author | Initials | Review | Initials | Approval | Initials |
|---|---|---|---|---|---|---|---|
| 1 | Sep. 2018 | E. Rosenbrand MSc<br>B. Robbins<br>D.V. Griffiths | | V.M. van Beek | | L. Voogt | |
| 2 | Nov. 2018 | E. Rosenbrand MSc<br>B. Robbins<br>D.V. Griffiths | 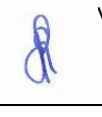 | V.M. van Beek |  | L. Voogt |  |

**Status**
final

# Contents

**1 Introduction** **1**

**2 Model description** **3**

**3 Model input** **7**
3.1 Mesh 7
3.2 Geometry 7
3.3 Boundary conditions 10
3.4 Numerical analysis parameters 11
3.5 Soil parameters 11
3.5.1 Hydraulic conductivity 12
3.5.2 Primary erosion 14
3.5.3 Secondary erosion criterion 23
3.6 Overview of simulations 25

**4 Results** **29**
4.1 Results of the basis simulations and comparison to experiments 29
4.1.1 Qualitative pipe progression 29
4.1.2 Critical head drop 32
4.1.3 Flux 36
4.2 Sensitivity analyses 36
4.2.1 Qualitative pipe progression 36
4.2.2 Critical head drop 38

**5 Analysis and discussion** **43**
5.1 Progression parallel to barrier interface in background sand 43
5.2 Number of pipes inside the barrier 43
5.3 Critical growth steps in medium-scale tests 45
5.4 Progression parallel to the upstream barrier interface in medium-scale tests 48
5.5 Progression of pipe backwards from barrier 49
5.6 Critical head drop 49
5.6.1 Basis simulations 49
5.6.2 Sensitivity analysis 51
5.7 Effect of barrier depth 55
5.8 Flux 56
5.8.1 Analysis with modified hydraulic conductivity of the background sand 57
5.9 Flow regime in the pipe 59
5.10 Summary 60

**6 Conclusions and Outlook** **61**
6.1 Conclusions 61
6.2 Outlook 62

**7 References** **64**

## Appendices

**A Progression of the pipe in medium-scale experiments** **A-1**
A.1 Coarse sand barrier GZB 1 A-2
A.2 Coarse sand barrier GZB 2 A-3

**B Properties of sands in cylinder experiments** **B-1**

**C Images of medium scale basis simulations** **C-1**
C.1 Simulation MSP_26 C-2
C.2 Simulation MSP_23 C-3
C.3 Simulation MSP_25 C-4
C.4 Simulation MSP_27 C-5
C.5 Simulation MSP_24 C-6
C.6 Simulation MSP_28 C-7

**D Effect of scaling of primary erosion criterion** **D-1**
D.1 Medium-scale simulation MSP_26 D-1
D.2 Small-scale simulations D-2

**E Effect of number of pipe elements activated per step** **E-1**

**F Effect of barrier thickness** **F-2**

**G Discussion of pipe progression steps** **G-1**
G.1 Progression parallel to the barrier interface in the background sand G-1
G.2 Number of pipes inside the barrier G-2
G.3 Critical growth steps in medium-scale tests G-3

# 1 Introduction

Backward erosion piping is a failure mechanism that poses a major threat to dams and embankments worldwide. The process occurs in situations where a granular aquifer is overlain by a cohesive cover layer. If a defect (crack or hole) in the cover layer concentrates flow, grains can be eroded from the aquifer. This leads to the formation of an erosion lens and a pipe that progresses backwards below the embankment. The blanket layer acts as a roof for the progressing pipe. When the pipe reaches the upstream water body, excessive scour and erosion can lead to embankment collapse. A coarse sand barrier (CSB) is a measure of preventing the pipe from progressing upstream. This consists of a trench of coarser material that is placed below the embankment at the top of the aquifer, at the interface with the cover layer where it will obstruct the pipe progression. The pipe will still form and progress backwards; however, the increased erosion resistance of the barrier is intended to stop further progression.

Dutch Water Authority Rivierenland intends to apply the coarse sand barrier at the pilot location Gameren as an innovative measure. Although experiments in the laboratory and at the IJkdijk (a former full-scale test facility in the North-Eastern part of the Netherlands), indicate the potential of the method, it is required to conduct a feasibility study to investigate whether the method offers sufficient resistance against piping in the field, both for the intended pilot location and for other comparable locations. Based on the result of this feasibility study and the exploration of alternative measures, a preferential measure will be selected for the pilot location. The approach to the feasibility study is described in (Deltares, 2017a) and consists of the following phases:

- Phase 1: Literature study of filter requirements and pre-selection of barrier material.
- Phase 2a: Small-scale experiments and numerical simulation.
- Phase 2b: Medium-scale experiments and numerical simulation.
- Phase 2c: Large-scale experiments and numerical simulation.

The purpose of the study is to assess the feasibility of the application of a coarse sand barrier as a piping measure for the location of Gameren, and for other locations along the main rivers in a more generic sense. To quantify the strength of the barrier, a criterion needs to be identified that reliably predicts failure of the barrier. Damage to the barrier – i.e. initial pipe formation into the barrier, caused by primary erosion – was initially considered as failure of the barrier. The hypothesis is that the local horizontal gradient in the barrier just upstream of the pipe characterizes the strength of a given barrier material at a given relative density, i.e. implying that different tests with the same material show the same local critical gradient in the barrier, regardless of the configuration or dimensions of the barrier.
After Phase 2a (Deltares, 2017b, Deltares 2017c) it was decided that the local critical gradient at which a pipe enters the barrier might be insufficient as a failure criterion, as it was observed that after the pipe damaged the barrier, a significant head increase was required in order for the pipe to progress through the barrier. In order to take full advantage of the strength of the barrier in design and assessment of embankments with a barrier, progression of the pipe through the barrier became an additional study focus as a possible failure criterion for barrier design.

The progression of a pipe is related to primary erosion (erosion at the pipe tip, resulting in lengthening of the pipe) and secondary erosion (resulting in widening and deepening of the pipe) (e.g. van Beek, 2015). Primary erosion controls the lengthening of the pipe, whereas secondary erosion results in a reduction of head loss in the pipe. The Sellmeijer (1988) model describes the progression of the pipe through secondary erosion alone. This assumes that the pipe will progress when the limit state equilibrium of particles on the pipe bottom has been exceeded near the pipe tip. A calibration study was done using experiments on different scales to fit model parameters (Sellmeijer, et al. 2011). Using the calibrated parameters, the model appears to work for homogeneous sands in configurations (geometry and boundary conditions) comparable to the ones used in the calibration study. For these situations, the gradient at the pipe tip and the gradient in the pipe are related to each other by the coupling between pipe flow and groundwater flow. For configurations, like the coarse sand barrier, this configuration is changed, and the primary erosion criterion will have to be accounted for explicitly. Several institutes are working on an improvement of the piping model in this respect.

The U.S. Army Corps of Engineers Engineer Research and Development Center (USACE-ERDC) is developing a preliminary finite element model that includes both primary and secondary erosion (Robbins & Griffiths, 2018a, 2018b). The current report presents the application of the model to model the small-scale and medium-scale experiments that were conducted in Phase 2a and 2b (Deltares 2017b and Deltares 2018a). The local criteria for primary erosion are derived based on the experiments that were conducted at the USACE-ERDC facilities in April 2017 (Deltares, 2018).

This report first briefly presents the model in Chapter 2. The model input is presented in Chapter 3, with particular emphasis on the determination of the primary erosion criterion. In Chapter 4 the results are presented, and these are discussed in Chapter 5. Chapter 6 presents the first conclusions based on the models and sketches an outlook for further experimental and numerical work.

# 2 Model description

This Chapter describes the 3D finite element model that is used for the simulations. This model is already presented in Robbins and Griffiths (2018a, 2018b), and the reader is referred to those papers for a detailed description. The current report is largely a reproduction of Robbins and Griffiths (2018b), modified where relevant to be specific to 3D.

The finite element model was developed by modifying the steady state groundwater program documented in Smith and Griffiths (2004).

The entire domain is constructed of hexahedral elements. The domain is divided into the pipe domain $\Omega_p$ and a soil domain $\Omega_s$. The pipe domain consists of the top plane of elements and the soil domain is the remainder of the domain. This implies that pipe progression is restricted to the progression of a horizontal pipe in the *x-y* plane, the *z* direction being the vertical direction. A cross section through a simple mesh illustrating the problem discretization is shown in Figure 2.1.

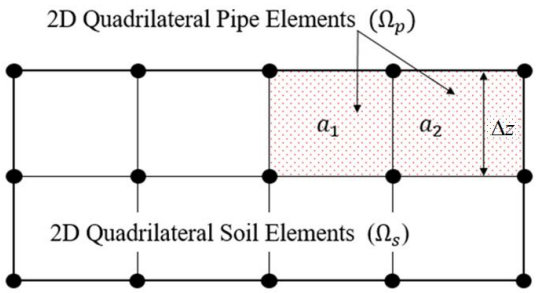


*Figure 2.1 Finite element discretization of the domain, profile view of the x-z plane, from Robbins and Griffiths (2018b)*

Flow in the soil is governed by the Laplace equation, which is solved by finite elements as an equivalent matrix problem

$$[K_e]\{H\} = \{Q\} \qquad (1)$$

where $\{H\}$ and $\{Q\}$ are vectors of the total head and net flow at the FEM nodes, and $[K_e]$ is the global conductivity matrix involving an assembly of element conductivity matrices given by

$$[K_e] = \int k_x \frac{\partial N_i}{\partial x}\frac{\partial N_j}{\partial x} + k_y \frac{\partial N_i}{\partial y}\frac{\partial N_j}{\partial y} + k_z \frac{\partial N_i}{\partial z}\frac{\partial N_j}{\partial z} d\Omega_s \qquad i,j=1,2,\ldots 8 \qquad (2)$$

with $k_x$, $k_y$, and $k_z$ denoting the hydraulic conductivity in the coordinate directions and $N_i$ denoting the finite element shape functions.

Flow in the pipe is assumed to be similar to unidirectional flow in between parallel plates, as in the Sellmeijer (1988) model. As the pipe is only allowed to progress horizontally in the *x-y* plane, the flow ($\overrightarrow{q_p}$) through the pipe is related to the hydraulic gradient in the *x-y* plane by

$$\overrightarrow{q_p} = -\frac{a^3 \rho g}{12\mu}\left[\frac{\partial H}{\partial x} \;\; \frac{\partial H}{\partial y}\right] \tag{3}$$

where $a$ denotes the depth of the eroded pipe, $g$ is the acceleration of gravity, and $\mu$ and $\rho$ represent the dynamic viscosity and density of water, respectively. From continuity,

$$\nabla \cdot \overrightarrow{q_p} + S = 0 \tag{4}$$

where $S$ is a sink/source term due to flow along the pipe. Substitution of Eq. 3 into Eq. 4 yields the differential equation governing the pipe flow in $\Omega_p$.

$$\frac{a^3 \rho g}{12\mu}\left(\frac{\partial^2 H}{\partial x^2} + \frac{\partial^2 H}{\partial y^2}\right) = S \tag{5}$$

Robbins and Griffiths (2018b) demonstrated that Eq. 5 is satisfied in the pipe elements ($\Omega_p$) by assembling the pipe elements into Eq. 1 using Eq. 2 with an equivalent hydraulic conductivity ($k_{pipe}$) substituted for $k_x$ and $k_y$ where

$$k_{pipe} = \frac{a^3 \rho g}{12\mu \Delta z} \tag{6}$$

with $\Delta z$ denoting the height of the pipe element as shown in Figure 2.1 and $a$ denoting the depth of the erosion pipe in the element. This approximation provided an adequate solution provided the element size used was sufficiently small. Robbins and Griffiths (2018a) show that for a 2D comparison, elements of 0.25 m gave essentially the same solution as representing the pipe using 1D rod elements as is done in D-Geo Flow software (van Esch, 2013).

In addition to satisfying the pipe hydraulics given by Eq. 5, the sand grains in the bottom of the erosion pipe must be in equilibrium. If equilibrium conditions do not prevail, sand would be transported resulting in a deeper pipe (increased value of $a$) yielding a different hydraulic solution. The hydraulic shear stress at the bottom of the pipe is determined from force equilibrium to be

$$\vec{\tau} = \frac{a \rho g}{2}\left[\frac{\partial H}{\partial x}, \frac{\partial H}{\partial y}\right] . \tag{7}$$

The equilibrium condition that must be satisfied is simply given by $|\tau| < \tau_c$ where $\tau_c$ denotes the critical shear stress for incipient motion of the soil being eroded, referred to in this report as the secondary erosion criterion.

As the pipe depths required for equilibrium are unknown, Picard iterations over the pipe depth are conducted to arrive at a satisfactory hydraulic solution satisfying grain equilibrium, pipe hydraulics, and the groundwater flow for a given erosion pipe location. The pipe depth was incremented by one half of the median grain diameter ($d_{50}$) of the sand each iteration for the current analysis. The starting depth of the pipe is $3 \times d_{50}$.

Once a hydraulic solution is obtained for a fixed pipe location, the potential for progression of the erosion pipe must be assessed. The magnitude of the horizontal gradient $i_h$ is used to assess whether the primary erosion criterion $i_{crit}$ is exceeded. Thus if $i_h > i_{crit}$ where

$$i_h = \sqrt{\left(\frac{\partial H}{\partial x}\right)^2 + \left(\frac{\partial H}{\partial y}\right)^2} \qquad (8)$$

in the elements immediately bordering the pipe, elements are switched to pipe elements, and the hydraulic solution must be iteratively solved for once again with the new pipe geometry. The maximum number of elements that is switched to a pipe state in a single iteration is an input parameter. If Equation 8 is satisfied in multiple elements, the elements with the highest gradient, up to the maximum number of elements, are switched to pipe elements.

This process is repeated to evaluate the potential for a pipe to progress through the domain of interest. The algorithm structure is illustrated in Figure 2.2.

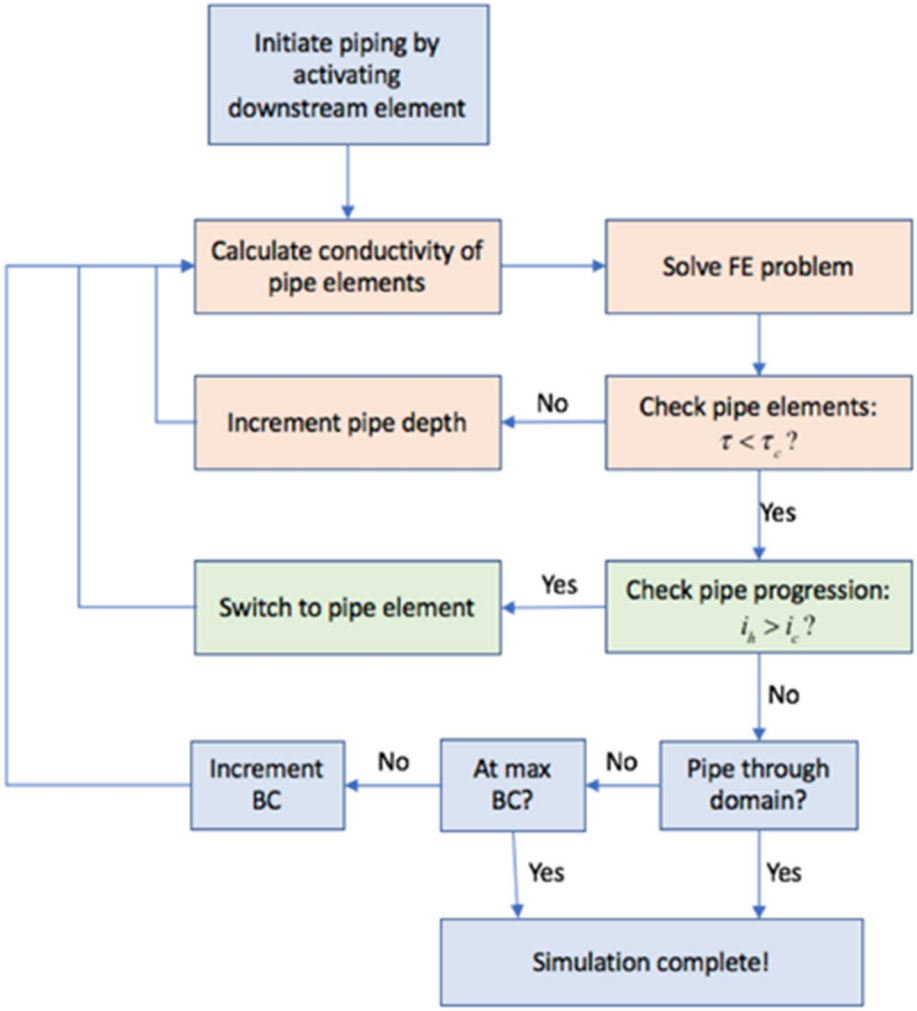


*Figure 2.2 Program algorithm for simulating pipe progression*

# 3 Model input

## 3.1 Mesh

A uniform mesh is used. The criterion for primary erosion is computed over the elements upstream of the pipe, therefore the element size dictates the distance over which this criterion is evaluated. The element size is selected based on a combination of computational efficiency and consideration of the problem addressed. For the small-scale models, 1 cm hexahedral cubes are used. As the median grain size of the barrier grains is in the order of 1 mm, elements smaller than 1 cm were considered unsuitable in this continuum model. For the medium-scale models, 4 cm hexahedral elements are used. A computation using 2 cm hexahedral cubes was performed to analyze the effect of element size for two models, MSP_26_2 and MSP_25_2. These computations took in the order of 2-3 days to run.

It was observed that the element size that was created was slightly smaller than specified, for dimensions where the combination of element size and model length would result in 10 elements. Thus, rather than having ten 1 cm elements for the depth of the small-scale models, these had eleven 0.9 cm elements. This was found to be due to rounding of element size in the numerical code. This is this not expected to affect the computed results significantly.

## 3.2 Geometry

The geometry of the CSB experiments in the models is based on the dimensions of the experimental set-up that is described in Deltares (2017b) and Deltares (2018a). Dimensions were rounded in order to match the element size. A photograph showing the small-scale set-up is shown in Figure 3.1.

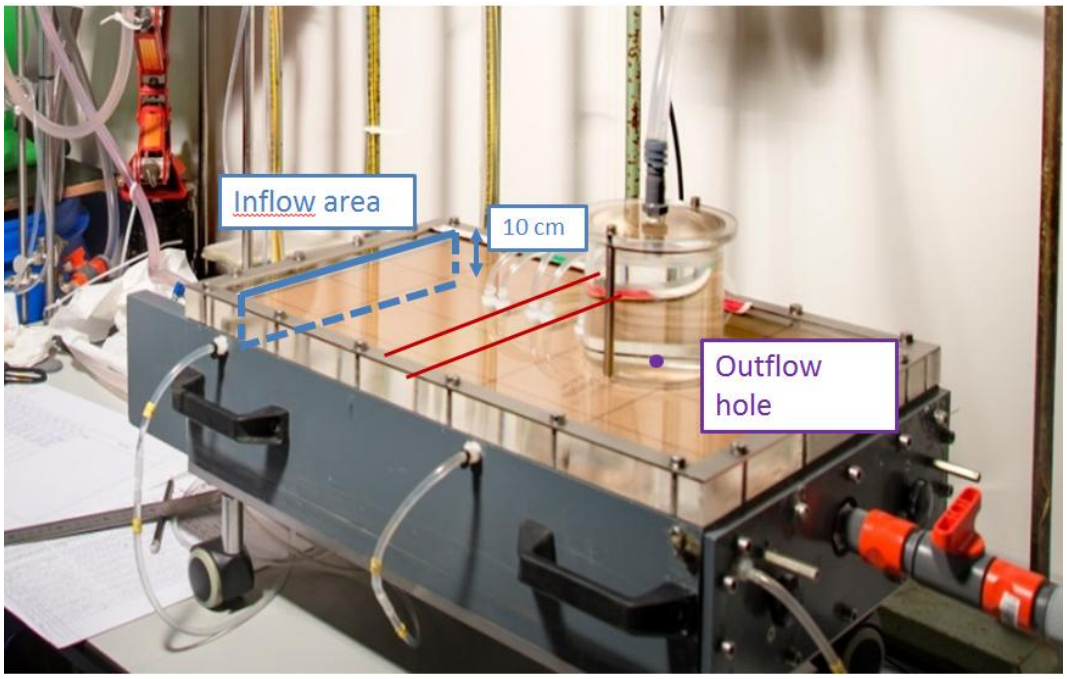


*Figure 3.1 Small-scale set-up. The location of the barrier is indicated by red lines, inflow is through the left side of the model (blue lines indicate inflow area), outflow is through a hole in the top of the cover (purple circle) The cylinder on the top surrounds the outlet hole and allows for removal of sand from the sample which is deposited on top of the cover*

The model dimensions and barrier location are summarized in  for each experiment configuration, a 3D figure of the model for the medium-scale is shown in Figure 3.2.

| **Model names** | **Width model x dimensions, m** | **Length model *y* dimension, m** | **Depth model *z* dimension, m** | **Distance between upstream wall and barrier, m** | **Centre of outlet hole, x location, m** | **Centre of outlet hole, y location, m** | **Length and width of outlet hole, m** |
|---|---|---|---|---|---|---|---|
| Small-scale regular | 0.30 | 0.48 | 0.10 | 0.18 | 0.15 | 0.35 | 0.019 |
| Small-scale rotated | 0.10 | 0.48 | 0.30 | 0.18 | 0.05 | 0.35 | 0.019 |
| Medium-scale | 0.88 | 1.76 | 0.40 | 0.60 | 0.44 | 1.40 | 0.79 |

*Table 3.1Model dimension*

Barrier depth varied in the different experiments, the depth per simulation is shown in the overview of the simulations at the end of this Chapter.

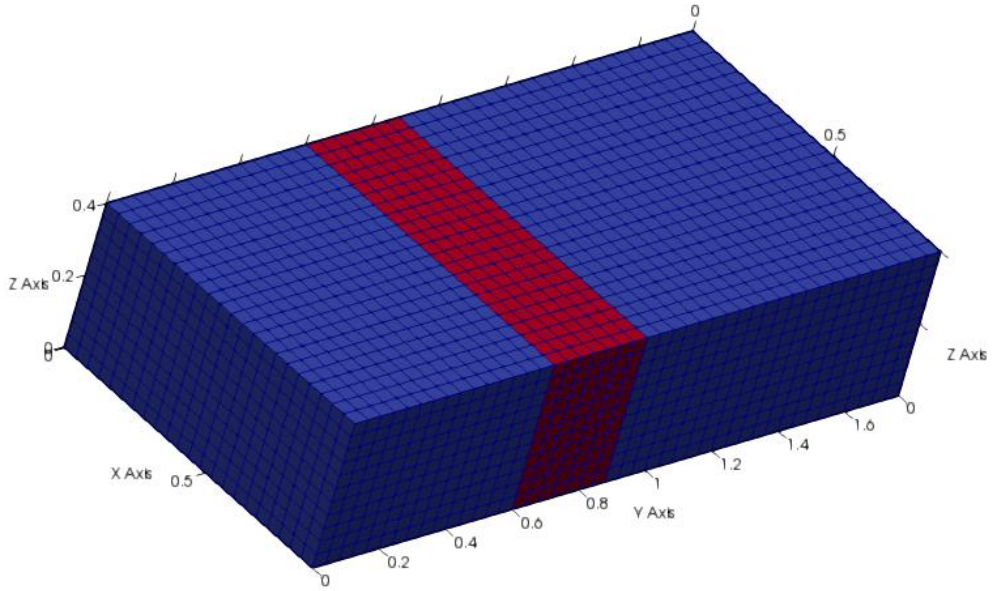


*Figure 3.2 3D view of the medium-scale model showing the background sand (blue) and the barrier material (red). Dark blue lines indicate the mesh. The inflow area is at y = 0 m, the center of the outflow hole is at x=0.44 m, y = 1.4 m*

The barrier thickness is 0.05 m in the small-scale experiments, and 0.30 m in the medium-scale experiments. In the medium scale models, the barrier is modelled as 0.28 m due to the element size. Therefore, a sensitivity analysis is done for two experiments with barrier thicknesses 0.24 m and 0.32 m, as shown in the overview of the simulations in Section 3.6. The distance of the barrier to the upstream interface is the same in these models, in order to have the same resistance in the fine sand up to the barrier.

The model consists of two soil types, the background sand and the barrier material, this is shown in Figure 3.3 along with the mesh.

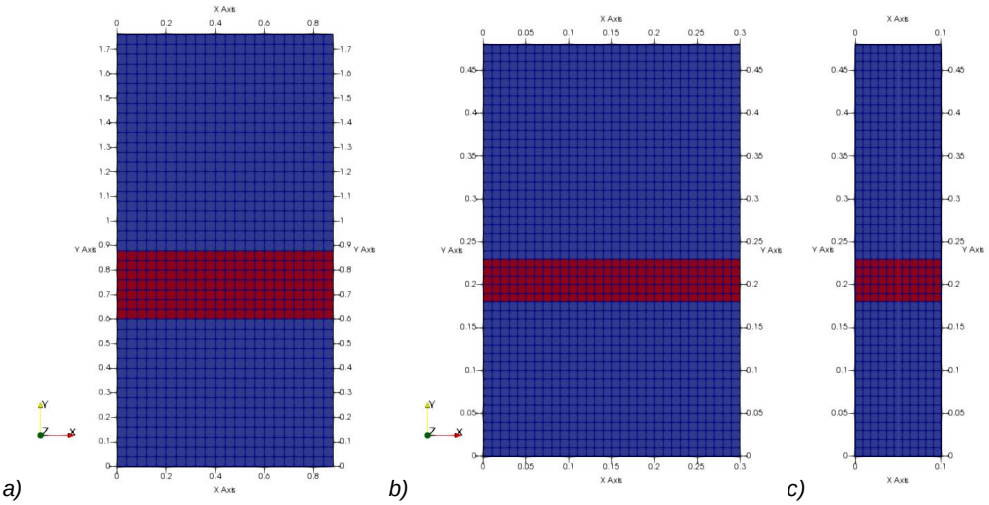


*Figure 3.3 Top view of the models showing the background sand (blue) and the barrier material (red). The barrier is typically 0.28 m (7 elements) thick in the medium-scale experiments (a) and 0.05 m (5 elements) thick in the small-scale experiments (b & c). Dark blue lines indicate the mesh. Flow enters the model through the plane y= 0*

## 3.3 Boundary conditions

The upstream boundary plane, at y=0, is a constant head boundary which represents the inlet of the model. The downstream boundary is a constant head assigned to the area corresponding to the outlet hole in the experiments. All other boundaries are closed. This approach neglects any head loss that may occur in the outlet hole.

The outlet hole is specified by the center of the outlet hole, and a region around this. The center is at (0.15 m, 0.35 m) for the small-scale regular model, at (0.05 m, 0.35 m) for the small-scale rotated model, and at (0.44 m, 1.40 m) for the medium-scale models respectively. The dimensions specified for length and width of this zone are 0.019 m for the small-scale models and 0.079 m for the medium-scale models.
In the initial condition, only the elements in the outlet hole are activated as pipe elements to provide a starting point for the pipe progression, and all other elements are soil elements as shown in Figure 3.4.
The 'rotated' small-scale models had an outlet hole of 3 elements rather than 2 elements due to the way in which element size was rounded off in the mesh (Figure 3.4c). This is not expected to have a significant effect on the critical head drops for damage and failure of the barrier.

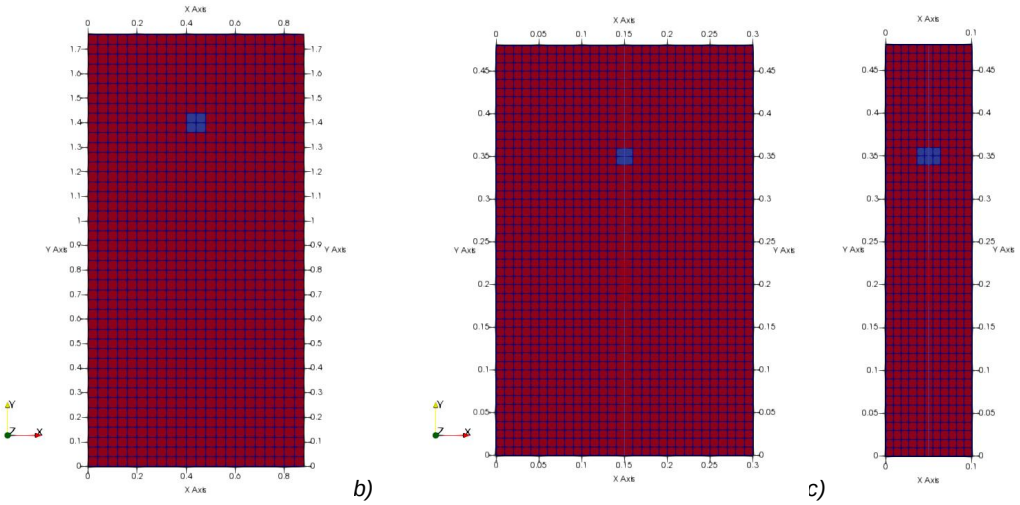


*Figure 3.4 View of the top of the model showing soil elements (red) and pipe elements (blue) in the initial condition. The medium-scale model is a), the small-scale models are b & c. The upstream side of the models is the x-z plane at y=0*

Initially an upstream head of 0.1 m is applied, and this head is increased incrementally by 10% of the current head each time the pipe progression stops. It is also possible to apply the full hydraulic load in one step, which was tested for the medium-scale simulation MSP_26 with 0.04 m elements and for MSP_26_2 with 0.02 m elements. This was found to yield results that appear unrealistic. In both models the pipe splits upon reaching the barrier, whereby one arm progresses into the barrier and the other arm progresses parallel to the barrier. Therefore, this option was not investigated further.

## 3.4 Numerical analysis parameters

The number of pipe elements that is switched on per iteration is an input parameter. This is set to two in the basis simulations, and the effect of using one and three is analyzed in simulations MSP_26_1el and MSP_26_3el.

As the basis simulation for test 199 did not yield failure of the barrier through piping (as shown in Chapter 4), the model simulations were also run with 1 and 3 pipe elements switched on per iteration. However, that did not lead to failure as observed in the experiment either.

## 3.5 Soil parameters

This Section presents the input soil parameters. As the primary and secondary erosion criteria are considered particularly important, the details on how these were determined are presented in detail.

The relative density (RD) of the materials is relevant for both hydraulic conductivity and the primary erosion criterion. Relative density ($RD_n$) was determined based on the porosity of the sample during preparation; these values are shown in .

| Experiment name* | Background sand | Barrier material | Relative density ($RD_n$)** background sand upstream | Relative density ($RD_n$)** barrier | Relative density ($RD_n$)** background sand downstream |
|---|---|---|---|---|---|
| KSP 191 | Metselzand | GZB 2 | 0.95 | 0.95 | 0.60 |
| KSP 192 | Metselzand | GZB 2 | 0.95 | 0.95 | 0.60 |
| KSP 196 | Metselzand | GZB 3 | 0.90 | 0.90 | 0.60 |
| KSP 198 | Metselzand | GZB 2 | 0.95 | 0.90 | 0.60 |
| KSP 199 | Metselzand | GZB 2 | 0.95 | 0.90 | 0.60 |
| MSP 24 | Baskarp 25 | GZB 2 | 1.07 | 1.05 | 0.93 |
| MSP 28 | Metselzand | GZB 2 | 1.07 | 0.83 | 0.97 |
| MSP 26 | Baskarp 25 | GZB 1 | 1.07 | 0.87 | 0.94 |
| MSP 23 | Baskarp 15 | GZB 1 | 0.91 | 0.79 | 0.84 |
| MSP 25 | Baskarp 25 | GZB 1 | 1.10 | 1.01 | 0.95 |
| MSP 27 | Baskarp 25 | GZB 1 low RD | 0.57 | 0.55 | 0.63 |

*Table 3.2 Overview of experiments that are modelled in this report. Relative density is based on reported values in Deltares (2017b) and Deltares (2018a)*

* Experiment name refers to the short names of the tests also used in Deltares (2018c) KSP referring to small-scale test and MSP referring to medium-scale test.

** $RD_n$ subscript n indicates relative density is based on porosity not void ratio.

The relative density of the background sand was different on the upstream side of the barrier than on the downstream side of the barrier in the experiments, due to the method of preparation. This is particularly the case for the small-scale experiments.

### 3.5.1 Hydraulic conductivity

The hydraulic conductivity of the soil for the simulations is based on the relative density that was achieved in the experiments, using the relationships between $RD_n$ and hydraulic conductivity that were determined in the small-scale phase and in the medium-scale phase (Deltares 2017b and Deltares 2018a). Different relationships were found for GZB 2 material for the two phases, which is probably due to a different batch of filter sand being used in the medium-scale tests, therefore the different relationships are also used for the different phases.

For the current simulations, the flow that enters the pipe at a given head drop over the model is of importance, therefore the relative density of the background sand upstream of the barrier is used to determine the hydraulic conductivity of the background sand in the simulations. The consequence of this is that the hydraulic conductivity of the background sand on the downstream side of the barrier is underestimated in the simulations relative to the experiments. This results in a higher hydraulic conductivity contrast on the downstream side of the barrier in the simulations, and therefore a greater convergence of flow towards the pipe on the downstream side of the barrier than in the experiments. Additionally, prior to the pipe reaching the barrier, the gradient in the background sand downstream of the barrier at a given head drop will also be higher which affects the initiation of piping in the background sand. In the current analysis the focus is on the piping in the barrier, therefore this second effect is not considered to be significant for the results.

In order to give an impression of the differences in hydraulic conductivity contrast based on the $RD_n$ upstream and downstream of the barrier, the resulting contrasts are shown in Figure 3.5 and . In order to qualitatively assess the effect on the pipe progression a simulation is done using the hydraulic conductivity of the downstream material for test MSP 26 (Simulation MSP_26HCdownstream).

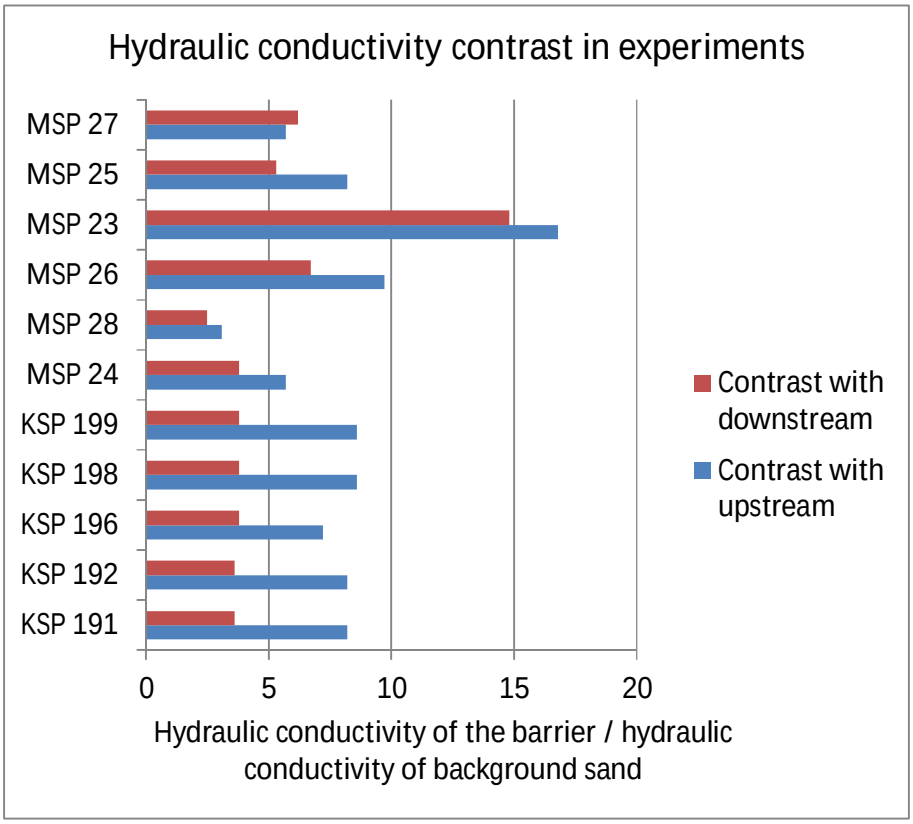


*Figure 3.5 Hydraulic conductivity contrast between the barrier and the background sand on the upstream and downstream side of the barrier in the experiments. This is based on the relative density ($RD_n$) of the samples as estimated during preparation*

| Experiment name* | Background sand | Barrier material | Hydraulic conductivity contrast upstream | Hydraulic conductivity contrast downstream |
|---|---|---|---|---|
| KSP 191 | Metselzand | GZB 2 | 8.2 | 3.6 |
| KSP 192 | Metselzand | GZB 2 | 8.2 | 3.6 |
| KSP 196 | Metselzand | GZB 3 | 7.2 | 3.8 |
| KSP 198 | Metselzand | GZB 2 | 8.6 | 3.8 |
| KSP 199 | Metselzand | GZB 2 | 8.6 | 3.8 |
| MSP 24 | Baskarp 25 | GZB 2 | 5.7 | 3.8 |
| MSP 28 | Metselzand | GZB 2 | 3.1 | 2.5 |
| MSP 26 | Baskarp 25 | GZB 1 | 9.7 | 6.7 |
| MSP 23 | Baskarp 15 | GZB 1 | 16.8 | 14.8 |
| MSP 25 | Baskarp 25 | GZB 1 | 8.2 | 5.3 |
| MSP 27 | Baskarp 25 | GZB 1 low RD | 5.7 | 6.2 |

*Table 3.3Hydraulic conductivity contrast in experiments on the upstream and downstream side of the barrier*

In the small-scale experiments a “filter cake”, a zone of lower hydraulic conductivity, formed on the upstream side of the barrier (Deltares, 2017c). This caused a steeper head drop over the upstream section of the barrier. This cannot be modelled using the preliminary FEM model. The filter cake would be expected to provide an extra strength to the barrier, thus the head drop at failure may be expected to be underpredicted in the simulations.

The values for the hydraulic conductivity that are used in the simulations are shown in .

| Simulation name | Background sand | Barrier material | Hydraulic conductivity background sand, m/s | Hydraulic conductivity barrier material, m/s |
|---|---|---|---|---|
| KSP_191 | Metselzand | GZB 2 | 2.5E-04 | 2.0E-03 |
| KSP_192 | Metselzand | GZB 2 | 2.5E-04 | 2.0E-03 |
| KSP_196 | Metselzand | GZB 3 | 2.9E-04 | 2.1E-03 |
| KSP_198 | Metselzand | GZB 2 | 2.5E-04 | 2.1E-03 |
| KSP_199 | Metselzand | GZB 2 | 2.5E-04 | 2.1E-03 |
| MSP_24 | Baskarp 25 | GZB 2 | 1.0E-04 | 5.7E-04 |
| MSP_28 | Metselzand | GZB 2 | 3.0E-04 | 9.3E-04 |
| MSP_26* | Baskarp 25 | GZB 1 | 1.0E-04 | 9.8E-04 |
| MSP_23 | Baskarp 15 | GZB 1 | 6.7E-05 | 1.1E-03 |
| MSP_25 | Baskarp 25 | GZB 1 | 9.0E-05 | 7.4E-04 |
| MSP_27 | Baskarp 25 | GZB 1 low RD | 2.7E-04 | 1.5E-03 |

*Table 3.4 Hydraulic conductivity in the numerical simulations*

* A sensitivity analysis is done with the hydraulic conductivity of the background sand downstream, 5.6E-4 m/s

### 3.5.2 Primary erosion

The primary erosion criterion is determined based on experiments. The USACE-ERDC laboratories have developed an experimental set-up in which piping can be investigated in a horizontal tube (Robbins et al. 2018). These experiments allow for direct measurement of horizontal gradients upstream of the pipe tip, in order to determine the primary erosion criterion. Robbins et al. (2018) used this set-up with measurements every 10 cm upstream of the pipe tip. This set-up was further modified to increase the sensor density, with pore pressure transducers every 2 cm upstream of the pipe tip, as shown in Figure 3.6. A first series of experiments using the modified set-up was conducted in this set-up in April 2018 using the coarse sand barrier soils, this is reported in Deltares (2018b).

*Figure 3.6 Photograph of the cylinder experimental set-up showing the transducer ports in the top of the sample. The spacing between ports is 2 cm in the center of the cylinder, and 10 cm at the ends (Deltares, 2018c)*

In this test series, only a limited number of tests were conducted, and some corrections of measured data were required due to difficulties with the data acquisition system. This led to a re-fitting of the equipment, and a second series of experiments on coarse sand barrier soils was conducted in June 2018. Results of those tests still need to be analyzed and will provide further insight into the value of the primary erosion criterion. However, the first set of results appears suitable in order to give a first indication of the primary erosion criteria for the barrier soils (Deltares, 2018b).

Both the barrier materials GZB 2 and GZB 3 have a slightly different grainsize distribution in the small- and in the medium-scale experiments. This is due to the different batch of fine filter sand that has a slightly finer grain size in the phase of medium-scale experiments. The latter batch was also used for the cylinder experiments. The effect of this difference is expected to be negligible for the primary erosion criterion. The criterion is found to be more sensitive to the coefficient of uniformity (Cu) than to the grain size in Deltares (2018b). Therefore, the same criteria are used for the small- and medium-scale models. Soil properties for the sands used in the cylinder experiments are shown in Appendix B.

A primary erosion criterion was also estimated directly based on the medium-scale experiments in Deltares (2018c). This was done by modelling the medium-scale experiments in a 2D groundwater flow model using DgFlow. The pipe progresses through the barrier in steps, these are shown in Appendix A. The so-called long growth step was considered as the best step to provide an estimate of the primary erosion criterion. Those simulations only give an estimate of the possible critical gradient as:

- The head measurements that are used to fit the simulations were not always made directly upstream of the pipe tip.
- The pipe did not always progress parallel to the flow direction (as shown in Appendix A).
- A 2D simulation is used to model 3D flow.

The values determined in the cylinder experiments are considered to provide a more reliable indication of the critical gradient for primary erosion for modelling in 3D, therefore these are used to compute the primary erosion criterion for the simulations in this analysis. The primary erosion criteria resulting from the 2D simulations are shown for comparison in Section 3.5.2.1.

#### 3.5.2.1 *Critical gradients over 10 centimeters*

In the cylinder experiments, the head profile upstream of the pipe tip is measured. A question is: over which distance upstream of the pipe tip does the hydraulic gradient uniquely characterize the resistance of the material against piping?
The hypothesis is that the critical gradient upstream of the pipe tip is a material property, however, the head profile as a function of distance from the pipe tip is affected by the geometry of the model and the permeability of the materials. Thus, two simulations with the same barrier material but a different geometry, or hydraulic conductivity contrast in the case of a background sand and a barrier, will only have the same critical gradient over one distance, and over other distances the gradients differ (Deltares, 2018c).

In Deltares (2018c), the 2D models of the experiments at the critical step for long growth are used to compute gradients over different distances, in order to see which distance yields the most constant gradient for experiments with the same barrier material. No definitive conclusion could be drawn based on the experimental results. For GZB 1 (3 tests) the coefficient of variation (CoV = standard deviation/mean) of the horizontal gradients over 0.02 m and 0.10 m were similar and the CoV was higher over 0.28 m and 0.30 m. This might be expected, more variation for gradients over larger distances. But for GZB 2 the CoV over 0.28 and 0.30 m was less than the CoV over 0.02 or 0.10 m, however, with two tests for GZB 2 the value of using the CoV is limited.

A gradient over a shorter distance has as disadvantage that flow converges strongly at the pipe tip in numerical models; this might not be representative for the physical reality where the pipe has a physical depth and there may be some crumbling of grains of the barrier. Therefore, in Deltares (2018c) 10 cm was selected as the distance over which to characterize the critical gradient for progression.
The critical gradients over 10 cm as determined in the cylinder experiments (Deltares, 2018b) are shown in . Critical gradients over that same distance as determined for 2D simulation of the experiments in Deltares (2018c) are shown in .

| Test | Relative density of the material ($RD_n$) | Computed critical gradient for primary erosion over 10** cm |
|---|---|---|
| Test 8* Baskarp B15 | 0.59 | 0.39 |
| Test 9 Baskarp B15 | 0.78 | 0.37 |
| Test 10 Baskarp B25 | 0.90 | 0.43 |
| Test 11 Baskarp B25 | 0.61 | 0.40 |
| Test 7 GZB 3 | 0.83 | 0.49 |
| Test 12 GZB 2 | 0.62 | 0.87 |
| Test 15 GZB 2 | 0.68 | 0.97 |
| Test 14 GZB 1 barrier. | 0.52 | 1.14 |

*Table 3.5 Critical progression gradients for experiments in Deltares (2018b)*

* *This test is considered unreliable due to presence of air bubbles in the sample.*

** *In order to reduce effects of noise, a polynomial function was fit to the measured head profile at the tip of the pipe. The linear gradient over 10 cm is shown (i.e. not the derivative of the head profile at 10 cm) as this corresponds to how gradients over the element are determined in the numerical model (Deltares 2018b).*

| Test description | Relative density of the material ($RD_n$) | Critical gradient for primary erosion in the barrier upstream of the pipe tip over 10 cm |
|---|---|---|
| MSP 24<br>GZB 2 & Baskarp B25 | 1.05 | 0.90 |
| MSP 28<br>GZB 2 & Metselzand | 0.83 | 0.76 |
| MSP 23<br>GZB 2 & Baskarp B15 | 0.79 | 2.94 |
| MSP 26<br>GZB 2 & Baskarp B25 | 0.87 | 2.93 |
| MSP 25<br>GZB 2 & Baskarp B25 shallow barrier | 1.01 | 2.74 |

*Table 3.6 Critical progression gradients for experiments in Deltares (2018c) based on long growth*

#### 3.5.2.2 *Correction of gradient over 10 centimeters for relative density*

The relative density affects the critical gradient for primary erosion as shown in Robbins et al. (2018). The set of cylinder experiments from April 2018 shows a similar effect of relative density (Deltares (2018b). Although the effect of RD on the critical gradient may be specific to a specific material, the number of samples reported in Deltares (2018b) is insufficient to be able to derive an individual correlation for the separate materials. Therefore, the correlation published in Robbins et al. (2018) is used for all soils in the current numerical analysis.

This correlation was derived for critical gradients over 10 cm upstream of the pipe tip. As this correlation relates to RD based on void ratio ($RD_e$), the data is first recomputed to derive the relation in terms of RD based on porosity, giving $i_{crit,10cm} \propto 0.2311 RD_n$. The results from the cylinder experiments, and the gradient over 10 cm as function of $RD_n$ are shown for the background sands in Figure 3.7 and for the barrier sands in Figure 3.8.

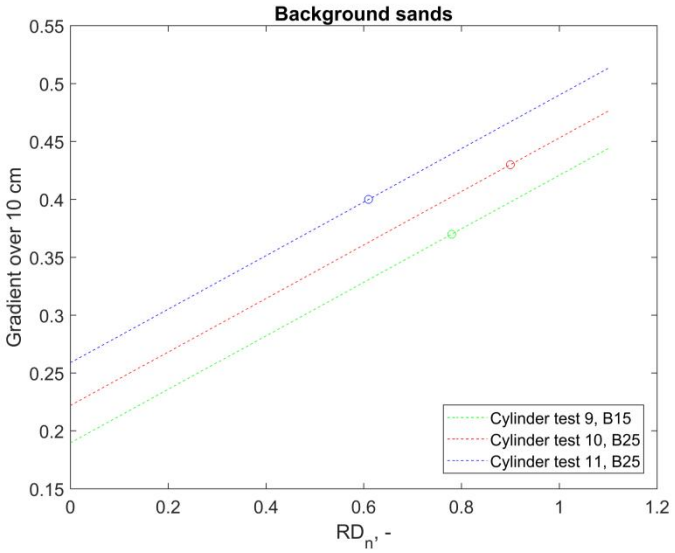


*Figure 3.7 Critical gradient over 10 cm as a function of relative density for background sands. Results from cylinder tests (Deltares, 2018b) (circles), the slope of the dashed lines is based on the correlation published in Robbins et al. (2018)*

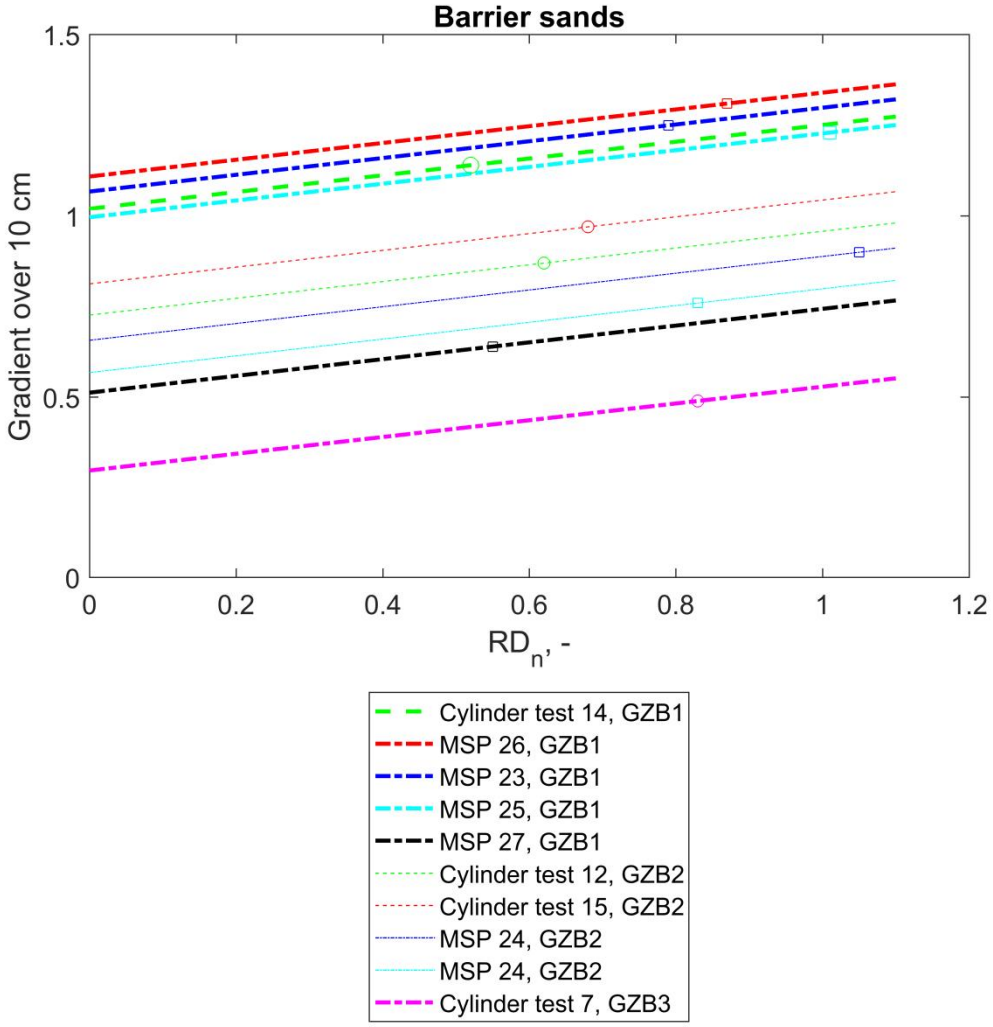


*Figure 3.8 Critical gradient over 10 cm as a function of relative density for barrier materials. Results from cylinder tests (Deltares, 2018b) (circles) and numerical modelling of box experiments (Deltares, 2018c) squares, the slope of the dashed lines is based on the correlation published in Robbins et al. (2018)*

In order to compute the critical gradient over 10 cm for the simulations in the current report, the critical gradient at relative density of 0 has to be found for each material. Then the critical gradient at the $RD_n$ of the background sand *downstream* of the barrier is computed as;

$$i_{crit,10cm,RD_n test} = i_{crit,10cm,RD_n=0} + 0.2311 RD_{test} \quad (9)$$

The $RD_n$ of the background sand downstream of the barrier is used, as the progression of the pipe from the background sand downstream into the barrier is of interest. Once the pipe progressed through the barrier, gradients in the background sand upstream are so high that failure will follow without further increases of the head drop.

The value of $i_{crit,10cm,RD_n=0}$ is determined per test as:

- For Baskarp B 15 there is only one reliable experiment, this is used;
- For Baskarp B 25 the average of the values from the two experiments is used;
- For GZB 1 there is only one cylinder experiment, this value is used. This value matches well with the values that are estimated based on numerical simulations of the box experiments at a high RD:
  - The box experient with a lower RD, MSP 27, results in a significantly lower value for the critical gradient. This might suggest a stronger effect of RD in the barrier material than is currently assumed using the correlation from Robbins et al. (2018). On the other hand, this result may also be affected by the fact that the gradient is not measured directly upstream of the pipe in the box experiments that are used to calibrate the simulation of the experiment, and by the fact that the pipe did not progress entirely parallel to the flow direction (Appendix A). Results from the additional cylinder experiments that were performed in June 2018 can give more insight into the effect of RD on the critical gradient for the different materials. In the current report the critical gradient based on the relation in Robbins et al. (2018) is used.
- For GZB 2, two cylinder experiments are available. The average of these values is used. The values based on the box experiments are consistently lower than the values based on the cylinder experiments, however, the difference is smaller than the difference for experiment MSP 27. The lower values for the box experiments may be due to not measuring the gradient directly upstream of the pipe tip, and, for test MSP 24, because the pipe progressed diagonally through the barrier (Appendix A).
- For GZB 3, only one value is measured in cylinder tests, and this barrier was not used in the medium-scale experiments. The critical gradient is significantly lower than for GZB 2, which qualitatively corresponds to the findings in the small-scale experiments that showed a lower strength with GZB 3 than with GZB 2.
- For Metselzand, there was no cylinder experiment to determine the critical gradient in the set of experiments from April 2018. This background sand has a d30 and d60 that are most comparable to the 40/70 sand that was used in cylinder experiments in Deltares (2018b) (soil properties are shown in Appendix B). The Cu is 2.4 as compared to 1.4 for the 40/70 sand. As Cu has a significant effect on the critical gradient, the correlation between Cu and critical gradient from Deltares (2018b) (with a slope of 0.34) is used to estimate the critical gradient for Metselzand.

The critical gradients at $RD_n = 0$ ($i_{crit,10cm,RD_n=0}$) are shown in , and the values of $i_{crit,10cm,RD_n test}$ that are used for the simulations are shown in .

| Soil | Critical gradient at $RD_n = 0$ |
|---|---|
| Baskarp B15 | 0.19 |
| Baskarp B25 | 0.24 |
| Metselzand | 0.60 |
| GZB 1 | 1.0 |
| GZB 2 | 0.77 |
| GZB 3 | 0.30 |

*Table 3.7 Critical gradients over 10 cm at $RD_n$= 0 that are used to compute critical gradients over 10 cm for simulations*

The value at $RD_n = 0$ for GZB 3, which has a mean grain size similar to GZB 2, but a Cu similar to the Baskarp sands, is much closer to the value for the Baskarp sands. This

indicates the relative importance of the effect of Cu as compared to the effect of grain size for the primary erosion criterion. The estimated critical gradient for Metselzand is actually higher than the estimated critical gradient for GZB 3 in test KSP 196.

| Simulation name | Background sand | Barrier material | Critical progression gradient over 10 cm background sand | Critical progression gradient over 10 cm barrier material |
|---|---|---|---|---|
| KSP_191 | Metselzand | GZB 2 | 0.74 | 0.99 |
| KSP_192 | Metselzand | GZB 2 | 0.74 | 0.99 |
| KSP_196 | Metselzand | GZB 3 | 0.74 | 0.51 |
| KSP_198 | Metselzand | GZB 2 | 0.74 | 0.98 |
| KSP_199 | Metselzand | GZB 2 | 0.74 | 0.98 |
| MSP_24 | Baskarp 25 | GZB 2 | 0.46 | 1.0 |
| MSP_28 | Metselzand | GZB 2 | 0.83 | 0.96 |
| MSP_26 | Baskarp 25 | GZB 1 | 0.46 | 1.2 |
| MSP_23 | Baskarp 15 | GZB 1 | 0.38 | 1.2 |
| MSP_25 | Baskarp 25 | GZB 1 | 0.46 | 1.3 |
| MSP_27 | Baskarp 25 | GZB 1 low RD | 0.39 | 1.2 |

*Table* 3.8*Critical gradients over 10 cm at the $RD_n$* of the experiments using the $RD_n$ of the background sand downstream of the barrier

| |
|---|
| |

*3.5.2.3 Scaling primary erosion criterion over element size*

As the primary erosion criterion in the simulations is computed over the length of one element, the critical gradient over 10 cm needs to be scaled to the critical gradient over 1 cm for the small-scale tests, and to the gradient over 4 cm and over 2 cm for the medium-scale tests.

In the tube experiments, gradients were measured every 2 centimeters, therefore these cannot be directly used to estimate the gradient over 1 cm. A polynomial is fit to the measured heads upstream of the pipe tip in Deltares (2018b), and this can be used for computing gradients over shorter distances. However, due to the interpolation from the pipe tip to the first measurement at 2 cm upstream of the pipe tip, this is likely to underestimate the convergence of flow at the pipe tip, and therefore under predict the gradient at the pipe tip.

The relation between the gradient over 10 cm to the gradient over other lengths is also dependent on the geometry and hydraulic conductivity contrast as those affect the head profile in the barrier. The situation in a tube with only one soil type will be different from the situation in a box model with a barrier configuration.

A 2D sensitivity analysis is done in Deltares (2018c) to model the relation of the gradient over different distances in a barrier configuration. Results in the sensitivity analysis for a configuration with a deep barrier and a pipe of 12 cm into the barrier match quite well with ratios that were found in the simulations of the long growth step in the box experiments, which would be expected as the models have a similar geometry.

Therefore, the gradients over 10 cm are scaled using the ratios obtained from the simulation from the sensitivity analysis with a 12 cm pipe, a hydraulic conductivity contrast of 3 and a deep barrier. For the scaling from 10 cm to 2 cm this gives a factor of 2.2, which is similar to what is found in four of the cylinder experiments. For the scaling of the gradient over 10 cm to the gradient over 1 cm this gives a factor 3.1 and for the conversion of the gradient over 10 cm to the gradient over 4 cm a factor 1.6. The critical gradients in the basis simulations are shown in .
These scaling factors are derived based on a 2D model of a 3D situation, when the pipe is already 12 centimeters into the barrier. As the pipe that has progressed along the barrier in the fine sand, the difference between the gradient upstream of the pipe tip in the 2D and in the 3D model would be smaller than in tests with a uniform sand and one straight pipe, there could be a difference between the scaling factor in 2D and 3D.
Furthermore, currently it is not clear over which distance the failure criterion should be determined, the 10 cm is used based on practical considerations, and as the model computes critical gradients over the elemental size a rescaling is necessary. Future work should focus on determining the optimum length, and ideally the gradient is also computed over this distance in order to evaluate the primary erosion criterion.

| Simulation name | Background sand | Barrier material | Critical progression gradient background sand | Critical progression gradient barrier material |
|---|---|---|---|---|
| KSP_191 | Metselzand | GZB 2 | 2.3 | 3.1 |
| KSP_192 | Metselzand | GZB 2 | 2.3 | 3.1 |
| KSP_196 | Metselzand | GZB 3 | 2.3 | 1.6 |
| KSP_198 | Metselzand | GZB 2 | 2.3 | 3.0 |
| KSP_199 | Metselzand | GZB 2 | 2.3 | 3.0 |
| MSP_24 | Baskarp 25 | GZB 2 | 0.7 | 1.6 |
| MSP_28 | Metselzand | GZB 2 | 1.3 | 1.5 |
| MSP_26 | Baskarp 25 | GZB 1 | 0.7 | 2.0 |
| MSP_23 | Baskarp 15 | GZB 1 | 0.6 | 1.9 |
| MSP_25 | Baskarp 25 | GZB 1 | 0.7 | 2.0 |
| MSP_27 | Baskarp 25 | GZB 1 low RD | 0.6 | 1.8 |

*Table 3.9 Critical gradients in the simulations for the basis simulations (the critical gradient is over 1 cm and therefore higher than the gradient over 4 cm for the medium-scale tests)*

In order to analyze the effect of the scaling factor that is used, a sensitivity analysis is also conducted using a lower scaling factor. The reduction of the scaling factor is based on the results from the cylinder experiments. The scaling factor of ca 1.5 (for scaling from gradients over 10 cm to gradients over 2 cm) that is indicated by the three cylinder experiments on barrier material is ca. 70% of the scaling factor of 2.2 that is used in the basis simulations. Therefore, in the sensitivity analysis the scaling factors are also reduced to 70% of the value in the basis simulation. For the small-scale models, the effect is expected to be more significant than for the medium scale models, therefore simulations are done for all small-

scale tests where the gradient over 10 cm is scaled by a factor 2.2 instead of by 3.1. For the medium-scale models one simulation is done, with MSP_26_scaling using a scaling factor of 1.1 instead of 1.6.

| Simulation name | Background sand | Barrier material | Critical progression gradient background sand | Critical progression gradient barrier material |
|---|---|---|---|---|
| KSP_191_Scaling | Metselzand | GZB 2 | 1.6 | 2.2 |
| KSP_192__Scaling | Metselzand | GZB 2 | 1.6 | 2.2 |
| KSP_196__Scaling | Metselzand | GZB 3 | 1.6 | 1.1 |
| KSP_198__Scaling | Metselzand | GZB 2 | 1.6 | 2.2 |
| KSP_199__Scaling | Metselzand | GZB 2 | 1.6 | 2.2 |
| MSP_26__Scaling | Baskarp 25 | GZB 1 | 0.50 | 1.4 |

*Table* 3.10 Critical gradients in the simulations with a 70% lower scaling factor than in the basis simulations

### 3.5.3 Secondary erosion criterion

Secondary erosion is modelled using White's (1940) approach for laminar flow to determine the critical shear stress at which particles are eroded from the bottom of the pipe as in van Beek (2015). The secondary erosion criterion, $\tau_c$ is given as:

$$\tau_c = \eta \frac{\pi}{6} \gamma_p' d_{50} tan\theta \qquad (10)$$

where $\eta$ is White's constant set at 0.30, $\gamma_p$' is the submerged unit weight of the soil particles, 2650*9.81, $d_{50}$ is the median grain size and $\theta$ is the bedding angle.

The bedding angle is computed based on the $d_{50}$ using the correlation derived in van Beek (2015)

$$\theta = -8.125 \ln(d_{50}) - 38.777 \qquad (11)$$

This correlation was derived using data for laminar flow using data from experiments in which sands had $d_{50}$ up to 1 mm. The barrier materials are outside this range. Therefore, alternative methods of computing shear stress as suggested by Brownlie (1988), Cao et al. (2016), and Briaud et al. (2017) were also used to compute the critical shear stress. The relation between the critical shear stress and $d_{50}$ is shown in Figure 3.9, which also contains a dataset collected and published by van Beek et al. (2018) including literature data and results from new cylinder experiments that are reported in Robbins et al (2018).

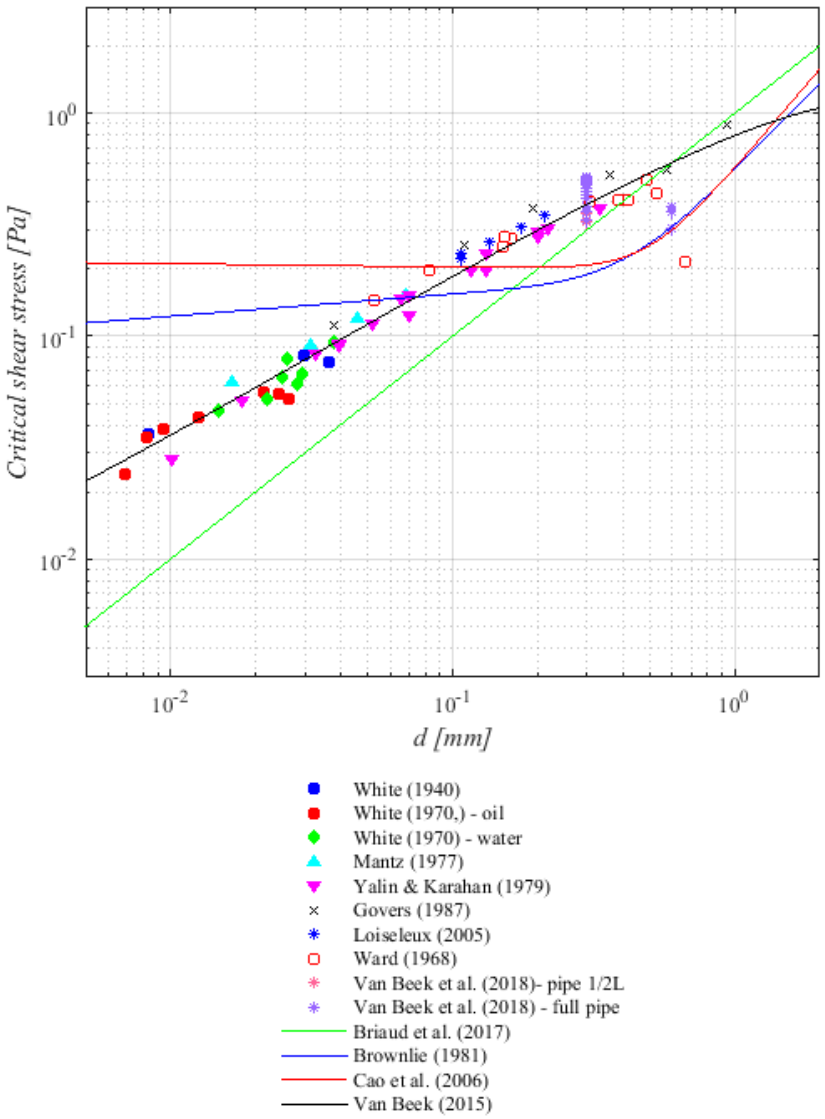


*Figure 3.9 Relation between grain size and critical shear stress according to different models (solid lines) data is from van Beek et al. (2018)*

Figure 3.9 shows that the correlation in van Beek (2015) fits data for small grain sizes significantly better than the other models. This would be expected as that relation is calibrated to a large portion of that data. The four relations show different trends for larger grain sizes, the relations from Cao et al. (2016) and Brownlie (1981) show a sharper increase in shear stress with increasing $d_{50}$, whereas the relation in van Beek (2015) levels off at high $d_{50}$.
The limited number of data points at a large grain size makes it difficult to assess which relation performs best in this area. Therefore, the relation in van Beek is used for both the barrier material and the background sand.

The input critical shear stress in this relation (or in the other three relations analyzed here) does not depend on relative density or on Cu. The input critical shear stresses for the simulations are shown in Table 3.11.

| Simulation name | Background sand | Critical shear stress background sand, Pa | Barrier material | Critical shear stress barrier material, Pa |
|---|---|---|---|---|
| KSP_191 | Metselzand | 0.45 | GZB 2 | 0.82 |
| KSP_192 | Metselzand | 0.45 | GZB 2 | 0.82 |
| KSP_196 | Metselzand | 0.45 | GZB 3 | 0.85 |
| KSP_198 | Metselzand | 0.45 | GZB 2 | 0.82 |
| KSP_199 | Metselzand | 0.45 | GZB 2 | 0.82 |
| MSP_24 | Baskarp 25 | 0.33 | GZB 2 | 0.75 |
| MSP_28 | Metselzand | 0.45 | GZB 2 | 0.75 |
| MSP_26 | Baskarp 25 | 0.33 | GZB 1 | 0.93 |
| MSP_23 | Baskarp 15 | 0.25 | GZB 1 | 0.93 |
| MSP_25 | Baskarp 25 | 0.33 | GZB 1 | 0.93 |
| MSP_27 | Baskarp 25 | 0.33 | GZB 1 low RD | 0.93 |

*Table 3.11 Critical shear stress in the numerical simulations*

## 3.6 Overview of simulations

An overview of the simulations is provided in .

| Simulation name | Model size | Barrier depth, m | Barrier thick-ness, m | k back ground, m/s | k barrier, m/s | $i_{crit}$ back-ground | $i_{crit}$ barrier | $\tau_c$ back-ground, Pa | $\tau_c$ barrier, Pa | Nr of pipe elements switched on per step |
|---|---|---|---|---|---|---|---|---|---|---|
| KSP_191 | Small-scale regular | 0.10 | 0.05 | 2.5E-04 | 2.0E-03 | 2.3 | 3.1 | 0.45 | 0.82 | 2 |
| KSP_192 | Small-scale regular | 0.03 | 0.05 | 2.5E-04 | 2.0E-03 | 2.3 | 3.1 | 0.45 | 0.82 | 2 |
| KSP_196 | Small-scale regular | 0.10 | 0.05 | 2.9E-04 | 2.1E-03 | 2.3 | 1.6 | 0.45 | 0.85 | 2 |
| KSP_198 | Small-scale rotated | 0.03 | 0.05 | 2.5E-04 | 2.1E-03 | 2.3 | 3.0 | 0.45 | 0.82 | 2 |
| KSP_199 | Small-scale rotated | 0.10 | 0.05 | 2.5E-04 | 2.1E-03 | 2.3 | 3.0 | 0.45 | 0.82 | 2 |
| MSP_24 | Medium-scale | 0.40 | 0.28 | 1.0E-04 | 5.7E-04 | 0.71 | 1.6 | 0.33 | 0.75 | 2 |
| MSP_28 | Medium-scale | 0.40 | 0.28 | 3.0E-04 | 9.3E-04 | 1.3 | 1.5 | 0.45 | 0.75 | 2 |
| MSP_26 | Medium-scale | 0.40 | 0.28 | 1.0E-04 | 9.8E-04 | 0.72 | 2.0 | 0.33 | 0.93 | 2 |
| MSP_23 | Medium-scale | 0.40 | 0.28 | 6.7E-05 | 1.1E-03 | 0.60 | 1.9 | 0.25 | 0.93 | 2 |
| MSP_25 | Medium-scale | 0.12 | 0.28 | 9.0E-05 | 7.4E-04 | 0.72 | 2.0 | 0.33 | 0.93 | 2 |
| MSP_27 | Medium-scale | 0.40 | 0.28 | 2.7E-04 | 1.5E-03 | 0.60 | 1.8 | 0.33 | 0.93 | 2 |

*Table 3.12 Overview of input parameters for basis simulations*

| Simulation name | Model size | Barrier depth, m | Barrier thick-ness, m | k back ground, m/s | k barrier, m/s | $i_{crit}$ back ground | $i_{crit}$ barrier | $\tau_c$ back ground, Pa | $\tau_c$ barrier, Pa | Nr of pipe elements switched on per step |
|---|---|---|---|---|---|---|---|---|---|---|
| KSP_191_Scaling | Small-scale regular | 0.10 | 0.05 | 2.5E-04 | 2.0E-03 | 1.6 | 2.2 | 0.45 | 0.82 | 2 |
| KSP_192_Scaling | Small-scale regular | 0.03 | 0.05 | 2.5E-04 | 2.0E-03 | 1.6 | 2.2 | 0.45 | 0.82 | 2 |
| KSP_196_Scaling | Small-scale regular | 0.10 | 0.05 | 2.9E-04 | 2.1E-03 | 1.6 | 1.1 | 0.45 | 0.85 | 2 |
| KSP_198_Scaling | Small-scale rotated | 0.03 | 0.05 | 2.5E-04 | 2.1E-03 | 1.6 | 2.2 | 0.45 | 0.82 | 2 |
| KSP_199_Scaling | Small-scale rotated | 0.10 | 0.05 | 2.5E-04 | 2.1E-03 | 1.6 | 2.2 | 0.45 | 0.82 | 2 |

*Table 3.13 Sensitivity analysis: Small-scale models with primary erosion criterion over 10 cm scaled by factor 2.20 (instead of scaled by factor 3.10)*

| Simulation name | Variation | Barrier thick-ness, m | k back ground, m/s | k barrier, m/s | $i_{crit}$ back-ground | $i_{crit}$ barrier | $\tau_c$ back-ground, Pa | $\tau_c$ barrier, Pa | Nr of pipe elements switched on per step |
|---|---|---|---|---|---|---|---|---|---|
| MSP_26_2_ | Element size 2 cm | 0.28 | 1.0E-04 | 9.8E-04 | **1.0** | **2.8** | 0.33 | 0.93 | 2 |
| MSP_26_1el | Nr elements switched on per step | 0.28 | 1.0E-04 | 9.8E-04 | 0.72 | 2.0 | 0.33 | 0.93 | **1** |
| MSP_26_3el | | 0.28 | 1.0E-04 | 9.8E-04 | 0.72 | 2.0 | 0.33 | 0.93 | **3** |
| MSP_26_B24 | Barrier thickness | **0.24** | 1.0E-04 | 9.8E-04 | 0.72 | 2.0 | 0.33 | 0.93 | 2 |
| MSP_26_B32 | | **0.32** | 1.0E-04 | 9.8E-04 | 0.72 | 2.0 | 0.33 | 0.93 | 2 |
| MSP_26_Hc downstream_ | Hydraulic conductivity based on downstream fine sand | 0.28 | **1.5E-04** | 9.8E-04 | 0.72 | 2.0 | 0.33 | 0.93 | 2 |
| MSP_26_ Scaling | Primary erosion criterion over 10 cm scaled by 1.10 instead of by 1.57 | 0.40 | 1.0E-04 | 9.8E-04 | **0.50** | **1.4** | 0.33 | 0.93 | 2 |

*Table 3.14 Sensitivity analysis: medium scale simulations variations on simulation for test MSP 26, bold values indicate variables that are different than in the basis schematization*

| Simulation name | Variation | Barrier thick-ness, m | back-ground, m/s | barrier, m/s | $i_{crit}$ back ground | $i_{crit}$ barrier | $\tau_c$ back ground, Pa | $\tau_c$ barrier, Pa | Nr of pipe elements switched on per step |
|---|---|---|---|---|---|---|---|---|---|
| MSP_23_B24 | Barrier thickness | **0.24** | 6.7E-05 | 1.1E-03 | 0.60 | 1.9 | 0.25 | 0.93 | 2 |
| MSP_23_B32 | Barrier thickness | **0.32** | 6.7E-05 | 1.1E-03 | 0.60 | 1.9 | 0.25 | 0.93 | 2 |

*Table 3.15 Sensitivity analysis: medium scale simulations variations on simulation for test MSP 23, bold values indicate variables that are different than in the basis schematization*

# 4 Results

The simulations show the progression of the pipe as the head drop is increased. In order to analyze the results, we consider quantitative and qualitative pipe progression. Results were analyzed using ParaView (version 5.4.1 64 bit).

For quantitative analysis, the head drop over the model is analyzed at damage and at failure, and the flow rate is compared to the experimentally measured flow rate. Damage is considered to be the point at which a first pipe develops in the barrier; failure is the point at which the pipe passes through the upstream interface of the barrier in the models. In experiments, damage was difficult to register. Crumbling of the barrier into the pipe that had formed parallel to the barrier interface was not considered as damage. Damage was considered to be the point where a pipe 'shape' could be distinguished in the barrier. However, the difference is to some extent subjective.

For qualitative analysis of pipe progression, the emphasis is on the medium-scale models. During the small-scale experiments, the barrier was only 5 cm thick and observations were aimed at identifying the head drops at damage and at failure. In the medium-scale experiments it was observed that the pipe progressed through the barrier in discrete steps, rather than gradually lengthening and these steps were analyzed (Deltares, 2018c). The pipe shape after specific progression steps are sketched in Appendix A.

The following aspects are considered in the qualitative analysis of pipe progression in the simulations:

- Progression of the pipe parallel to the barrier in the background sand prior to damage of the barrier.
- The number of pipes entering the barrier at damage.
- The maximum distance that a pipe progresses inside the barrier at the damage head drop.
- The number of pipes entering the barrier in total.
- The number of pipes that progress past half way through the barrier and come to a stop, i.e. an additional head raise is required to cause failure.
- Progression of the pipe inside the barrier parallel to the interface between the background sand upstream and the barrier.

## 4.1 Results of the basis simulations and comparison to experiments

### 4.1.1 Qualitative pipe progression

In order to compare the simulations of the pipe progression to the pipe progression sketched in Appendix A, the output of the simulations at the end of the damage step and at the first step after the pipe has progressed through the upstream interface of the barrier are shown in Appendix C for the basis simulations of the medium-scale experiments.

A summary of the qualitative pipe progression in the simulations is given in , a summary of qualitative pipe progression in experiments is given in .

| | Progression of pipe parallel to the barrier in background sand prior to entering barrier | Number of pipes entering the barrier at damage | Maximum distance that a pipe progresses inside the barrier in the damage step, m | Number of pipes that enter the barrier in total | Number of pipes that progress past half way through the barrier and come to a stop. | Progression of pipe parallel to the barrier at the upstream interface + |
|---|---|---|---|---|---|---|
| MSP_26 | yes | 1 | 0.24 | 2 | 2 | yes[++] |
| MSP_23 | yes | 2 | 0.24 | 2 | 2 | no |
| MSP_25 | yes | 1 | 0.28 | 1 | 0 | no |
| MSP_27 | yes | 1 | 0.24 | 1 | 1 | no |
| MPS_24 | yes | 1 | 0.24 | 1 | 1 | no |
| MSP_28 | yes | 1 | 0.28 | 1 | 0 | no |
| | | | | | | |
| KSP_191 | yes | 2 | 0.01 | 3 | 3 | no |
| KSP_192 | yes | 2 | 0.04 | 2 | 2 | no |
| KSP_196 | no | 1 | 0.01 | 1 [=] | 1 | yes |
| KSP_198 | yes | 1 | 0.04 | 1 | 1 | no |
| KSP_199 | no** | 1** | 0.04 | 1** | Multiple* | no |

*Table 4.1Summary of qualitative pipe progression steps in the basis simulations*

* pipe forms prior to failure (not before damage as in other simulations). Prior to damage pipe goes back from outlet hole

**when the pipe reaches the barrier, it branches; one pipe progresses parallel to the barrier interface and one pipe enters the barrier, but the pipe branches again once inside the barrier and both branches progress and subsequently branch further, all at the same applied head drop as for damage

[+] as the pipe sometimes moves sideways through the barrier, progression parallel to the barrier interface is only considered as such if the pipe stops and an additional head increment is required in order to proceed to failure.

[++] only 2 elements

[=] the pipe branches inside the barrier

| Test | Progression of pipes parallel to the barrier interface | Number of pipes entering barrier at damage* | Number of pipes that enter barrier in total | Number of pipes that progress past half way through barrier and come to a stop. | Progression of pipe parallel to barrier upstream interface |
|---|---|---|---|---|---|
| MSP 26 | Yes | multiple | multiple | 1 | yes |
| MSP 23 | Yes | multiple | multiple | 1 | yes |
| MSP 25 | Yes | multiple | multiple | 0 | no |
| MSP 27 | Yes | multiple | multiple | 1 | yes |
| MSP 24 | Yes | 1 | 1 | 1 | yes |
| MSP 28 | No | 1 | 1 | 1 | no |
| | | | | | |
| KSP 191** | Yes | *1 that progresses 4 cm through barrier in damage step* | *Multiple* | *Multiple* | *Widening of pipe at upstream interface* |
| KSP 192** | Yes | *1 but difficult to distinguish crumbling and pipes and several pipes do enter in following head increments.* | *Multiple* | *Probably 0* | *No* |
| KSP 196** | Yes | *1 short pipe, 2 head increments later another pipe enters* | *Multiple* | *Multiple* | *No* |
| KSP 198** | Yes | *1 at next head increment next pipe enters* | *Multiple* | *Probably 1* | *No* |
| KSP 199** | Yes | *1 at next head increment next pipe enters* | *Multiple* | *Multiple* | *No* |

*Table 4.2Summary of qualitative pipe progression steps in the experiments*

* refer to sketches in Appendix A for pipe extent inside the barrier at critical steps.

** no sketch was made of the pipes during the small-scale experiments and progression of the pipes inside the barrier was not the subject of investigation. The current summary is an interpretation based on observations reported in Deltares (2017b)

### 4.1.2 Critical head drop

The critical head drop at the damage step and at the failure step in the simulations, are shown in . This also shows the experimental heads for damage, long growth, and failure. The ratio of the heads in the simulations to the heads in the tests are shown in .

| Simulation | Modelled critical damage head, m | Modelled critical failure head drop, m | Experimentally measured critical damage head *, m | Experimentally measured critical head for short growth *, m | Experimentally measured critical head for long growth*, m | Experimentally measured critical failure head drop *, m |
|---|---|---|---|---|---|---|
| MSP_26 | 2.55 | 3.74 | 0.51 | 0.84 | 1.71 | 2.59 |
| MSP_23 | 3.74 | 4.98 | 2.87 | 3.32 | 3.47 | >5.33 |
| MSP_25** | 2.55 | 2.55 | 0.81 | 1.17 | 1.57 | 1.89 |
| MSP_27 | 1.59 | 1.74 | 0.35 | 0.63 | 0.81 | 1.31 |
| MSP_24 | 1.44 | 1.59 | 0.60 | 0.70 | 1.07 | 1.31 |
| MSP_28 | 0.90 | 0.90 | 0.19 | 0.48 | 0.59 | 0.63 |
| | | | | | | |
| KSP_191[+] | 0.90 | 1.31 | 0.40 | n.a. | n.a. | 1.01 |
| KSP_192[+] | 0.99 | 1.19 | 0.41 | n.a. | n.a. | 0.74 |
| KSP_196[+] | 0.12 | 0.67 | 0.55 | n.a. | n.a. | 1.00 |
| KSP_198[+] | 0.74 | 0.89 | 0.26 | n.a. | n.a. | 1.05 |
| KSP_199[+] | 0.13 | n.a.[++] | 0.28 | n.a. | n.a. | 0.76 |

*Table 4.3Overview of modelled and measured critical heads for basis simulations*

* This is the head drop between the inlet of the sample, corrected for loss at the upstream filter, and the head measurements that are made inside the sample at the location in the background sand at the downstream interface of the barrier.

** In test MSP 25 there was no long growth step therefore the critical head for medium growth II is used.

[+] In the small scale tests, progression steps were not recorded.

[++] During this simulation the pipe formed throughout the barrier, but the head drop could not be increased to cause failure, this was observed in the simulations where 1, 2 or 3 elements were switched on per pipe progression step.

| Simulation | Ratio modelled head for damage/ measured head for damage | Ratio modelled head for damage/ measured head for short growth | Ratio modelled head for damage/ measured head for long growth | Ratio modelled head for failure/ measured head for failure |
|---|---|---|---|---|
| MSP_26 | 5.0 | 3.0 | 1.5 | 1.4 |
| MSP_23 | 1.3 | 1.1 | 1.1 | <0.9 |
| MSP_25* | 3.2 | 2.2 | 1.6 | 1.4 |
| MSP_27 | 4.5 | 2.5 | 2.0 | 1.3 |
| | | | | |
| MSP_24 | 2.4 | 2.1 | 1.3 | 1.2 |
| MSP_28 | 4.7 | 1.9 | 1.5 | 1.4 |
| | | | | |
| KSP_191+ | 2.2 | n.a. | n.a. | 1.3 |
| KSP_192+ | 2.4 | n.a. | n.a. | 1.6 |
| KSP_196+ | 0.2 | n.a. | n.a. | 0.7 |
| KSP_198+ | 2.8 | n.a. | n.a. | 0.9 |
| KSP_199+= | 0.5 | n.a. | n.a. | n.a.= |

*Table 4.4 Ratio of modelled critical head to measured critical head*

* In test MSP 25 there was no long growth step therefore the critical head for medium growth II is used.

\+ In the small scale tests, progression steps were not recorded.

\= During this simulation the pipe formed throughout the barrier, but the head drop could not be increased to cause failure, this was observed in the simulations where 1, 2 or 3 elements were switched on per pipe progression step.

#### 4.1.2.1 *Head loss in the pipe*

Critical head drops in the simulations are compared to the head difference between the upstream side of the filter and the head measurements that are made in the pipe downstream of the barrier. The head at this location, rather than in the outlet tubing of the experiments, was used in order to exclude the head loss in the sand boil and the erosion lens that formed at the outlet hole during the experiments (Deltares, 2017c and Deltares 2018c). Thus, the resistance in the pipe is assumed to be negligible in this comparison.

This assumption is checked for simulation MSP_26; the head in the pipe parallel to the barrier at the critical states for damage and failure was less than 0.0015 m, as shown in Figure 4.2 and Figure 4.3. Thus, the assumption is considered appropriate for the comparison of the simulations to the experiments.

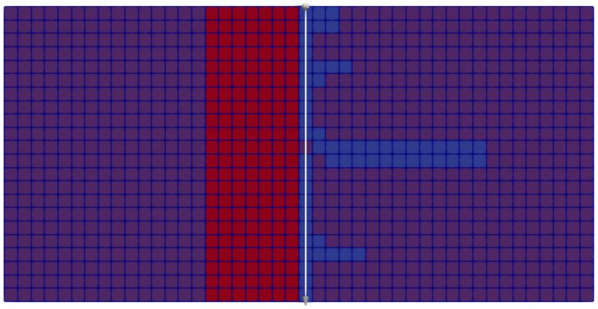

*Figure 4.1 The white line indicates the location of the pipe in the background sand downstream of the barrier in MSP_26 used to assess head and pipe depth in Figure 5.2 and Figure 5.3. Barrier is red, background sand is purple, the location of the pipe is in blue*

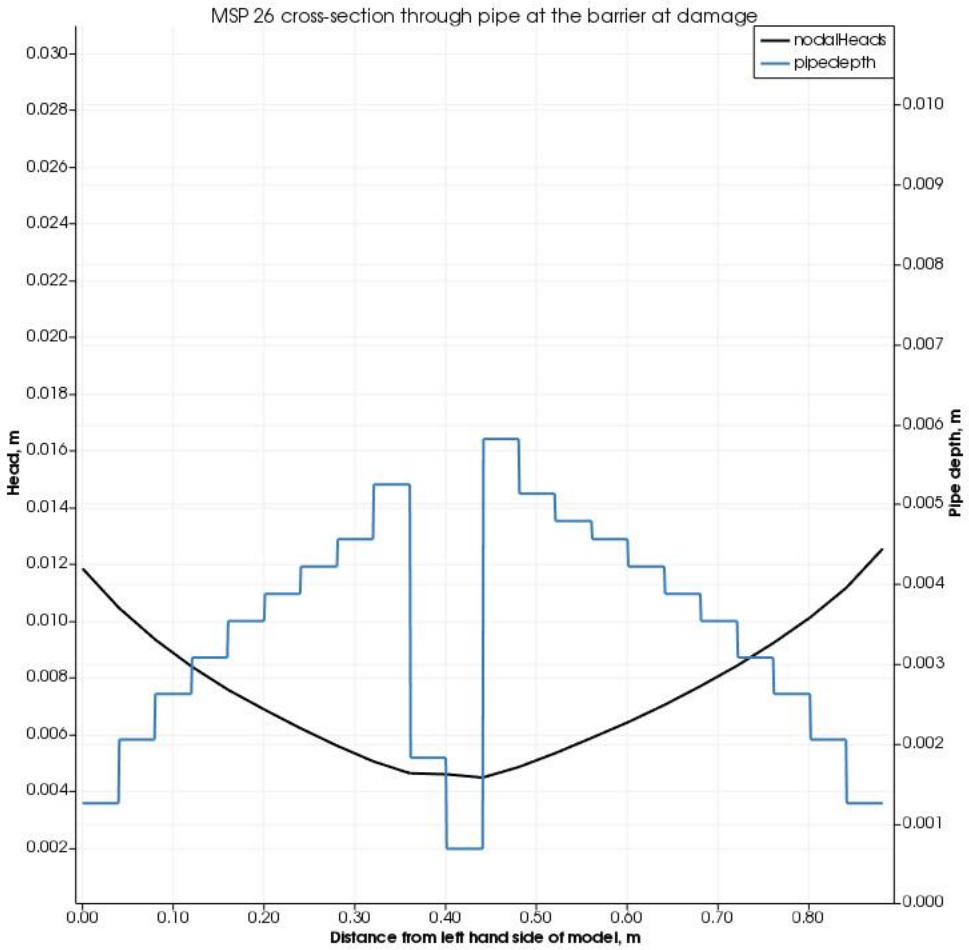


*Figure 4.2 Modelled head and pipe depth inside the pipe downstream of the barrier in simulation MSP_26 at the critical state for damage*

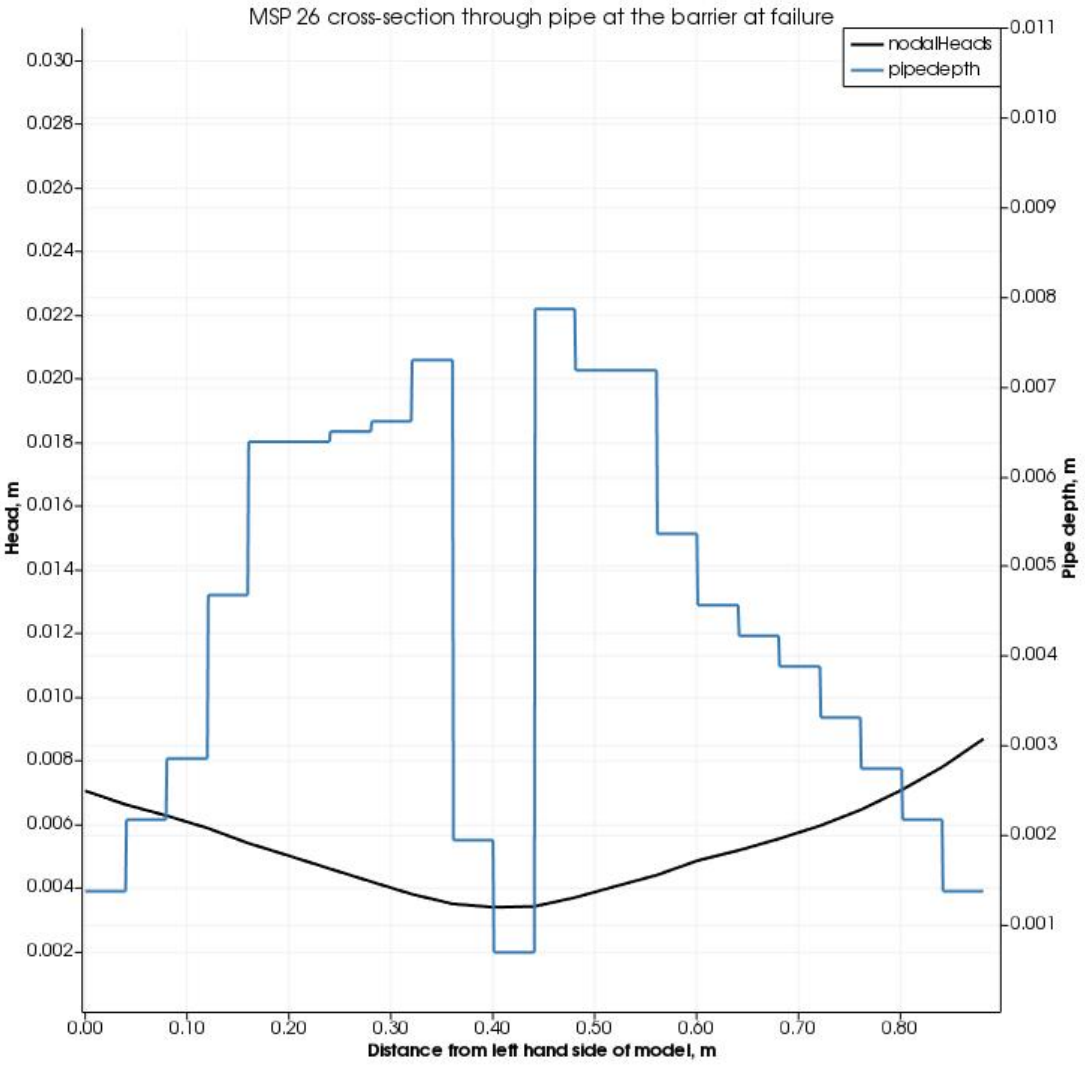


*Figure 4.3 Modelled head and pipe depth inside the pipe downstream of the barrier in simulation MSP_26 at the critical state for failure*

4.1.3 Flux

The flux that was measured during the experiments at the critical step for damage of the barrier is compared to the flux in the models at approximately the same head drop. These results are shown in .

| Experiment | Flux modelled, cc/min | Flux measured, cc/min |
|---|---|---|
| MSP_26 | 1521 | 2454 |
| MSP_23 | 6603 | 7244 |
| MSP_25* | 1996 | 4154 |
| MSP_27 | 2623 | 3186 |
| | | |
| MSP_24 | 1774 | 2966 |
| MSP_28 | 3719 | 4512 |
| | | |
| KSP_191$^{+}$ | 909 | 918 |
| KSP_192$^{+}$ | 846 | 987 |
| KSP_196$^{+}$ | 1498 | 1493 |
| KSP_198$^{+}$ | 383 | 635 |
| KSP_199$^{+=}$ | 419 | 728 |

*Table 4.5Flux in experiments and in the model at the head drop that corresponded to damage in the experiment*

## 4.2 Sensitivity analyses

This Section presents the results of the sensitivity analyses.

4.2.1 Qualitative pipe progression

The qualitative aspects of pipe progression were investigated by variations on the basis of simulation MSP_26.

As the effect of barrier thickness on the critical head drop was considered remarkable, this was varied additionally for MSP_23 in order to see whether the same behavior is observed with different models.

Mesh refinement affects the modelling of progression of the pipe parallel to the barrier interface, with more progression of the pipe parallel to the interface for simulations with a finer mesh. As this parallel progression was observed to occur in the majority of the medium-scale experiments, but not in experiment MSP 25, the effect of mesh refinement was also analyzed for that model.

The sensitivity analysis on the medium-scale models is summarized in .

| Simulation | Progression of pipe parallel to barrier in background sand prior to entering barrier | Number of pipes entering barrier at damage | Maximum distance that pipe progresses inside barrier in damage step, m | Number of pipes that enter barrier in total | Number of pipes that progress past half way through barrier and come to a stop. | Progression of pipe parallel to barrier upstream interface [+] |
|---|---|---|---|---|---|---|
| **MSP_26** | **Yes** | **1** | **0.24** | **2** | **2** | **yes[++]** |
| MSP_26_1el | Yes | 1 | 0.24 | 1 | 1 | no |
| MSP_26_3el | Yes | 1 | 0.24 | 1 | 1 | no |
| MSP_26_B24 | yes | 1 | 0.20 | 3 | 3 | yes[=] |
| MSP_26_B32 | yes | 1 | 0.28 | 1 | 1 | no |
| MSP_26_2 | yes | 1 | 0.18 | 1 | 1 | yes |
| MSP_26_Scaling | yes | 2 | 0.12 | 2 | 1 | no |
| MSP_26_Hcdownstream | yes | 1 | 0.24 | 1 | 1 | no |
| | | | | | | |
| **MSP_23** | **yes** | **2** | **0.24** | **2** | **2** | **no** |
| MSP_23_B24 | yes | 2 | 0.20 | 2 | 2 | no |
| MSP_23_B32 | yes | 2 | 0.24 | 2 | 2 | no |
| | | | | | | |
| **MSP_25** | **yes** | **1** | **0.28** | **1** | **1** | **no** |
| MSP_25_2 | yes | 1 | 0.28 | 1 | 1 | no |

*Table 4.6 Summary of qualitative pipe progression steps for sensitivity analysis on medium-scale models (basis simulations are bold)*

[+] As the pipe sometimes moves sideways through the barrier, progression parallel to the barrier interface is only considered as such if the pipe stops and an additional head increment is required in order to proceed to failure.

[++] Only 2 elements.

[=] Only 1 element.

For the small scale simulations, the effect of the scaling factor was investigated for all models. A summary of the qualitative comparison of the simulations is shown in .

| Simulation | Progression of pipe parallel to barrier in background sand prior to entering barrier | Number of pipes entering barrier at damage | Maximum distance that pipe progresses inside barrier in damage step, m | Number of pipes that enter barrier in total | Number of pipes that progress past half way through barrier and come to a stop | Progression of pipe parallel to barrier upstream interface [+] |
|---|---|---|---|---|---|---|
| **KSP_191** | **yes** | **2** | **0.01** | **3** | **3** | **no** |
| KSP_191_Scaling | yes | 2 | 0.02 | 3 | 3 | no |
| **KSP_192** | **yes** | **2** | **0.04** | **2** | **2** | **no** |
| KSP_192_Scaling | yes | 2 | 0.03 | 2 | 2 | no |
| **KSP_196** | **no** | **1** | **0.01** | **1 but splits** | **1** | **yes** |
| KSP_196_Scaling | no | 1 | 0.01 | 1 but splits | 2 | yes |
| **KSP_198** | **yes** | **1** | **0.04** | **1** | **1** | **no** |
| KSP_198_Scaling | yes | 1 | 0.04 | 1 | 1 | no |
| **KSP_199**** | **no**** | **1**** | **0.04** | **1**** | **Multiple**** | **no** |
| KSP_199_Scaling | Yes | 1 | 0.01 | 2 | 2 | no |

*Table 4.7 Summary of qualitative pipe progression steps for sensitivity analysis on small-scale models (basis simulations are bold)*

[+] As the pipe sometimes moves sideways through the barrier, progression parallel to the barrier interface is only considered as such if the pipe stops and an additional head increment is required in order to proceed to failure.

** During this simulation the pipe formed throughout the barrier, but the head drop could not be increased to cause failure, this was observed in the simulations where 1, 2 or 3 elements were switched on per pipe progression step

### 4.2.2 Critical head drop

The critical head drop in the simulations for the sensitivity analysis on test MSP 26 is shown in Figure 4.4 for damage and Figure 4.5 for failure. The critical head drop for all medium-scale sensitivity computations is shown in . Simulations with a different barrier thickness have the same distance between the upstream interface of the barrier and the inlet, so that the resistance in the background sand upstream of the barrier is comparable.

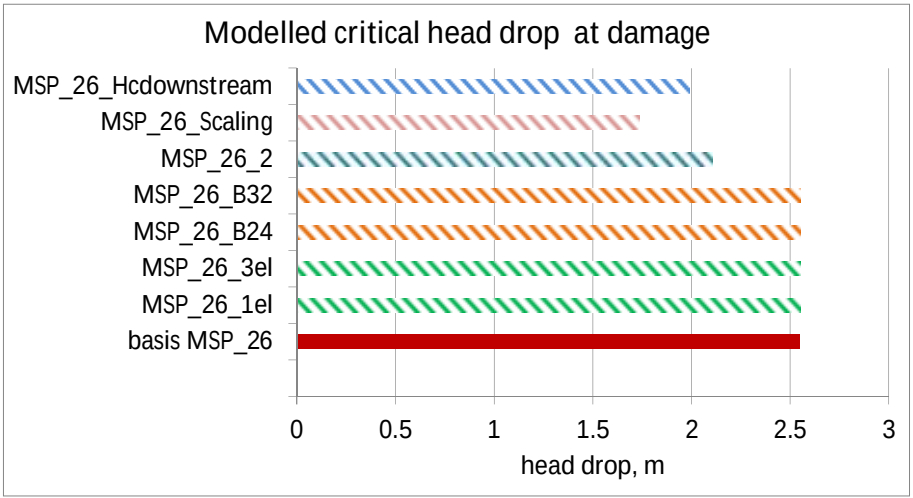


*Figure 4.4 Modelled critical head drop at damage for sensitivity analysis of MSP 26*

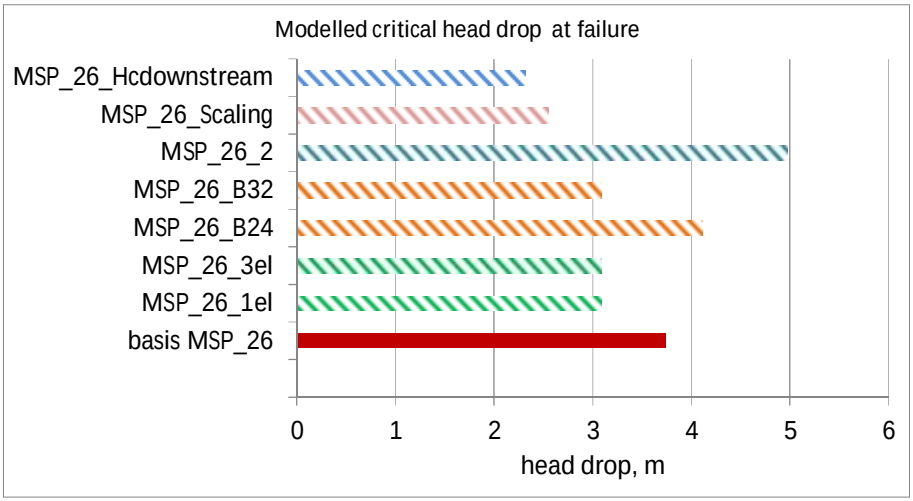


*Figure 4.5 Modelled critical head drop at failure for sensitivity analysis of MSP 26*

| Simulation | Modelled critical damage head, m | Modelled critical failure head drop, m | Ratio critical head variation/critical head basis damage | Ratio critical head variation/critical head basis failure |
|---|---|---|---|---|
| **MSP_26** | **2.55** | **3.74** | | |
| MSP_26_1el | 2.55 | 3.09 | 1.00 | 0.83 |
| MSP_26_3el | 2.55 | 3.09 | 1.00 | 0.83 |
| MSP_26_B24 | 2.55 | 4.11 | 1.00 | 1.10 |
| MSP_26_B32 | 2.55 | 3.09 | 1.00 | 0.83 |
| MSP_26_2 | 2.11 | 4.98 | 0.83 | 1.33 |
| MSP_26_Scaling | 1.74 | 2.55 | 0.68 | 0.68 |
| MSP_26_Hcdownstream | 1.99 | 2.32 | 0.78 | 0.62 |
| | | | | |
| **MSP_23** | **3.74** | **4.98** | | |
| MSP_23_B24 | 3.74 | 4.98 | 1.00 | 1.00 |
| MSP_23_B32 | 3.74 | 5.48 | 1.00 | 1.10 |
| | | | | |
| **MSP_25** | **2.55** | **2.55** | | |
| MSP_25_2 | 2.11 | 2.11 | 0.83 | 0.83 |

*Table 4.8 Overview of modelled heads in sensitivity analysis of medium scale models*

For the small scale sensitivity analysis, the critical head in the basis simulation and in the simulation with a smaller scaling factor is shown in Figure 4.6 for damage, and in Figure 4.7 for failure. A summary of the critical heads for the small-scale sensitivity analysis is given in . In the discussion, these results are compared to the experimentally measured head drops.

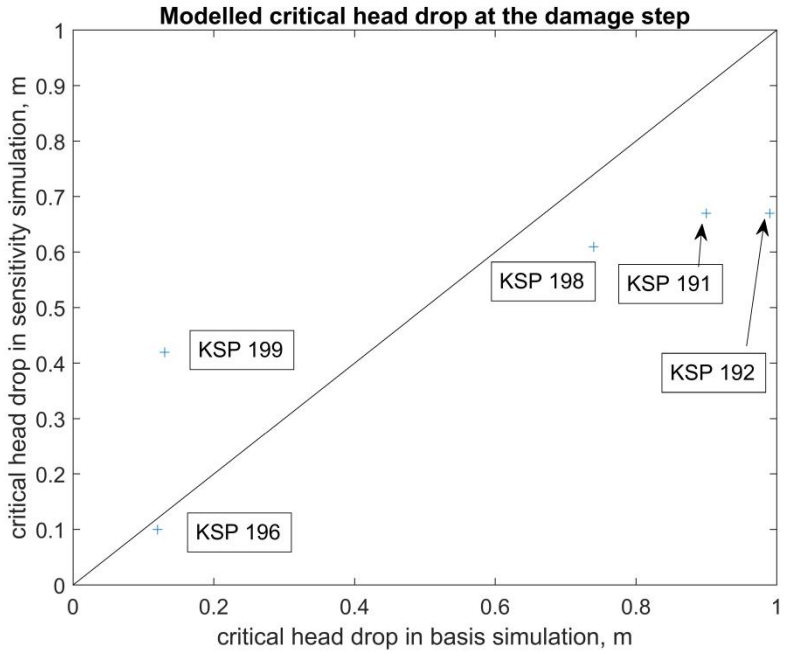


*Figure 4.6 Critical head drop at damage in the small scale simulations, sensitivity simulations have a lower factor for scaling the primary erosion criterion and therefore a lower primary erosion criterion than the basis simulations*

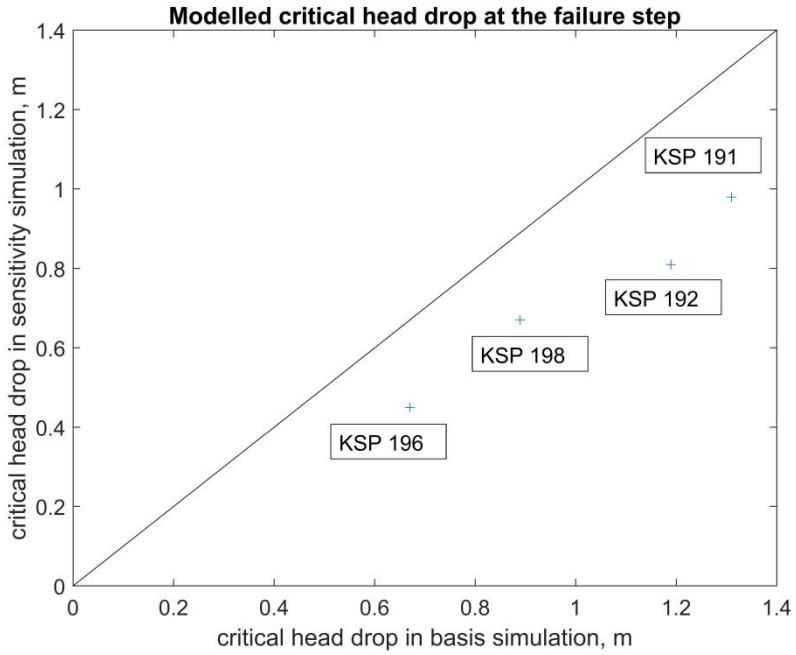


*Figure 4.7 Critical head drop at failure in the small scale simulations, sensitivity simulations have a lower factor for scaling the primary erosion criterion and therefore a lower primary erosion criterion than the basis simulations*

| Simulation | Modelled critical damage head, M | Modelled critical failure head drop, m | Ratio critical head variation/critical head basis damage | Ratio critical head variation/critical head basis failure |
|---|---|---|---|---|
| **KSP_191** | **0.90** | **1.31** | | |
| KSP_191_Scaling | 0.67 | 0.98 | 0.75 | 0.75 |
| **KSP_192** | **0.99** | **1.19** | | |
| KSP_192_Scaling | 0.67 | 0.81 | 0.68 | 0.68 |
| **KSP_196** | **0.12** | **0.67** | | |
| KSP_196_Scaling | 0.10 | 0.45 | 0.83 | 0.67 |
| **KSP_198** | **0.74** | **0.89** | | |
| KSP_198_Scaling | 0.61 | 0.67 | 0.82 | 0.75 |
| **KSP_199**[+] | **0.13** | **n.a.** | | |
| KSP_199_Scaling | 0.42 | 0.81 | 3.23 | |

*Table 4.9Overview of modelled heads in sensitivity analysis of medium scale models*

[+] During this experiment the pipe formed throughout the barrier, but the head drop could not be increased to cause failure, this was observed in the simulations where 1, 2 or 3 elements were switched on per pipe progression step.

# 5 Analysis and discussion

In the current analysis, a basis set of parameters for primary and secondary erosion was derived based on the available experimental data in (Deltares 2017b&c, and Deltares 2018a, b&c) and this was used to simulate the small-scale and medium scale coarse sand barrier experiments. Due to the relatively large number of input parameters (including hydraulic conductivity, primary erosion criterion, and secondary erosion criterion, as well as numerical iteration parameters and choices made in model discretization), and the relatively limited number of experiments, the parameters were not adapted to fit experimental results. Rather than parameter fitting, the sensitivity of the results to model decisions, mesh size, number of pipe elements increased, discretization of the barrier thickness, changing hydraulic conductivity of the background sand and scaling the primary erosion criterion were investigated in order to obtain a better understanding of the model and the results.

This Chapter presents an overview of the most important aspects of the numerical modelling. Appendix G discusses the results in more detail. First, qualitative aspects of pipe progression are discussed. The simulation results are compared to the experimental findings, in order to see which aspects of piping behavior are well modelled. Subsequently the critical head drops are analyzed and compared to experimental results. Then the effect of barrier depth is discussed explicitly as this is significant for relating results of experiments, in which the barrier typically has the full depth of the model, to field situations where this is not the case. Finally, the flow regime in the pipe is briefly discussed.

## 5.1 Progression parallel to barrier interface in background sand

All small-scale experiments, and all but one medium-scale experiments showed the pipe to progress parallel to the barrier interface in the background sand before damage. This behavior is reproduced well in all simulations except for two small-scale simulations KSP_196 and KSP_199. The causes of this are the probably the input parameters for the primary erosion criterion in KSP_196, and numerical artefacts in KSP 199. This is discussed in Appendix G1.

Overall this aspect of piping behavior is therefore considered to be represented well in the models.

## 5.2 Number of pipes inside the barrier

Considering the number of pipes that enter the barrier, there is a clear difference between GZB 1 and GZB 2 in the medium-scale experiments (). For GZB 2 only one pipe enters the barrier, whereas multiple pipes enter the barrier in tests with GZB 1 (refer to figures in Appendix A). In the small scale experiments, no significant difference was observed between tests with GZB 2 and GZB 2.

The difference between GZB 1 and GZB 2 is not observed in the simulations, the number of pipes entering the barrier in the basis simulation is shown in Figure 5.1.

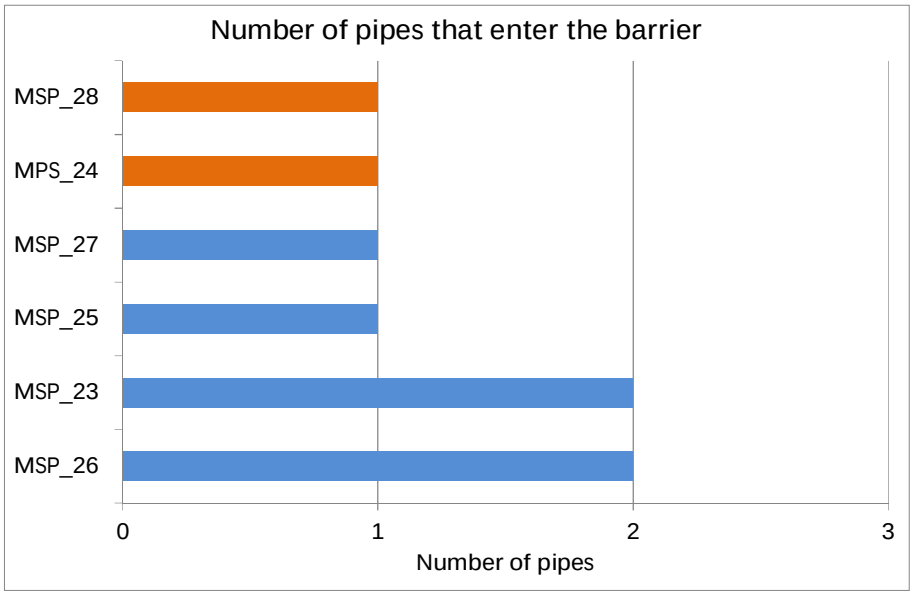


*Figure 5.1 Number of pipes that enter the barrier in the basis simulations*

The sensitivity analysis on MSP_26 (Figure 5.2) shows that the number of pipes that enter the barrier in the models is dependent on modelled barrier thickness, the number of elements that switched to pipe elements per step, the mesh size, and the height of the primary erosion criterion as discussed in Appendix G2.

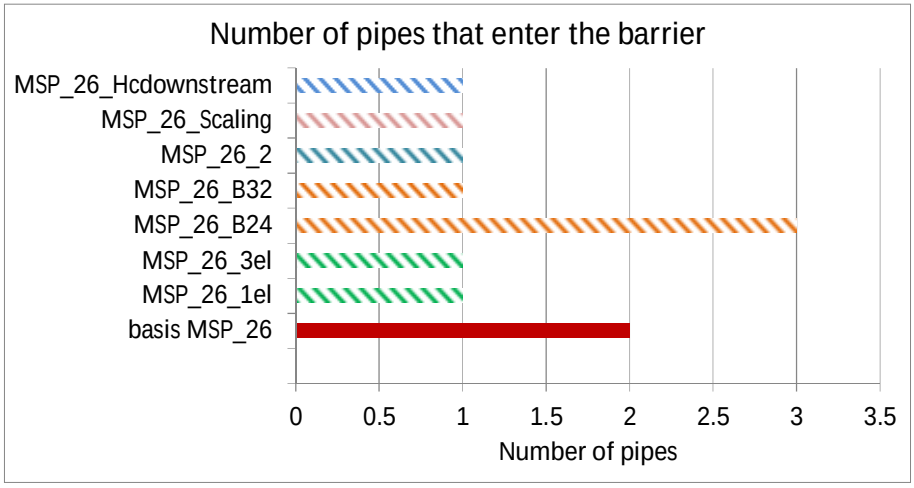


*Figure 5.2 Overview of the number of pipes that enter the barrier during the simulations in the sensitivity analysis on model MSP_26*

In the small-scale experiments multiple pipes entered the barrier in all experiments. The modelled number of pipes that entered the barrier is shown to be dependent on the height of the primary erosion criterion, as shown in Figure 5.3.

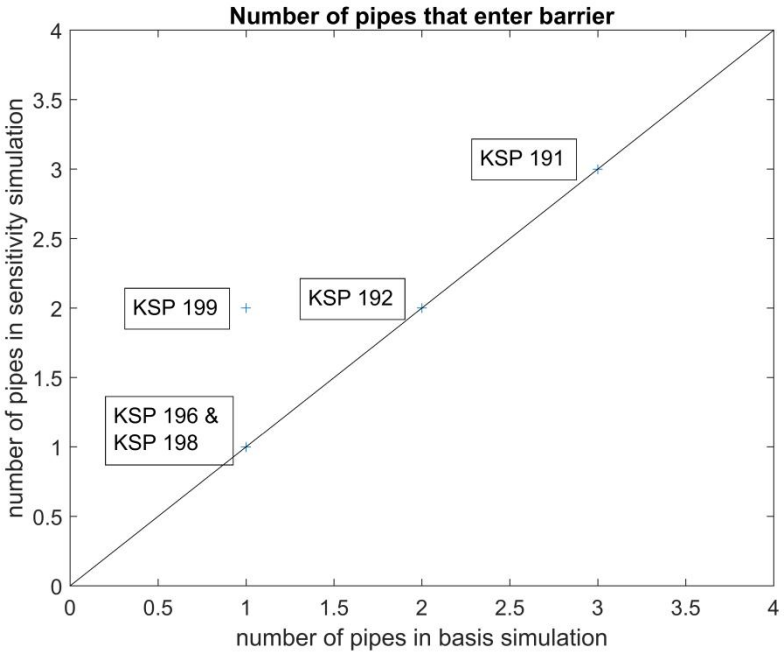


*Figure 5.3 Overview number of pipes that enter the barrier during the small-scale simulations, sensitivity simulations have a lower factor for scaling the primary erosion criterion and therefore a lower primary erosion criterion than the basis simulations*

The number of pipes is influenced by many factors and is therefore not yet well simulated.

## 5.3 Critical growth steps in medium-scale tests

In the medium-scale experiments the pipe is observed to progress through the barrier in discrete steps. Several steps that are considered to be significant have been distinguished (Deltares, 2018c):

- Damage: the point when the pipe first forms in the barrier, due to crumbling of the barrier this point was considered difficult to register and relatively uncertain. During damage one or multiple pipes formed in the barrier and progressed but typically only 2 to 4 cm. Due to the uncertainty of the pipe tip location due to crumbling no estimates of the pipe length after damage were reported.
- Short growth: where one or more pipes progress but not past half way through the barrier, sometimes forming a T-shape inside the barrier. Estimates of the pipe length after the short growth step were made in Deltares (2018c) with an uncertainty of 2 cm.
- Long growth: where one pipe progresses past half way through the barrier but not through the upstream interface. Estimates of the pipe length after the long growth step were made in Deltares (2018c).
- Failure: when a pipe progresses through the upstream interface.

In all tests except MSP 25 and MSP 28, when the head drop is further increased after the long growth step the pipe grows to a few centimeters short of the upstream interface of the barrier and then progresses parallel to the barrier interface prior to failure. Images of the estimated pipe outline are shown in Appendix A.

In the models the pipe progresses almost through the entire barrier at damage; except for two models, MSP_25 and MSP_28 where the pipe progresses directly through the entire barrier so that damage equals failure of the barrier. The comparison of the estimated length at the end of the short growth step, and at the end of the long growth step is shown in Figure 5.4 and Figure 5.5.

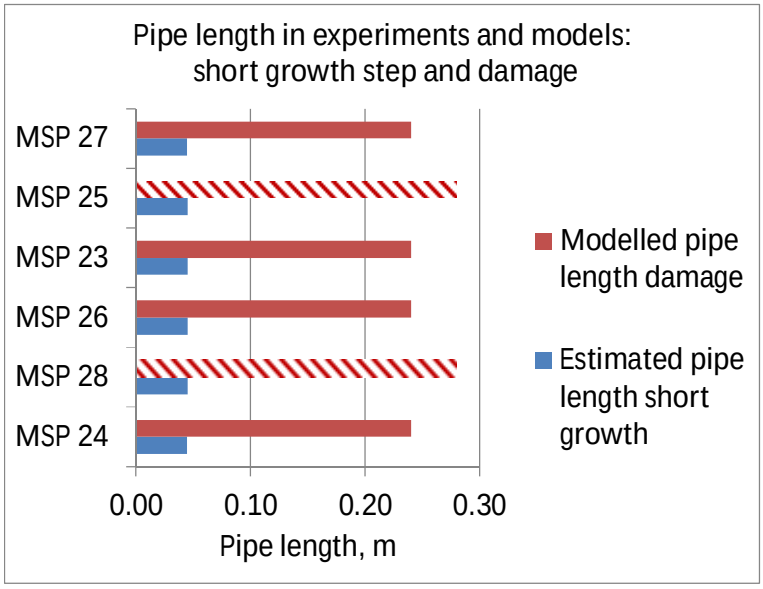


*Figure 5.4 Comparison of estimated pipe length inside the barrier after the short growth step in experiments and the modelled pipe length after damage. Pattern fill indicates that the pipe passed through the entire barrier in this step*

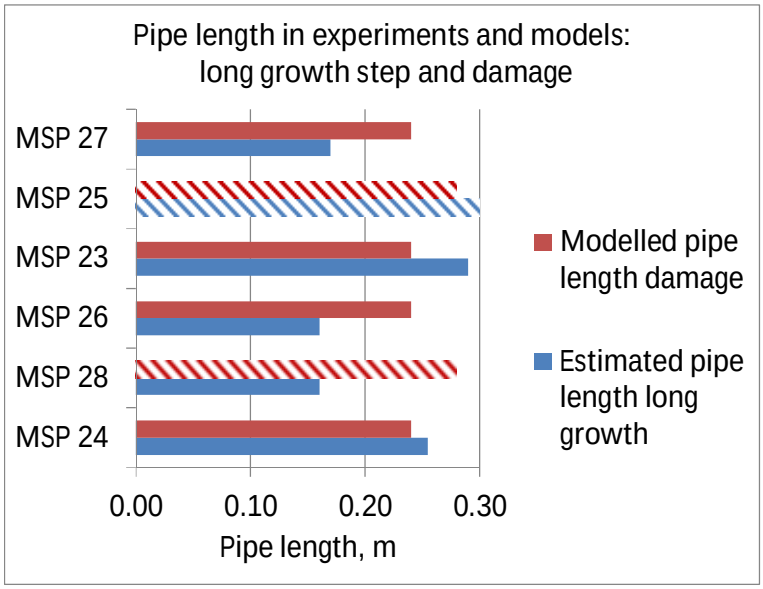


*Figure 5.5 Comparison of estimated pipe length inside the barrier after the long growth step in experiments and the modelled pipe length after damage. Pattern fill indicates that the pipe passed through the entire barrier in this step*

The length that the pipe progresses inside the barrier in the models at damage is more similar to the total that the pipe has progressed in the experiments during the long growth step. The critical gradient upstream of the pipe tip that is determined in the cylinder experiments in

(Deltares, 2018b) is also more similar to the critical gradient that is determined for the long growth step, than the gradients which are determined in the damage or short growth steps (Deltares, 2018c).
It is remarkable that the models of MSP 25 and MSP 28 show failure in the damage step. These are the two experiments where the pipe did not progress parallel to the upstream interface of the barrier inside the barrier in the experiments. In test MSP 25 no long growth step was observed, the pipe progressed to failure in the step where it past beyond half way through the barrier. This indicates that the observed damage and short growth steps in the experiments are not captured by the model, but that the model does captures the long growth step or failure. Possibly the crumbling of the barrier, which occurs due to the finite depth of the pipe in front of the barrier, plays a role in the observation of damage and short growth, which can occur at local gradients below the critical progression gradient.

Although the modelled distance of pipe progression at damage in the basis models indicates a resemblance to the long growth step observed in the experiments, the sensitivity analysis also shows that the size of this step can vary depending on the input parameters. The sensitivity analyses on MSP_26 are shown in Figure 5.6.

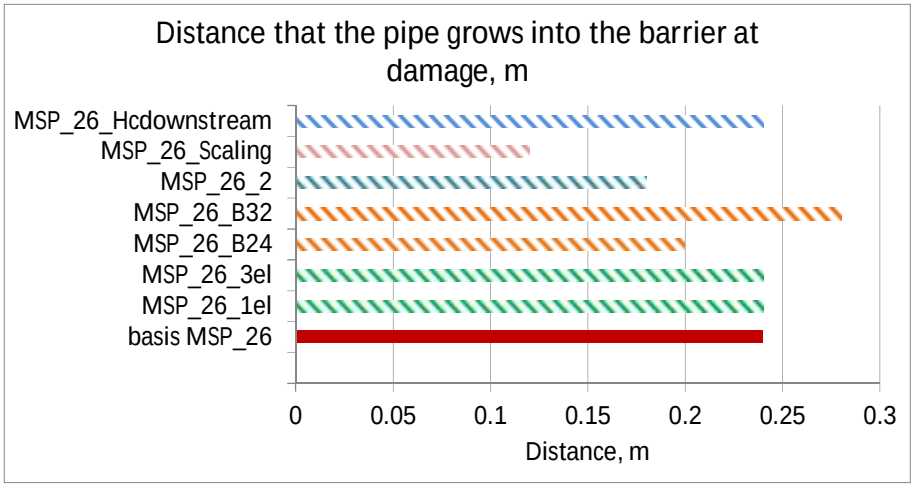


*Figure 5.6 Overview of the distance that the pipe progresses inside the barrier during the medium-scale simulations of test MSP 26*

The sensitivity analysis on the small-scale experiments in Figure 5.7 also shows that the distance of pipe progression into the barrier at the damage step is affected by the primary erosion criterion, as would be expected.

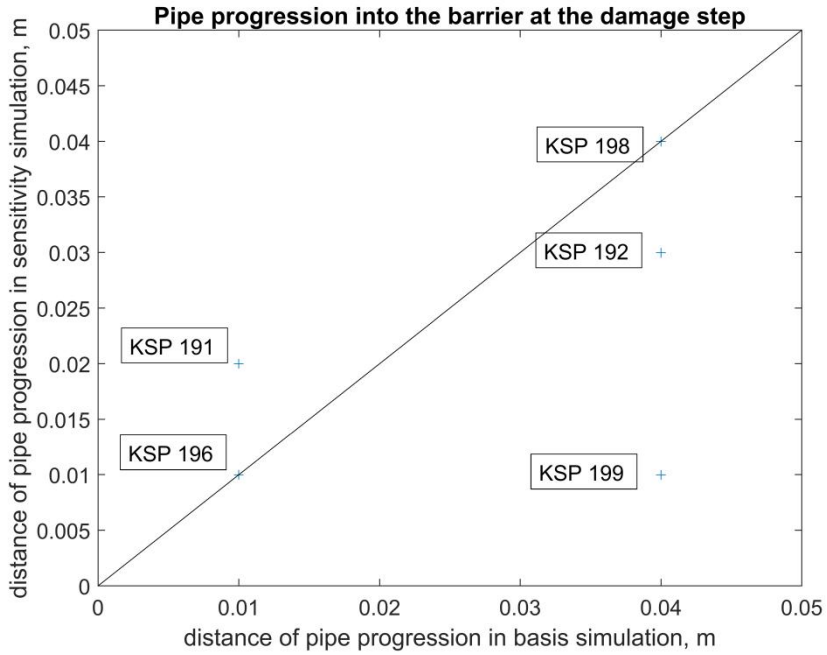


*Figure 5.7 Overview of the distance that the pipe progresses inside the barrier during the small-scale simulations, sensitivity simulations have a lower factor for scaling the primary erosion criterion and therefore a lower primary erosion criterion than the basis simulations*

## 5.4 Progression parallel to the upstream barrier interface in medium-scale tests

The pipe progresses parallel to the upstream interface of the barrier in the medium scale experiments MSP 23, MSP 24, MSP 26, and MSP 27 (). There is no progression parallel to the interface in MSP 25 and MSP 28.

In simulations of the medium-scale tests there is little to no progression parallel to the upstream interface in the basis simulations; only two elements in MSP_26 and not at all in the other models. This may be due to the mesh coarseness, with a finer mesh of 2 cm elements for test MSP_26_2 there is a significant amount of progression parallel to the upstream interface of the barrier as shown in Figure 5.8.

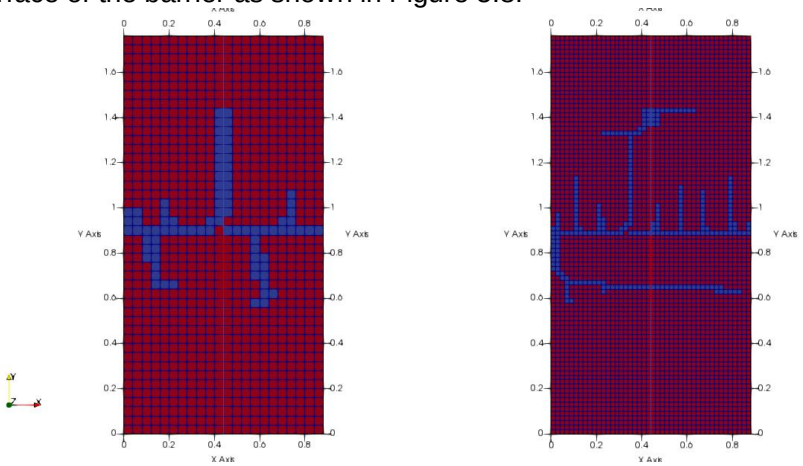

*Figure 5.8 Top view of the model, inflow is on the bottom. Left hand side, simulation MSP_26 one step after the failure state, right hand side, simulation MSP_26_2 one step after the failure state. (red is soil elements, blue is pipe elements)*

Even with a 2 cm mesh, there is no progression of the pipe parallel to the barrier for simulation MSP_25_2 (). In that simulation the pipe progresses through the upstream interface of the barrier in the damage step, in both the simulation with 4 cm elements and with 2 cm elements.

## 5.5 Progression of pipe backwards from barrier

In several simulations pipes form that progress downstream from the pipe along the barrier interface prior to damage, as shown in Appendix C. This is largely a numerical artefact due to the fact that no mechanism for pipe widening is programmed in the preliminary FEM program. It is expected that this would be much less pronounced in the model results if widening were allowed. The addition of widening is planned in future versions of the program. In some experiments, a widening of the pipe parallel to the barrier, or a shift of the pipe parallel to the barrier in the downstream direction is observed. There is no mention of individual pipes progressing downstream.

## 5.6 Critical head drop

This Section assesses the modelled critical head drop. When considering the differences between the modelled critical head drops and experiments, and the effect of the parameters in the sensitivity analysis, the size of the load increment (10% of the current head drop) must be considered. These are relatively large steps, with a smaller load increment the differences between models might be smaller.

### 5.6.1 Basis simulations

The models tend to over predict the critical head drops at damage and at failure, as shown in Figure 5.9 and Figure 5.10.

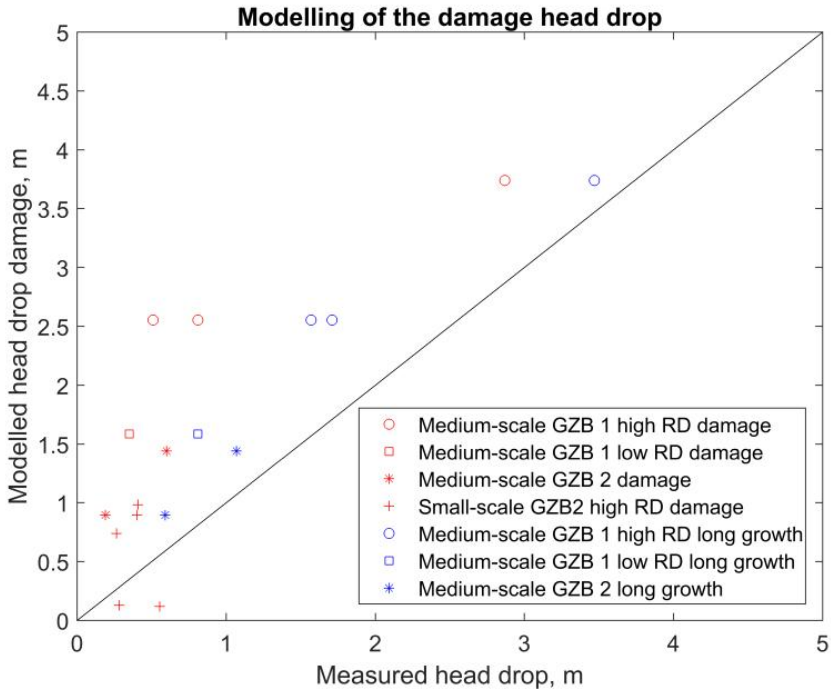


*Figure 5.9 Modelled critical head drop at damage, compared to measured head drop at damage and at long growth in the experiments. The long growth step was not explicitly recorded for the small-scale experiments*

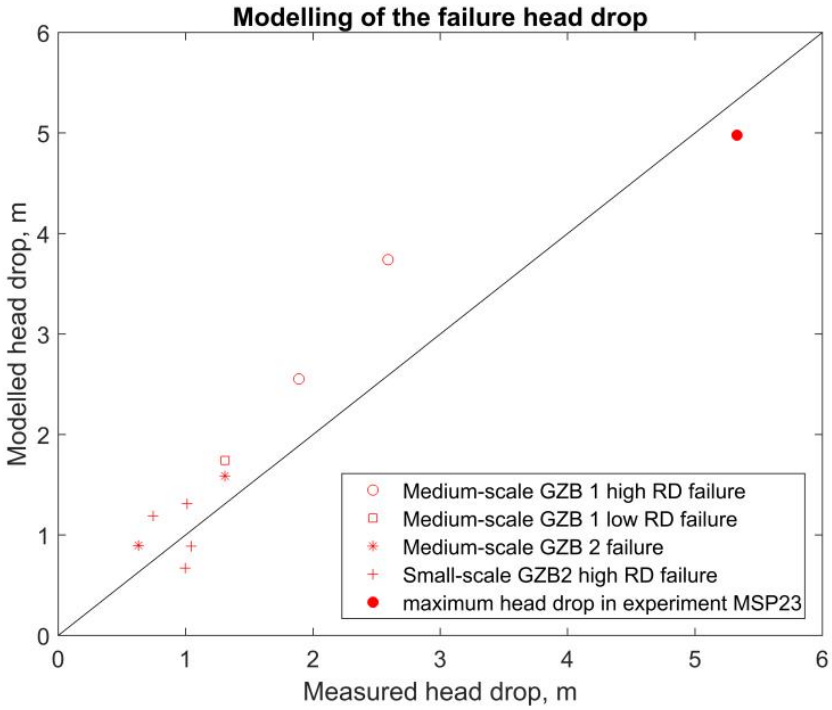


*Figure 5.10 Modelled critical head drop at failure of the barrier, compared to measured head drop at failure in the experiments*

As discussed in Section 5.3, the modelled damage step shows more resemblance to the experimentally recorded long growth step for the medium-scale experiments than to the experimentally recorded damage step. The critical head drop of the long growth step is also overpredicted, however the ratio of the modelled damage head drop to the experimental long growth head drop is more similar to the ratio of the modelled and experimental failure head drops as shown in Figure 5.11.

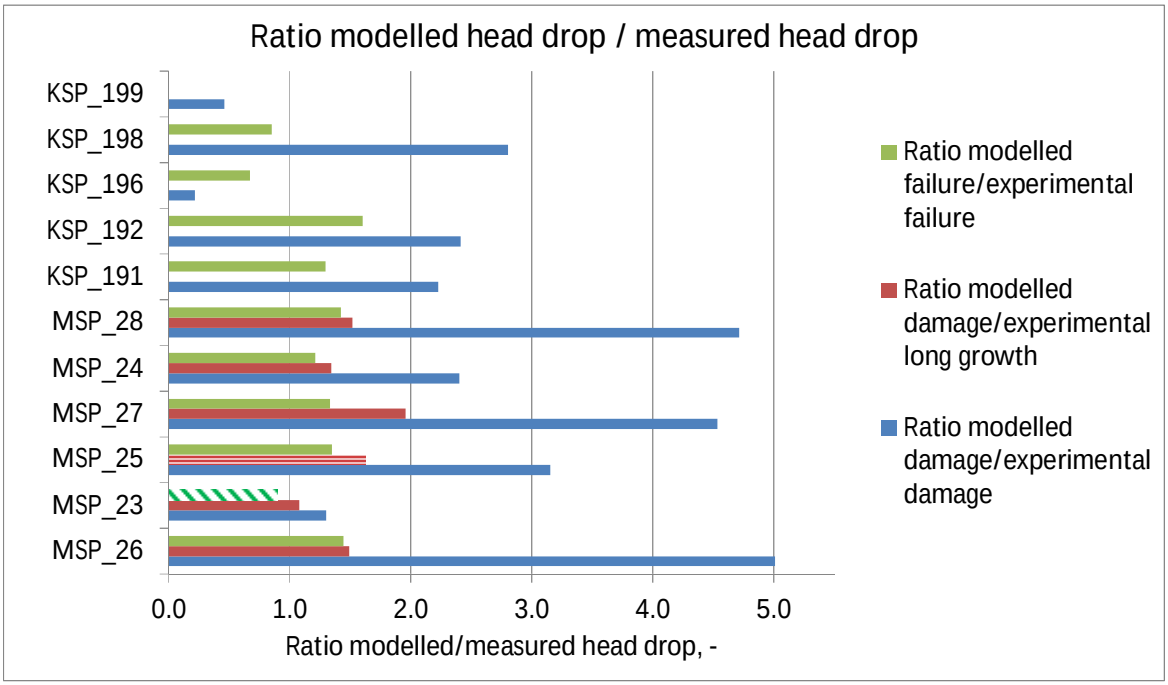


*Figure 5.11 Ratio of the modelled head drop to the measured head drop. Pattern fill for failure of MSP 23 indicates no failure took place during the experiment when the maximum head drop was applied. Pattern fill for long growth in MSP 25 indicates there was no long growth step and medium growth is used. In the small-scale experiments no long growth step was registered*

In the small-scale basis simulations, the critical head drop for damage is underpredicted in KSP_196, and in KSP_199, and overpredicted in the other experiments as shown in Figure 5.11. As discussed in Appendix G1, the input critical gradients for the barrier materials and background sand may be the cause of the mismatch with experimental results in KSP_196. In KSP_199 the simulation results appear to be affected by numerical artefacts.
The critical head drop for failure is also underpredicted in KSP_198, but only by a small amount (ratio 0.9). It is notable that the ratio of the modelled to the measured critical heads for this test (in the rotated set-up with a 0.03 m deep barrier) is smaller than for the other tests with the regular small-scale set up and with the medium-scale set-up.

### 5.6.2 Sensitivity analysis

#### *5.6.2.1 Critical gradient for primary erosion*

Various parameters will affect the simulated critical head drops. The critical gradient for primary erosion is one of them. The sensitivity analysis for MSP_26 and the small-scale models shows that reducing the primary erosion criterion to 70% of the criterion in the basis model yields critical head drops for damage and failure that are close to the experimental results as shown in  and Figure 5.12. The simulations still overpredict damage for the small-scale models, but for MSP_26_Scaling the simulated damage matches the experimental long growth well.

| Simulation | Modelled critical damage head drop, m | Measured critical damage head drop *, m | Ratio modelled/ measured damage head drop | Modelled critical failure head drop, m | Measured critical failure head drop *, m | Ratio modelled/ measured failure head drop |
|---|---|---|---|---|---|---|
| MSP_26_ Scaling | 1.74 | 1.71 | 1.0 | 2.55 | 2.59 | 0.98 |
| KSP_191_ Scaling | 0.67 | 0.40 | 1.7 | 0.98 | 1.01 | 0.97 |
| KSP_192_ Scaling | 0.67 | 0.41 | 1.6 | 0.81 | 0.74 | 1.09 |
| KSP_196_ Scaling | 0.10 | 0.55 | 0.2 | 0.45 | 1.00 | 0.45 |
| KSP_198_ Scaling | 0.61 | 0.26 | 2.3 | 0.67 | 1.05 | 0.64 |
| KSP_199_ Scaling | 0.42 | 0.28 | 1.5 | 0.81 | 0.76 | 1.06 |

*Table 5.1 Overview of modelled and measured critical heads for simulations with a lower primary erosion criterion*

* This is the head drop between the inlet of the sample, corrected for loss at the upstream filter, and the head measurements that are made inside the sample at the location in the background sand at the downstream interface of the barrier

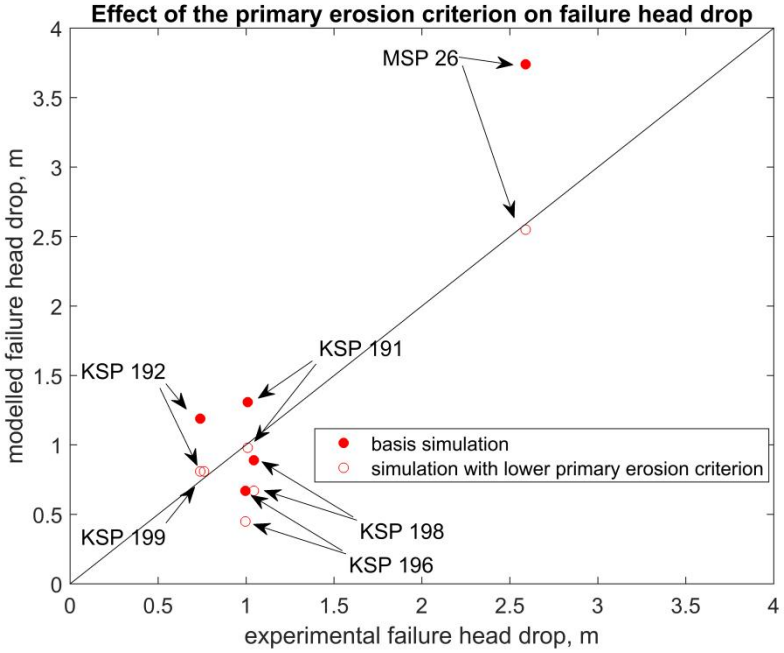


*Figure 5.12 Critical head drop for failure modelled with the basis simulation (red symbols) and with the lower primary erosion criterion (white symbol with red border) as compared to experimentally measured head drop. For basis simulation 199 no failure occurred*

Note that KSP_199 which suffered from numerical artefacts in the basis simulation does not do so in the simulation with a lower primary erosion criterion, and the ratio of the modelled and measured failure head drop is similar to that of the small scale regular models.

For KSP_196 and KSP_198, the basis simulation gave an underprediction of the measured failure head drop and this is worsened by the lower primary erosion criterion. For KSP_196, this can be due to the parameters used for the primary erosion criterion, as the barrier (GZB 3) is different than in the other small-scale models (GZB 2).
For KSP_198 the difference is not due to the parameter choice, as the same set of parameters is used in the other small-scale simulations. Further investigation would be required to determine whether this might possibly be an experimental artefact or whether it is related to the model. This is the only model in which the ratio of the barrier depth to the model depth is 1/10; this ratio is 1/3 in the other models with a shallow barrier.

There could be different reasons to reduce the primary erosion criterion that was used in the basis simulations. The primary erosion criterion that was used in the current analysis might be too high if the factor that was selected to scale the critical gradient over 10 cm to the critical gradient over the smaller element sizes was too high. This could be investigated by assessing the value of this ratio using data from the new experiments that were performed in June 2018, and possibly also by modelling the cylinder experiments in a 3D finite element model.

It is also possible that the effect of relative density is different for the barrier soils than for the 40/70 soil. Currently the correlation based on the latter soil in Robbins et al (2018) is used. Also, there is limited data of cylinder experiments on the barrier materials, and analysis of the additional experiments would indicate whether the values that are used are appropriate.

#### *5.6.2.2 Mesh size*

The mesh size also affects the critical head drop as shown for MSP 25 and for MSP 26 in Figure 5.13. Both models have a lower critical head drop for damage with a finer mesh. Probably the more refined mesh results in a higher computed gradient at the pipe tip at damage, and therefore a lower critical head drop. For MSP 25, damage equals failure. However, for MSP 26 the head drop for failure is higher with the 2 cm mesh. This is probably due to the extensive development of the pipe parallel to the upstream barrier interface which is modelled with the finer mesh.
The effect of the mesh on the critical head drop suggests that it is desirable to determine the primary erosion criteria based on cylinder experiments, rather than fitting this to the models. Any fit to the models would be mesh dependent and could therefore not confidently be extrapolated to other geometries.

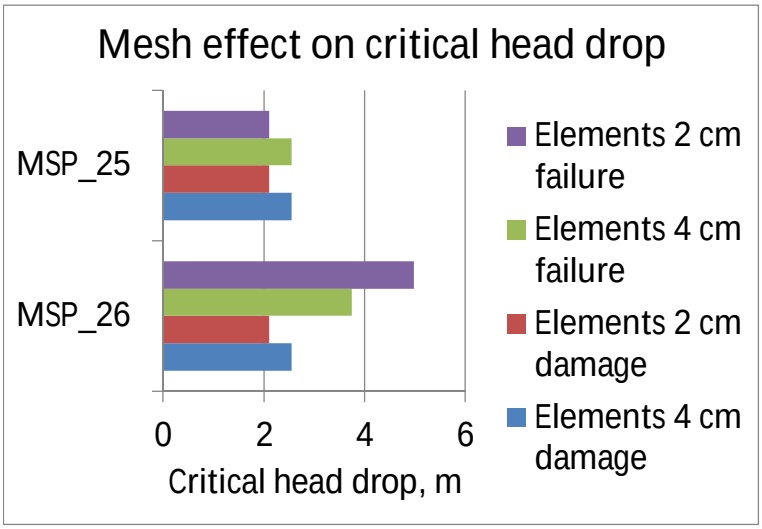


*Figure 5.13 Critical head drops for damage and for failure with different mesh sizes for models MSP_26 and MSP_25*

#### 5.6.2.3 *Modelled barrier thickness*

The modelled barrier thickness also affects the critical head drop. It would be expected that a thicker barrier results in a higher critical head drop for failure, as the pipe has to progress through a longer distance inside the barrier. However, this is not clearly demonstrated by the sensitivity analysis in Figure 5.14. The lower critical head drop at failure for simulation MSP_26_B32 is remarkable and it is not clear why this is the case. For MSP_23, the computed critical head drop for failure is higher for the barrier that is 0.32 m thick.

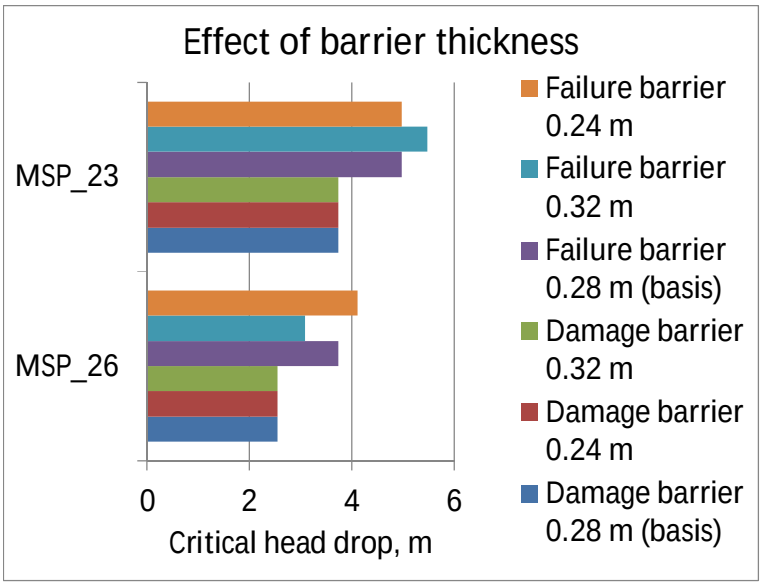


*Figure 5.14 Modelled effect of barrier thickness in simulations MSP_26 and MSP_23*

#### 5.6.2.4 *Number of elements switched on*

The number of elements that is switched per pipe iteration also affects the computed critical head drop at failure. In the basis simulations, 2 elements can be switched per iteration. For MSP_26, the effect of switching 1 or 3 is simulated. Both give a critical head drop for damage

that is the same as in the basis model, but the critical head drop for failure is lower than in the basis model. The pipe pattern after failure is shown in Figure 5.16.

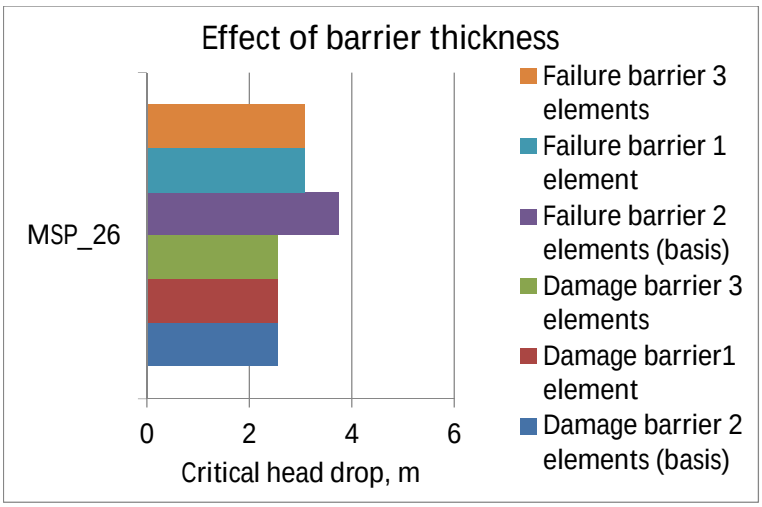


*Figure 5.15 Modelled effect of number of elements switched on per pipe iteration in simulations MSP_26*

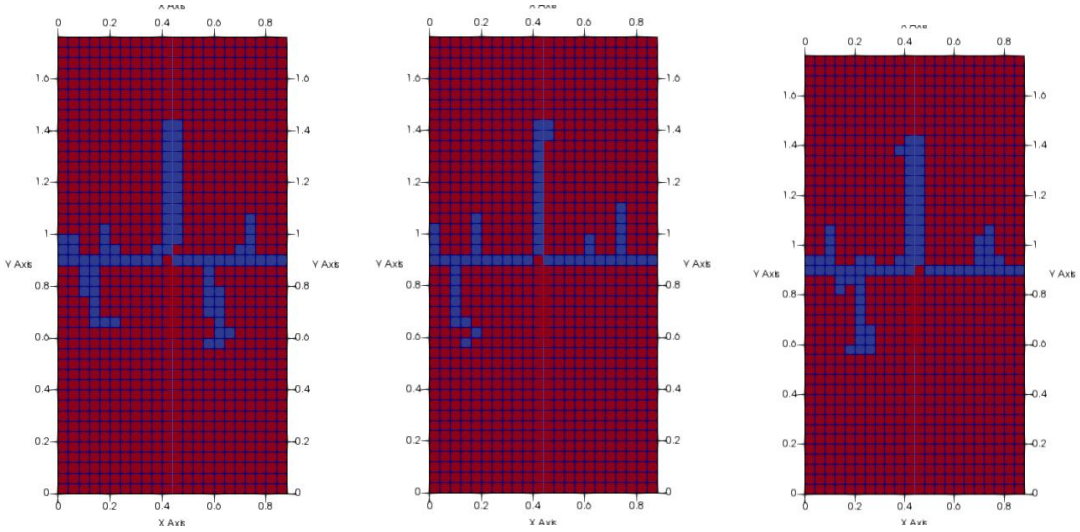

*Figure 5.16 Pipe pattern at failure in simulations with 2 elements switched (left),3 elements switched on (middle) and 1 elements switched on (right)*

## 5.7 Effect of barrier depth

In the medium-scale experiments there was only one experiment where the barrier did not have the full depth of the model, MSP 25 (GZB 1 and Baskarp B25). In this experiment, the pipe did not show a long growth step or progression parallel to the upstream interface of the barrier. When the pipe passed half way through the barrier it continued to failure without further raising the head drop. This is significantly different from the other MSP experiments with GZB 1. The simulation captures this difference, the pipe progresses entirely through the barrier at the damage step. As discussed earlier in this Chapter, the damage step in the models appears to relate well to the long growth step that was observed in the medium-scale experiments.

The critical head drop at damage is similar in the tests with a deep and shallow barrier, but the deep barrier has a higher critical head drop for failure. This is probably due to the higher pore pressures upstream of the barrier in models with a shallow barrier (Deltares, 2018c).

In the small-scale experiments, progression of the pipe through the barrier was not specifically monitored. Based on the observations, piping behavior seems similar for test KSP 192 and MSP 25. These are both experiments with the regular box and the shallow barrier which is 1/3 of the depth of the model. In both tests it appears that there were no pipes that had progressed further than half way through the barrier (long-growth) prior to failure. In the small-scale experiments with a full depth barrier it appears that there were pipes that progressed passed half way through the barrier prior to failure. However, whereas in the MSP_25 simulation, the pipe causes failure after the damage step, in the KSP_192 simulation that is not the case. The cause of this difference is unclear but may be related to the very limited thickness of the barrier in the small-scale experiments.

## 5.8 Flux

For the small-scale tests, the modelled flux matches the measured flux well in the 'normal' set-up but is significantly underestimated in the models of the 'rotated' set up as shown in Figure 5.17 (KSP198 and 199).

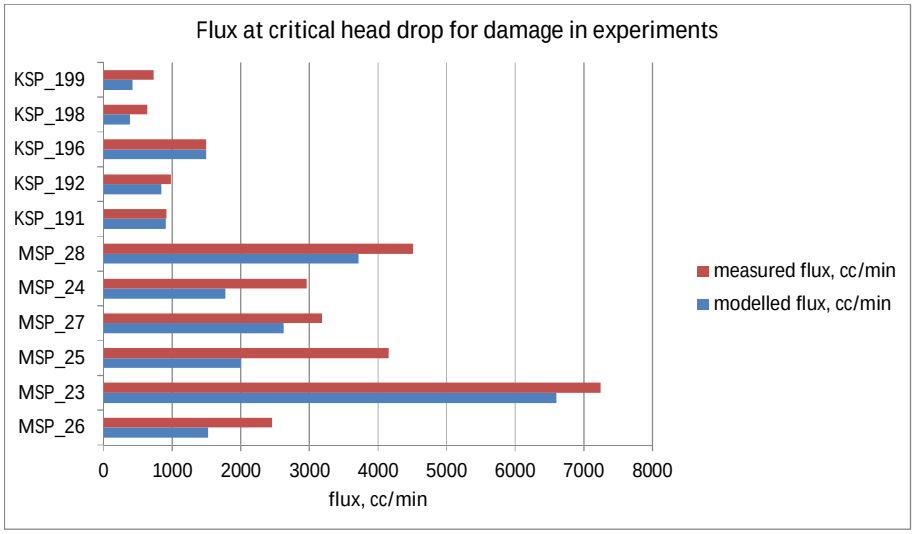


*Figure 5.17 Flux at measured critical head drop for damage, modelled and measured results*

A similar deviation was encountered in modelling the small-scale tests in 2D numerical models in Deltares (2017c). In those models, the hydraulic conductivity was fit to the measured head profile and flux. This fit also required a higher hydraulic conductivity of the background sand upstream of the barrier, than would be expected based on the reported $RD_n$. This possibly could be due to an underestimation of the relative density of the sample during preparation, however, the reason that this appeared for the 'rotated' models was not clear in Deltares (2017c). In the current models the hydraulic conductivity of the background sand is based on the relative density of the fine sand upstream of the barrier. This hydraulic conductivity is lower than the hydraulic conductivity downstream of the barrier in the experiments, which would also contribute to an underestimation of the flux in the models. This effect would be strongest in the rotated models as there would be more flow below the barrier to the background sand.

For the medium-scale tests, the modelled flux tends to overestimate the measured flux more significantly in some tests than in others. Again, the deviation in the current models is similar to what was observed in the 2D models in Deltares (2018c). The ratio of the measured flux over the modelled flux in the current model is 0.8 - 0.9, for MSP 23, MSP27 and MSP 28. For MSP 26, MSP 25 and MSP 24 the ratios are 0.5 - 0.6. The tests with a worse ratio are the three tests with high relative density Baskarp 25 as background sand. This suggests that possibly the correlation that was derived for the hydraulic conductivity of this sand is the cause of the deviation. However, there is no indication of a deviation in the results of the tests used to derive this correlation.

### 5.8.1 Analysis with modified hydraulic conductivity of the background sand

As the hydraulic conductivity contrast will have a strong effect on the modelled critical head drop, the medium scale simulations were repeated using a modified hydraulic conductivity of the background sand. The ratio of the modelled flux to the measured flux in the basis was used to scale the input hydraulic conductivity. This resulted in a relatively good match of the flux as shown in Figure 5.16. The head profile computed in the model using the hydraulic conductivity from the basis simulation, and the head profile computed in the model with a modified hydraulic conductivity are shown in Figure 5.16. The measured head profile is also shown. Due to the small difference between the two models, this does not provide a good indication of which model best matches the head measurements. However, based on the better approximation of the flux the models with the modified hydraulic conductivity can be considered better.

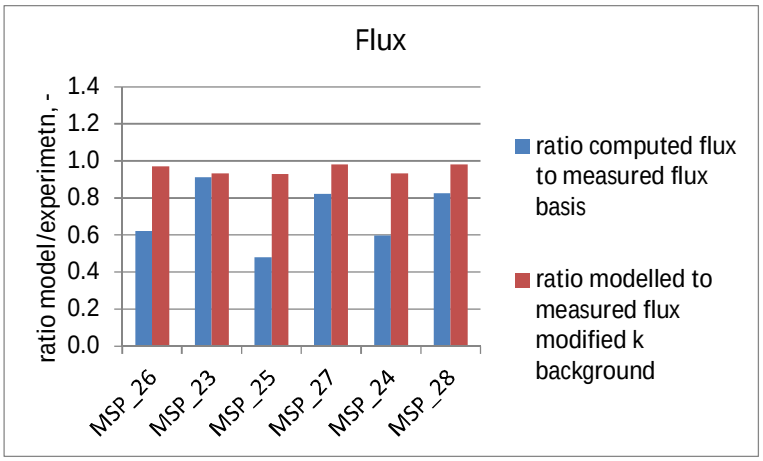


*Figure 5.18 Ratio of the modelled flux to the measured flux*

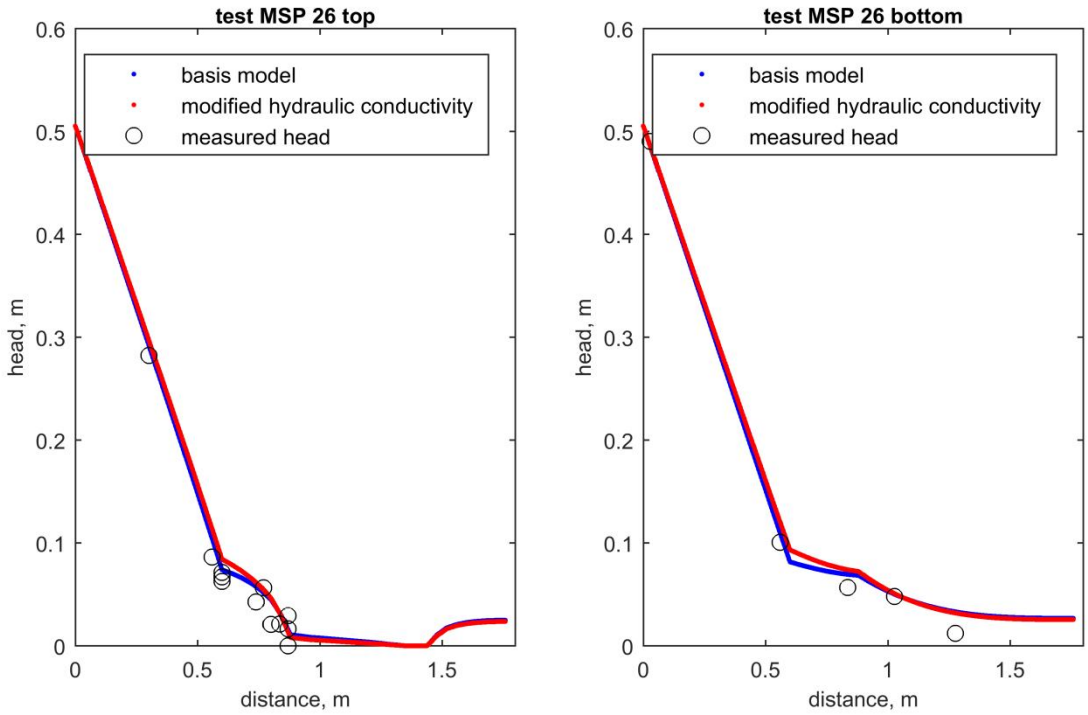


*Figure 5.19 Head profile modelled for experiment MSP 26 (red and blue lines) and head measurements during this test at the critical head drop for damage in the experiment*

The computed critical head drop (using the basis models and using the models with the modified hydraulic conductivity) and the measured head drop for damage and failure are shown in Figure 5.19 and Figure 5.20. Figure 5.19 compares the experimental long growth to modelled damage, Figure 5.20 shows modelled and measured results for failure.
As noted in Section 5.6, differences between models might be smaller when a smaller increment in the head drop is used.

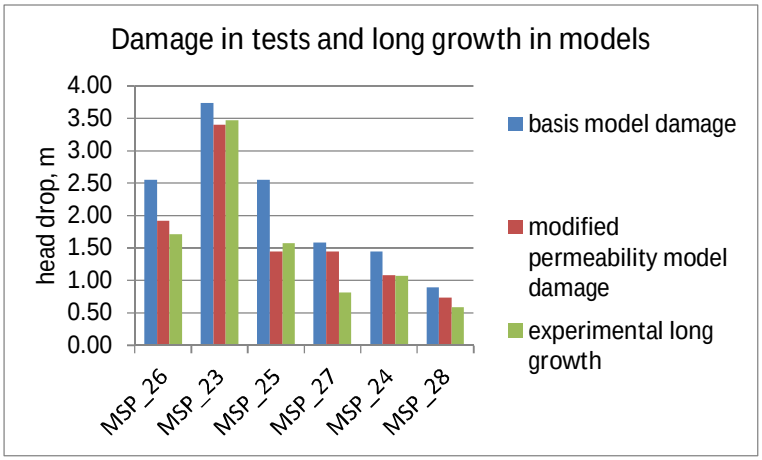


*Figure 5.20 Critical head drop at damage in medium-scale models and at long growth in experiments*

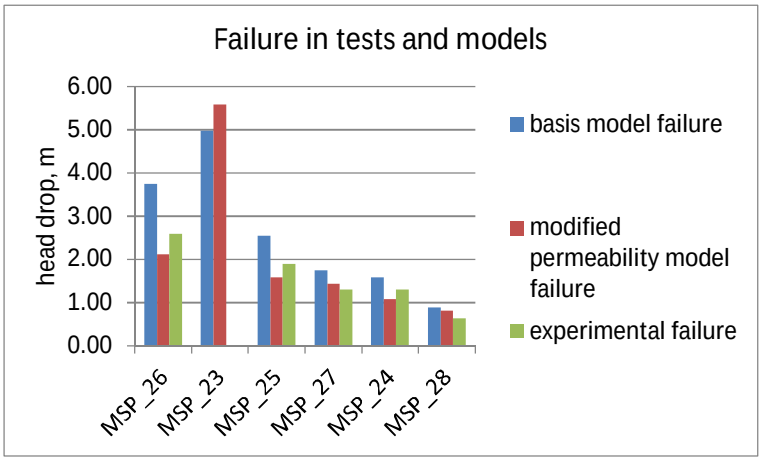


*Figure 5.21 Critical head drop at failure in medium-scale models and experiments (in test MSP 23 there was no failure at the maximum applied head drop of 5.3 m)*

The models with a modified hydraulic conductivity predict lower head drops for damage for all simulations, as would be expected with a lower hydraulic conductivity downstream. This is also the case for all failure head drops except for test MSP 23. In that model the critical head drop for failure is higher than in the basis simulation. However, the difference is only one load step, and the difference between the hydraulic conductivity in the two models is relatively small, the modified hydraulic conductivity in the conductivity is 1.1 times the hydraulic conductivity in the basis model.

Overall the modified hydraulic conductivity models provide a better estimate of the experimental critical head drops. However, whereas the basis models showed that failure occurred in the damage step for tests MSP 25 and MSP 28, which appeared to match the observed piping behavior in those experiments, this is not the case for the models with modified hydraulic conductivity. The modified models show failure in the damage step for MSP 24 and MSP 27, where there was a clear difference between long growth and failure in the experiments. Therefore, it appears that this qualitative aspect of the piping process is not reproduced as well with the modified hydraulic conductivity.

## 5.9 Flow regime in the pipe

The critical shear stress in the pipe is known to be a function of the flow regime. The current values are based on data from experiments with laminar flow (van Beek (2018)). Estimates of the flow regime in the pipe downstream of the barrier in small-scale experiments (Deltares, 2017b) suggest flow may be non-laminar for a large part of the experiment.

The effect of non-laminar flow in the pipe is not included in the current model. The question is also whether this would be significant. Non-laminar flow may lead to a lower critical shear stress, and a deeper pipe, however, as shown in Section 4.1.2, the modelled head drop in the pipe is relatively small.

In actual experiments the depth of the pipe causes the interface between the barrier and the pipe to crumble and establish a stable slope (Deltares, 2017c). A greater pipe depth would then be expected to cause more crumbling. Possibly this contributes to damage to the barrier being observed at lower head drops in the experiments than in the models.

## 5.10 Summary

This analysis shows that the model reproduces qualitative aspects of pipe progression and approximates the critical head drop in the presence of a coarse sand barrier for experiments at the small and the medium-scale. Figure 5.21 shows the modelled critical head drop for failure for the small-scale models, and the medium-scale models with the best estimates for hydraulic conductivity.

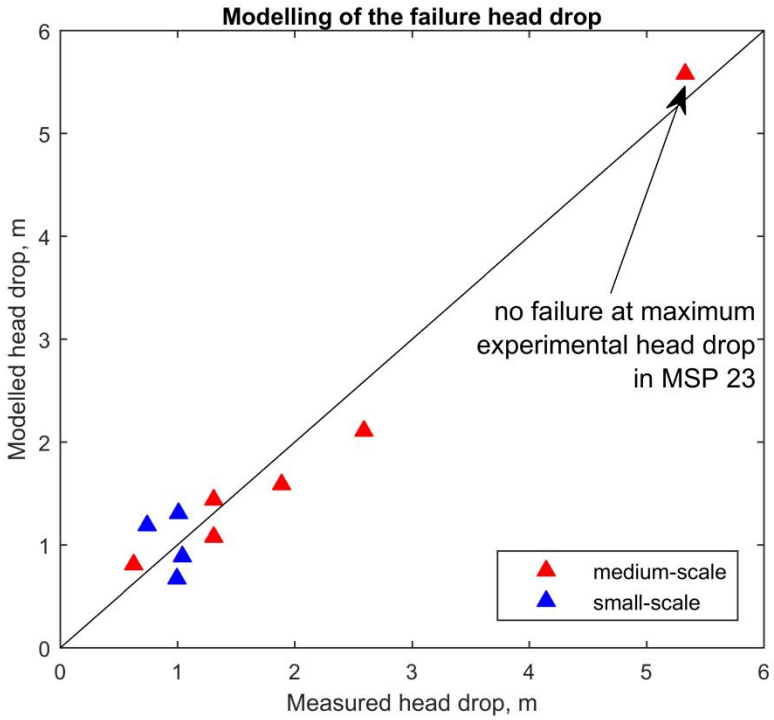


*Figure 5.22 Critical head drop at failure in medium-scale models and experiments (in test MSP 23 there was no failure at the maximum applied head drop of 5.3 m)*

The modelled critical head drop is sensitive to the hydraulic conductivity contrast and the primary erosion criterion. Applying a factor to the primary erosion criterion shifts the critical head drop by the same factor. This implies that for design, it would be possible to apply a safety factor to the primary erosion criterion in order to make a conservative prediction.

# 6 Conclusions and Outlook

## 6.1 Conclusions

The preliminary model is considered promising to model the piping behavior in the presence of a coarse sand barrier.

Quantitatively, the modelled critical head drops compare well to the experimental critical head drops for failure for both small- and medium-scale experiments. Modelling at the larger scale, such as the Delta Flume experiments, should indicate whether this is also the case at an even larger scale. If this is the case that implies that this model captures enough of the piping process to be used as a design tool.

Qualitatively, the model captures aspects of piping that were also observed in the tests, it:

- Shows pipe progression in the background sand parallel to the barrier interface when the pipe reaches the barrier, as is also observed in experiments.
- Shows that after the pipe damages the barrier, additional head increases may be required for failure, as is also the case in experiments.
    - The head drop at which the pipe damages the barrier is overestimated in the models. The distance of pipe progression into the barrier at damage is as well. It appears that the modelled damage step bears a closer resemblance to an observed ‘long growth’ step in experiments where the pipe progresses further through the barrier. This difference may indicate that the damage step observed in the experiments is affected by aspects, such as crumbling of the barrier into the pipe that are not captured in the model. As the establishment of the damage step is difficult in experiments, it is not considered a problem that this step is not modelled well. The long growth step is also used as an indicator for barrier strength in Deltares (2018c) therefore it is desirable that this step is modelled well, which appears to be the case.
- May be able to model pipe progression parallel to the upstream barrier interface with a higher degree of mesh refinement.
    - This progression is observed in several medium-scale experiments. The current model with 4 cm elements only shows a minor progression of the pipe parallel to the interface for one experiment, and not for the other tests where this progression was observed. Increasing the mesh refinement to 2 cm elements shows more extensive progression parallel to the interface for that model.

Model results are affected to some extent by mesh size and load step increment, which can be refined at higher computational cost. The hydraulic conductivity of the background sand is also an important parameter affecting the modelled critical head drop. A conservative estimate may need to be made for this for field situations, where hydraulic conductivity can be uncertain.

The modelled critical head drop at both scales is reduced by lowering the primary erosion criterion. This implies that a safety factor could be applied to this parameter for design computation.

## 6.2 Outlook

The current study has indicated several points that can be addressed in a follow up numerical investigation. These were not further analyzed in the current numerical investigation, as both additional experimental data and possibly model modification will significantly improve the effectiveness of this analysis.
The current investigation indicates that the primary erosion criterion that is used significantly affects critical head drops. Mismatches between current models and experiments could be due to several aspects, such as uncertainty regarding the primary erosion criterion, which is based on a small number of experiments, uncertainty regarding the effect of relative density on the criterion, and uncertainty regarding the conversion of the criterion over different distances. Besides uncertainty regarding the primary erosion criterion, differences between simulations and experimental results are shown to be sensitive to the hydraulic conductivity of the background sand in the models. Results can also be affected by: the modelling of the background sand with the same properties upstream and downstream of the barrier, and the mesh size which is used.

On the experimental side, it is therefore recommended to analyze the second round of experiments in the cylinder set-up that was performed at the USACE-ERDC facility in June 2018. This provides better insight into the appropriate values of the primary erosion criterion and the effect of relative density on the primary erosion criterion of the coarse sand barrier soils.
Additional experiments in the medium-scale set-up would also provide more insight into the experimentally observed piping behavior to which the models are being compared. The effect of barrier depth on the progression of the pipe is only investigated in one regular small-scale and in one medium-scale model, and in two ‘rotated’ small scale models. Barrier depth appears to have an important effect on the amount of residual strength after the pipe damages the barrier. Additional medium-scale experiments with a shallow barrier (possibly varying the barrier depth) could be used to gain confidence in the experimental results. Similarly, the lack of the pipe progressing parallel to the barrier interface in the fine sand could be investigated in an additional experiment with Metselzand.
In addition to analyzing the measured head profiles in the cylinder tests, it could possibly be beneficial to model these experiments in a (different) 3D finite element model of a cylinder. This would yield the gradients over different distances that can be compared to the experimental gradients over those distances in order to better determine the appropriate value to use to scale the critical gradient over 10 cm to the critical gradient over the element size.

On the modelling side an improvement of computational efficiency would also facilitate a mesh refinement analysis. In the current analysis the load step is incremented by 10% of the current head drop, a reduction of the step size might reduce the difference between simulations and the experiments, and the sensitivity of the modelled critical head drop to other model parameters. Although implementation of adaptive meshing could also be desirable, and contribute to improvement of computational efficiency, this is not considered as a pre-requisite for an additional numerical investigation of small- and medium-scale models. If adaptive meshing were to be implemented, this would also affect the implementation of the distance over which the primary erosion criterion is assessed. It might be desirable to evaluate this over a fixed distance, rather than over the element size, this would also make the scaling from 10 cm to the element size unnecessary.

The follow up numerical investigation could then assess the following questions:

- Which mesh size best reproduces the experimental results given the newly determined parameter set?
  This would regard both qualitative aspects, such as pipe progression parallel to the upstream barrier interface, and quantitative aspects, such as how well is the critical head drop at damage and failure are modelled?
- Why does the pipe progress diagonally from the outlet hole to the barrier in some models?
- How sensitive are results to the hydraulic conductivity that is used in the models?
  Hydraulic conductivity is already a source of uncertainty in laboratory tests, but especially in the Delta Flume and in the field, therefore the effect of a wider range of hydraulic conductivities on a field scale model would be of interest.
- What is the net effect of the relative density of the barrier on the critical head?
  A lower RD would reduce the strength criterion of the barrier, but also increase the hydraulic conductivity contrast which to some extent offsets this effect.
  The RD in the experiments is high but in the Delta Flume or in the field a lower RD may be present.
- What is the effect of barrier depth on the progression of the pipe through the barrier?
  Current medium-scale experiments indicate that with a shallow barrier the pipe progresses through the long growth step immediately to failure, whereas in experiments with a barrier that has the full depth of the model, the pipe halts at the upstream interface of the barrier. In the field the barrier will always only have a limited depth compared to the depth of the sand body, therefore it is important to understand the effect of barrier depth.
- How does the head profile in the 3D models at the critical progression steps (long growth and failure) compare to the 2D head profile modelled in Deltares (2018)?
  Practically speaking it is desirable to be able to model the critical steps in 2D especially for large scale models such as the Delta Flume or field situations.

# 7 References

Briaud, J., Govindasamy, I., Shafii, I. (2017). Erosion Charts for Selected Geomaterials. Journal of Geotechnical and Geoenvironmental Engineering. 143(10). 04017072

Brownlie (1981) “Prediction of flow depth and sediment discharge in open channels.” Report No. KH-R-43A, Keck Laboratory of Hydraulics and Water Resources, California Institute of Technology, Pasadena, California

Cao, Z., Pender, G. Meng, J. (2006) Explicit Formulation of the Shields Diagram for Incipient Motion of Sediment. Journal of Hydraulic Engineering. 132(10). pp1097-1099.

Deltares, (2017a). Feasibility study on the effectiveness of a coarse sand barrier as a piping measure. Report 1220240-004-GEO-0003.

Deltares, (2017b). Factual Report Small-scale experiments coarse sand barrier. Deltares report 11200952-004-GEO-0003.

Deltares, (2017c). Analysis report coarse sand barrier. Analysis of small-scale configuration (phase 2a). Deltares Report 11200952-006-GEO-0006.

Deltares, (2018a), Factual Report Medium-Scale Experiments Coarse Sand Barrier. Deltares 11200952-007-GEO-0004.

Deltares, (2018b) Primary Erosion Tests for the Coarse Sand Barrier. Deltares Report 11200952-035-GEO-0001.

Deltares, (2018c), Analysis Report Medium-Scale Experiments Coarse Sand Barrier. Deltares report 11200952-007-GEO-0005.

Robbins, B.A., & Griffiths, D.V. (2018a). A simplified finite element implementation of the Sellmeijer model for backward erosion piping. In Proceedings of the 9th European Conference on Numerical Methods in Geotechnical Engineering. Puerto, Portugal, June 25-27, 2018.

Robbins B.A. & Griffiths, D.V. (2018b) Modelling of backward erosion piping in two and three dimensional domains. In Internal Erosion in Earthdams, Dikes and Levees - Proceedings of EWG-IE 26th Annual Meeting 2018. Ed. Bonelli, S., Jommi, C., Sterpi, D. Politecnico di Milano 10-13 Sept. 2018.

Robbins, B.A., Van Beek, V.M., Lopez, J.F., Montalvo Bartolomei, A.M., Murphy, J., (2018). A novel laboratory test for backward erosion piping. International Journal of Physical Modelling in Geotechnics. Published ahead of print.

Sellmeijer, J.B. (1988). On the Mechanism of Piping Under Impervious Structures. Dissertation. Delft University of Technology.

Sellmeijer, J.B., Lopez de la Cruz, J., van Beek, V.M., Knoeff, H. (2011). Fine-tuning of the backward erosion piping model through small-scale, medium-scale and IJkdijk experiments. European Journal of Environmental and Civil Engineering 15(8): 1139-1154

Smith, I. M. & D. V. Griffiths (2004). Programming the finite element method (4th ed.). Hoboken, NJ, USA: John Wiley & Sons, Inc.

Van Beek, V.M. (2015). Backward Erosion Piping Initiation and Progression. Dissertation. Delft University of Technology.

Van Beek, V.M., Robbins, B.R., Hoffmans, G. J. C. M., Bezuijen, A., van Rijn, L., (2018). Use of incipient motion data for backward erosion piping models. International Journal of Sediment Research. To be published.

Van Esch, J.M., Sellmeijer, J.B., Stolle, D. (2013). Modeling Transient Groundwater Flow and Piping under Dikes and Dams. In 3rd International Symposium on Computational Geomechanics (ComGeo III), 9.

# A Progression of the pipe in medium-scale experiments

The figures in this Appendix show the extent of the pipe after a step in which there was significant progression of the pipe. The critical gradients are the gradients just prior to this step. In the current report, only critical gradients for the long growth step are used for analysis. These results are discussed in detail in Deltares (2018c).

Abbreviations in figures refer to steps in which there was significant progression of the pipe. These steps are listed below:

- *D = Damage*: a pipe shape is observed to enter the barrier; this step is difficult to register and therefore to some extent subjective.
- SG = Short growth: is the point where one or more of the pipes on the downstream end of the barrier progress by several cm but not beyond halfway through the barrier. In some experiments the point that the pipe formed a T-shape, i.e. split into two branches inside the barrier, was considered short growth (test MSP 24, MSP 28 and MSP 27). The determination of short growth is subjective as there is often some progression of the pipes after damage that could be considered more or less significant.
- MG Medium growth: in some experiments after the short growth there is another significant growth step, which still does not cause the pipe to lengthen past halfway through the barrier, this step was observed in experiments MSP 25 and MSP 22, as with short growth this is quite subjective.
- Long growth: the first progression step whereby one of the pipes progresses beyond halfway through the barrier. Typically, the pipe lengthens between ca. 9 to 24 cm during this step. Due to the longer distance over which the pipe progresses, this step is relatively easy to distinguish. An exception is experiment MSP 27 where the pipe progresses only a short distance at long growth, passing just 1 cm beyond half way through the model. Subsequently there is another long growth step where the pipe does proceed a larger distance upstream.

## A.1 Coarse sand barrier GZB 1

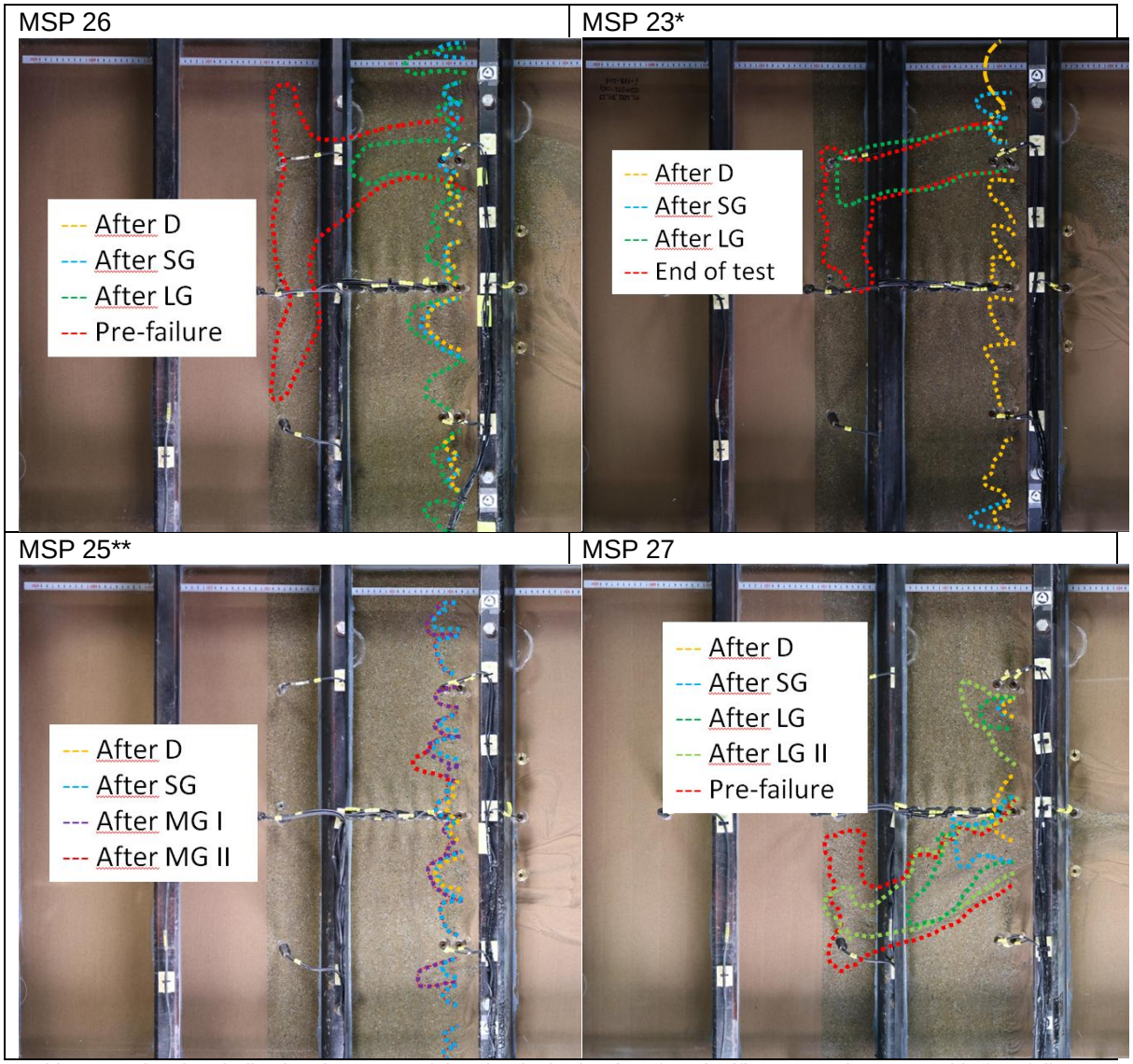


*Table A.1 Sketches indicating the extent of the pipe in the barrier after significant growth steps and before failure or the end of the experiment*

* there was no failure in this experiment.

** after MGII the pipe passes upstream to failure

## A.2 Coarse sand barrier GZB 2

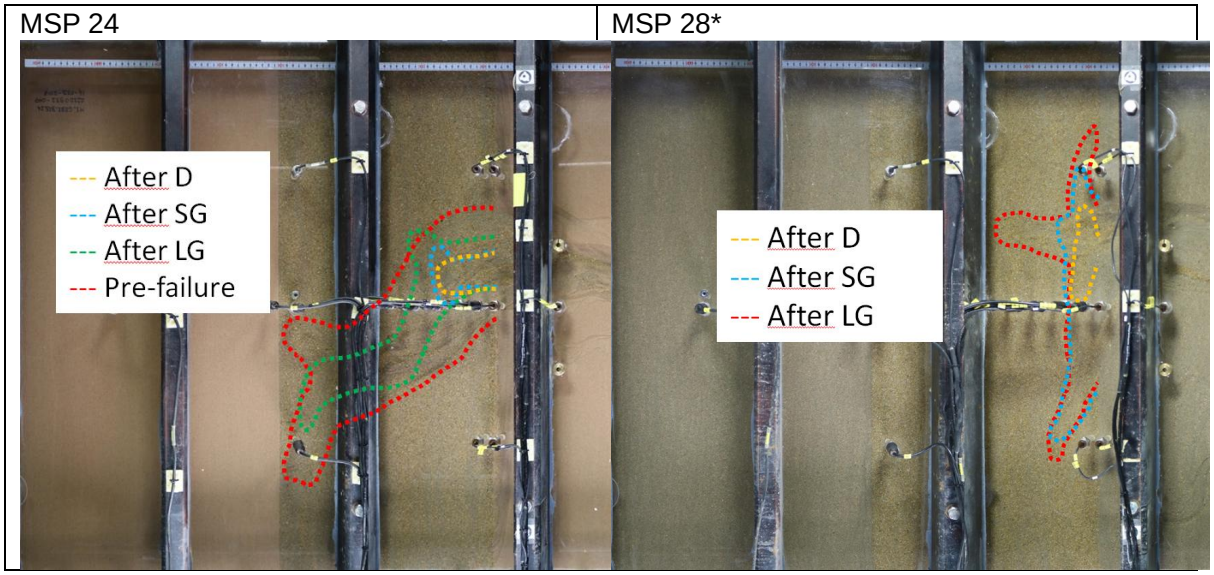


*Table A.2 Sketches indicating the extent of the pipe in the barrier after significant growth steps and before failure or the end of the experiment*

* after long growth the pipe proceeds upstream to failure.

# B Properties of sands in cylinder experiments

The physical properties of the soils used in the cylinder experiments in Deltares (2018b) and Deltares (2018 a & c) are shown in *Table B.1*.

| | **Metselzand** | **Baskarp B15** | **Baskarp B25** | **GZB 1** | **GZB 2** | **GZB 3** | **40/70 sand**** |
|---|---|---|---|---|---|---|---|
| d10, mm | 0.187 | 0.103 | 0.150 | 0.413 | 0.375 | 0.738 | 0.227 |
| d30, mm | 0.278 | 0.129 | 0.191 | 0.940 | 0.766 | 0.820 | 0.268 |
| d60, mm | 0.440 | 0.161 | 0.246 | 1.510 | 0.927 | 0.961 | 0.322 |
| $C_c$, mm | 0.9 | 1.0 | 1.0 | 1.4 | 1.7 | 0.9 | 1.0 |
| $C_u$, mm | 2.4 | 1.6 | 1.6 | 3.7 | 2.5 | 1.3 | 1.4 |
| minimum porosity* | 0.32 | 0.36 | 0.35 | 0.29 | 0.30 | 0.35 | 0.36 |
| maximum porosity* | 0.41 | 0.48 | 0.46 | 0.40 | 0.41 | 0.45 | 0.44 |

*Table B.1 Physical properties of the tested sands used in Deltares (2018b)*

*For all sands except for the 40/70 sand the maximum and minimum porosity values were determined using a combination between the maximum and minimum density that were obtained using the 'wet method' (van der Poel & Schenkeveld, 1998) and the relative density achieved in column permeability tests. Both those tests concern determining the void ratio limits of a saturated sample placed in water. For 40/70 sand, minimum and maximum porosities were determined according to ASTM D4254 -16 and ASTM D4253-16, respectively.

** Data from Robbins et al (2018)

A comparison of the grain size distribution of GZB 2 and GZB 3 in the small-scale and the medium-scale/cylinder experiments is shown in Figure B.1.

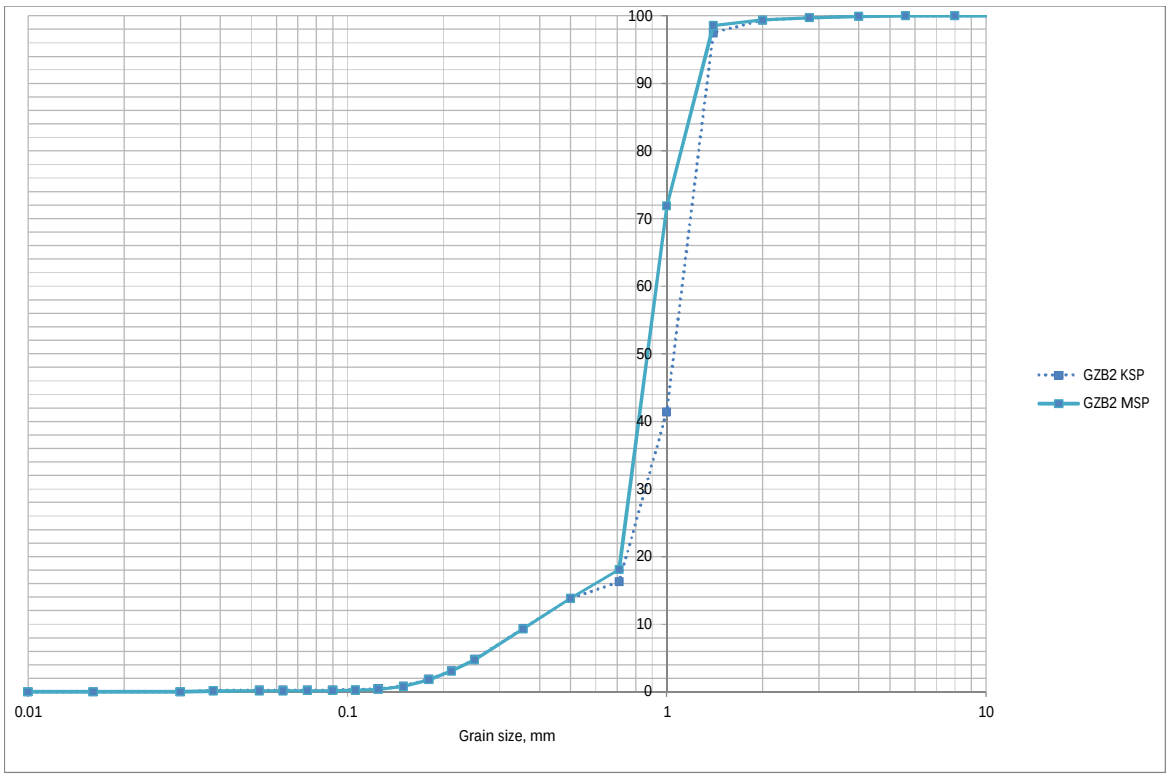


*Figure B.1 Comparison of particle size distribution of GZB 2 in the small-scale (KSP) experiments and the medium-scale (MSP) experiments. The same distribution was used for the medium-scale and the tube tests*

# C Images of medium scale basis simulations

In order to compare the simulations of the pipe progression to the observed pipe progression in experiments in Appendix A, the output of the simulations at the end of the damage step and at the first step after the pipe has progressed through the upstream interface of the barrier are shown in this appendix for the basis simulations of the medium-scale experiments.

## C.1 Simulation MSP_26

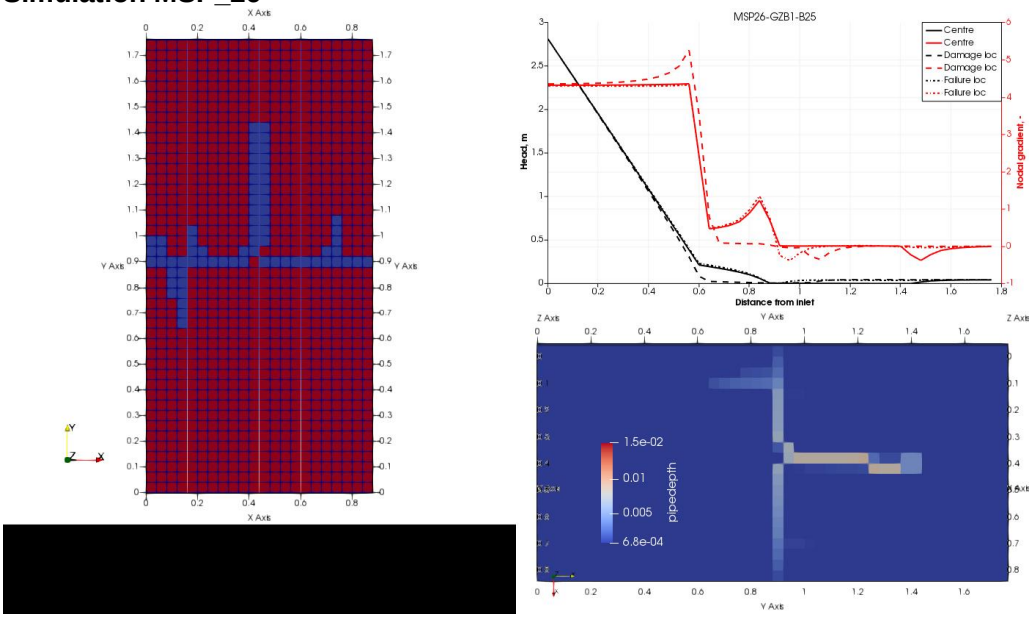


*Figure C.1 MSP_26 end of the damage step, the state of the simulation at the end of the damage step. Left hand side: indicates pipe progression (pipe is blue). Right hand side top: plots of heads and gradients along the y-axis at the top of the model at three locations: center of the model, the location where the pipe damages the barrier and the location where the pipe that causes failure occurs. Right hand side bottom: depth of the pipe*

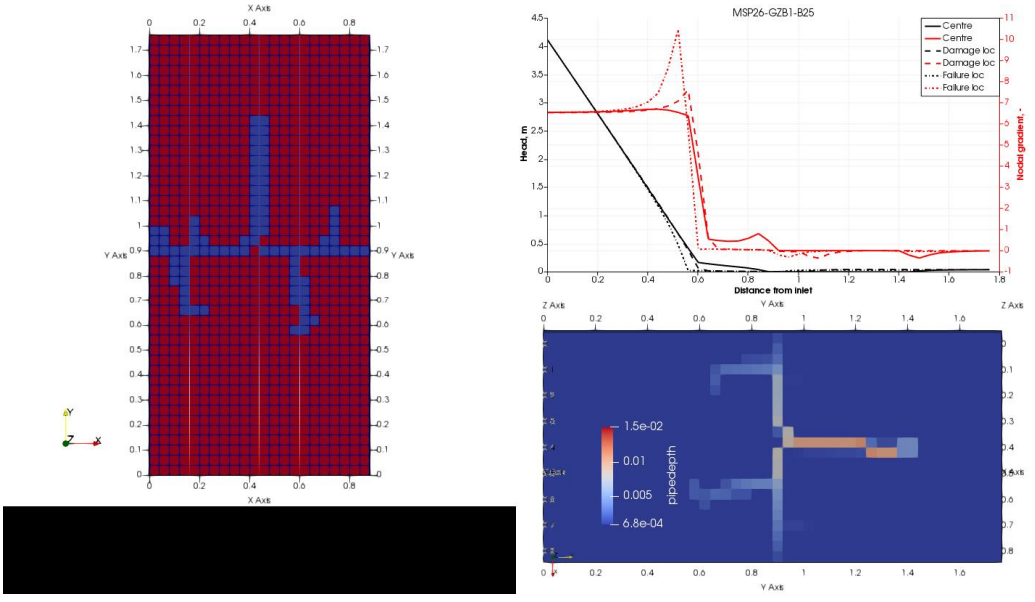


*Figure C.2 MSP_26 first step after pipe breaches through the barrier, the state of the simulation at the end of the damage step. Left hand side: indicates pipe progression (pipe is blue). Right hand side top: plots of heads and gradients along the y-axis at the top of the model at three locations: center of the model, the location where the pipe damages the barrier and the location where the pipe that causes failure occurs. Right hand side bottom: depth of the pipe*

## C.2 Simulation MSP_23

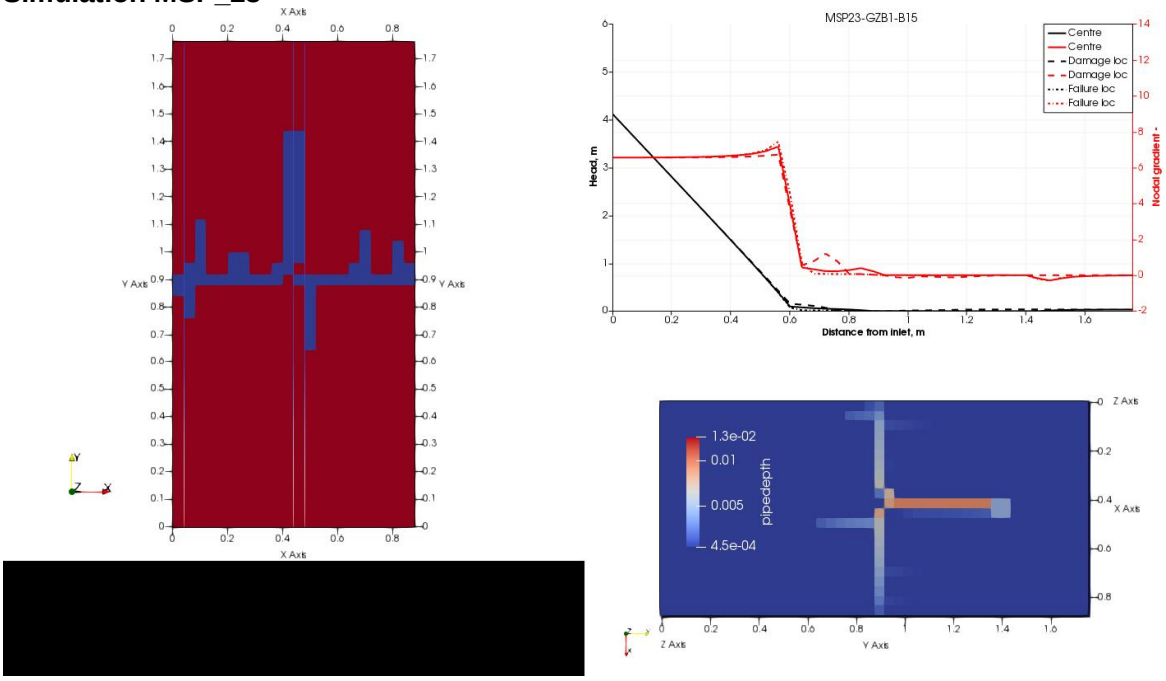


*Figure C.3 MSP_23 end of the damage step, the state of the simulation at the end of the damage step. Left hand side: indicates pipe progression (pipe is blue). Right hand side top: plots of heads and gradients along the y-axis at the top of the model at three locations: center of the model, the location where the pipe damages the barrier and the location where the pipe that causes failure occurs. Right hand side bottom: depth of the pipe*

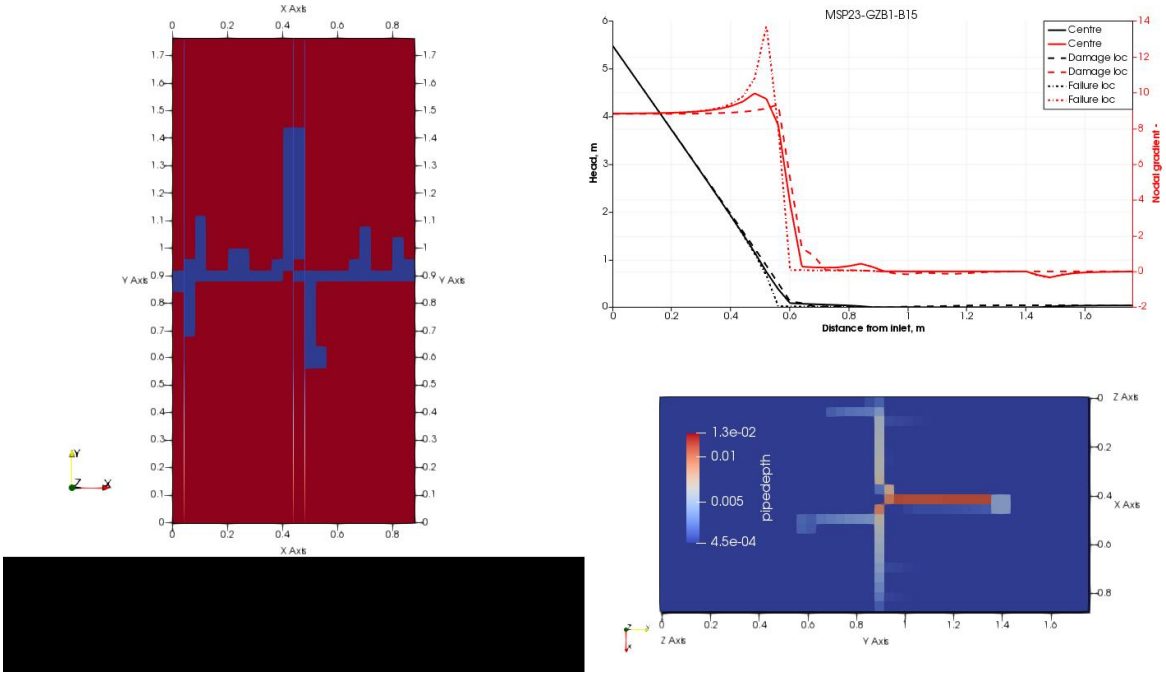


*Figure C.4 MSP_23 first step after pipe breaches through the barrier, the state of the simulation at the end of the damage step. Left hand side: indicates pipe progression (pipe is blue). Right hand side top: plots of heads and gradients along the y-axis at the top of the model at three locations: center of the model, the location where the pipe damages the barrier and the location where the pipe that causes failure occurs. Right hand side bottom: depth of the pipe*

## C.3 Simulation MSP_25

In this test, after the damage step the pipe progresses through the barrier to failure, therefore there is no image at the end of the damage step.

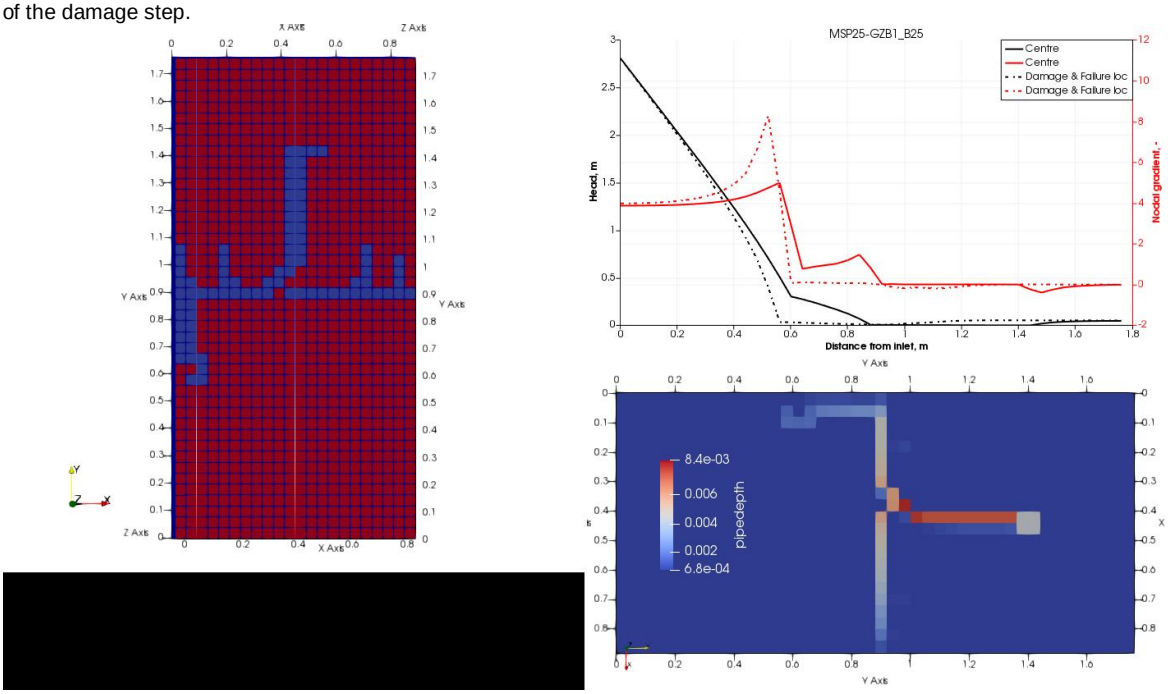


*Figure C.5 MSP_25 first step after pipe breaches through the barrier, the state of the simulation at the end of the damage step. Left hand side: indicates pipe progression (pipe is blue). Right hand side top: plots of heads and gradients along the y-axis at the top of the model at three locations: center of the model, the location where the pipe damages the barrier and the location where the pipe that causes failure occurs. Right hand side bottom: depth of the pipe*

## C.4 Simulation MSP_27

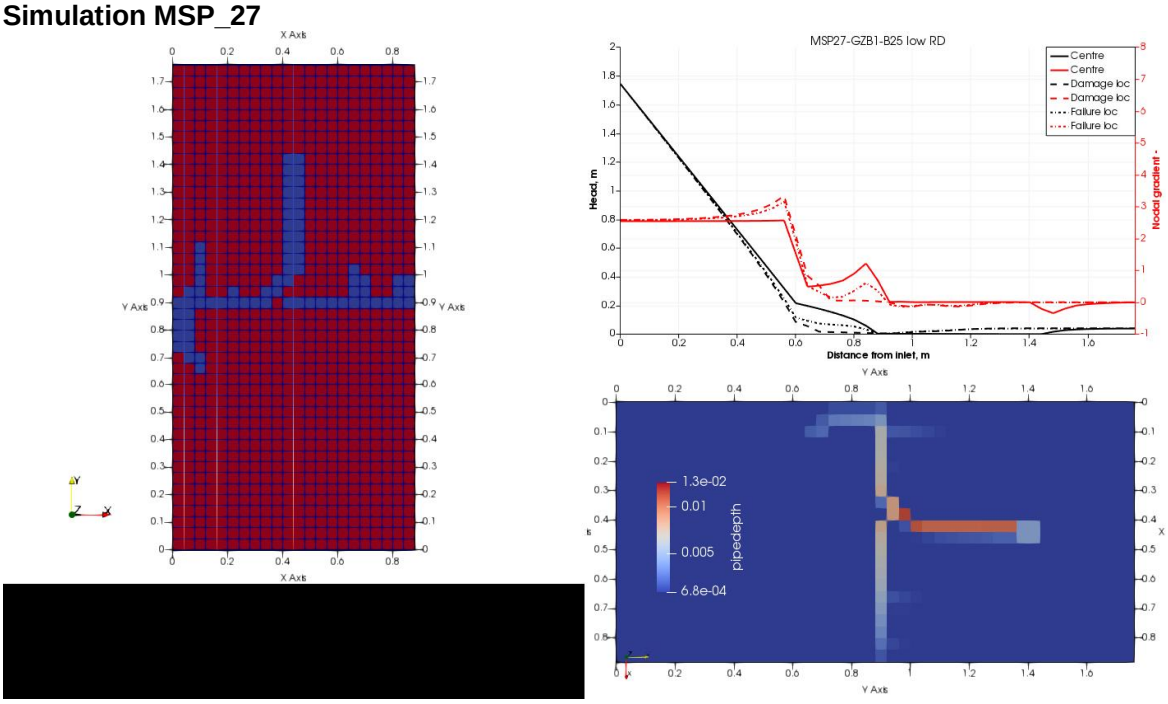


*Figure C.6 MSP_27 end of the damage step, the state of the simulation at the end of the damage step. Left hand side: indicates pipe progression (pipe is blue). Right hand side top: plots of heads and gradients along the y-axis at the top of the model at three locations: center of the model, the location where the pipe damages the barrier and the location where the pipe that causes failure occurs. Right hand side bottom: depth of the pipe*

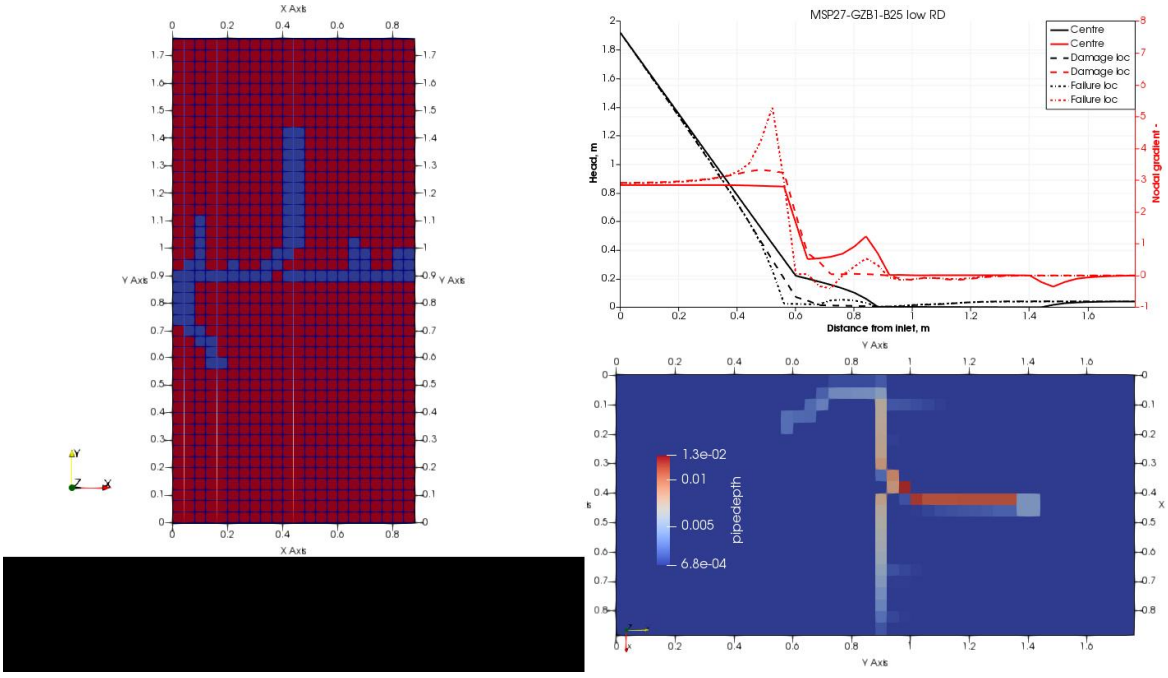


*Figure C.7 MSP_27 first step after pipe breaches through the barrier, the state of the simulation at the end of the damage step. Left hand side: indicates pipe progression (pipe is blue). Right hand side top: plots of heads and gradients along the y-axis at the top of the model at three locations: center of the model, the location where the pipe damages the barrier and the location where the pipe that causes failure occurs. Right hand side bottom: depth of the pipe*

## C.5 Simulation MSP_24

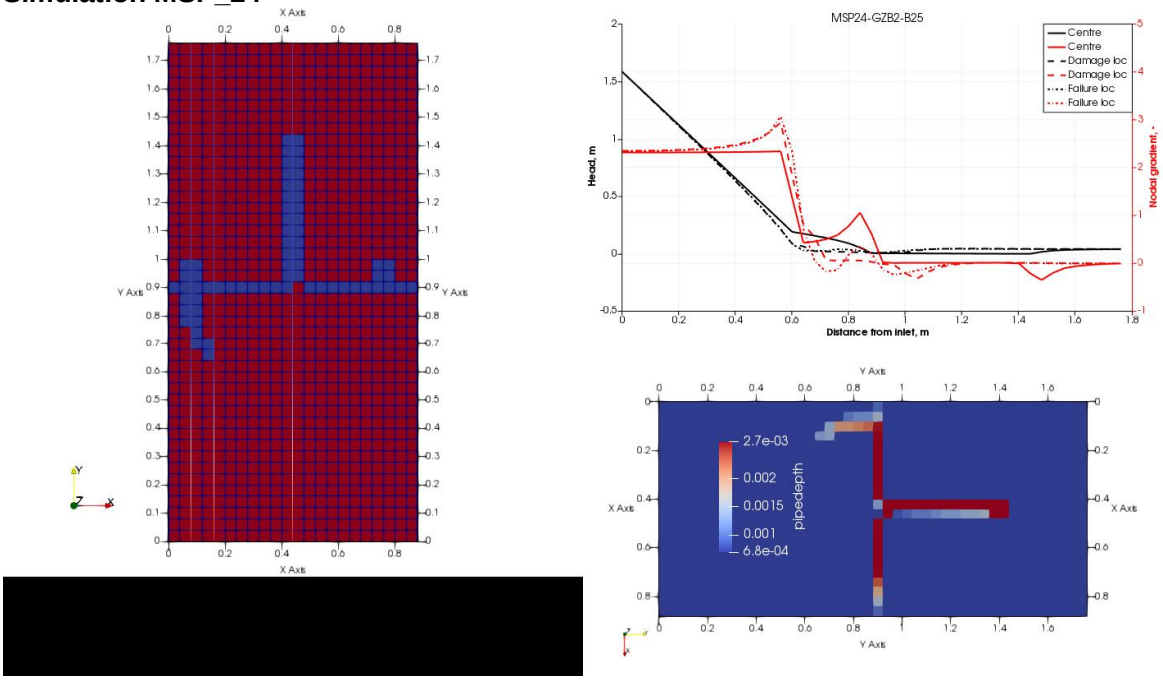


*Figure C.8 MSP_24 end of the damage step, the state of the simulation at the end of the damage step. Left hand side: indicates pipe progression (pipe is blue). Right hand side top: plots of heads and gradients along the y-axis at the top of the model at three locations: center of the model, the location where the pipe damages the barrier and the location where the pipe that causes failure occurs. Right hand side bottom: depth of the pipe*

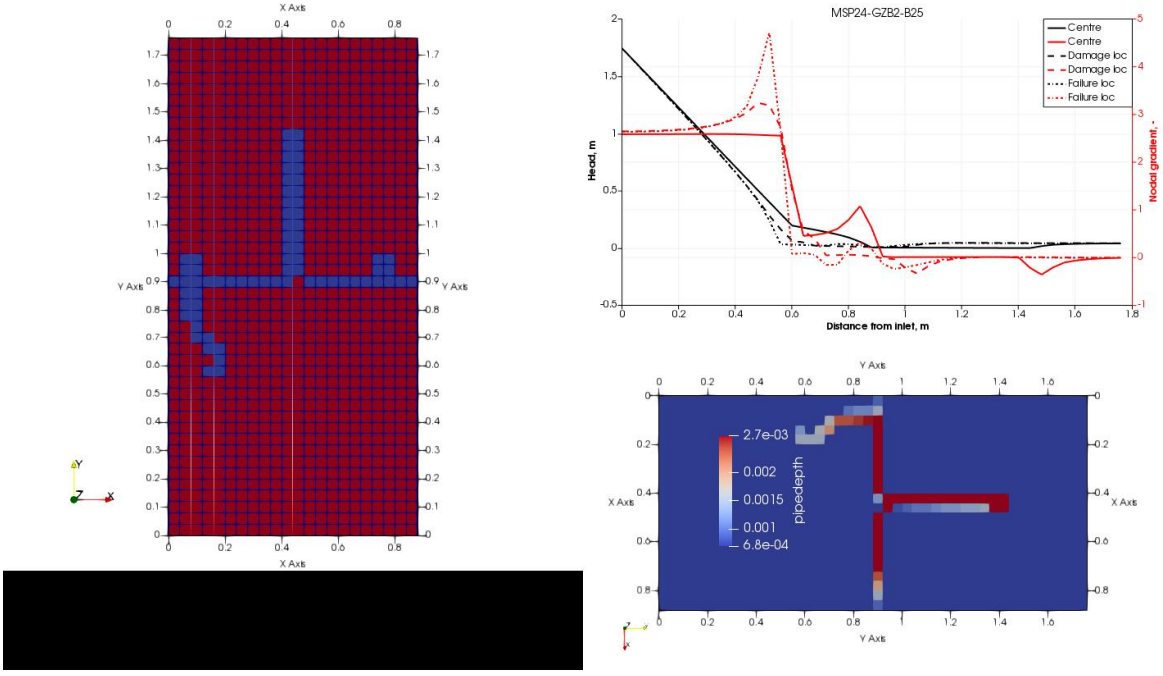


*Figure C.9 MSP_24 first step after pipe breaches through the barrier, the state of the simulation at the end of the damage step. Left hand side: indicates pipe progression (pipe is blue). Right hand side top: plots of heads and gradients along the y-axis at the top of the model at three locations: center of the model, the location where the pipe damages the barrier and the location where the pipe that causes failure occurs. Right hand side bottom: depth of the pipe*

## C.6 Simulation MSP_28

In this test, after the damage step the pipe progresses through the barrier to failure, therefore there is no image at the end of the damage step.

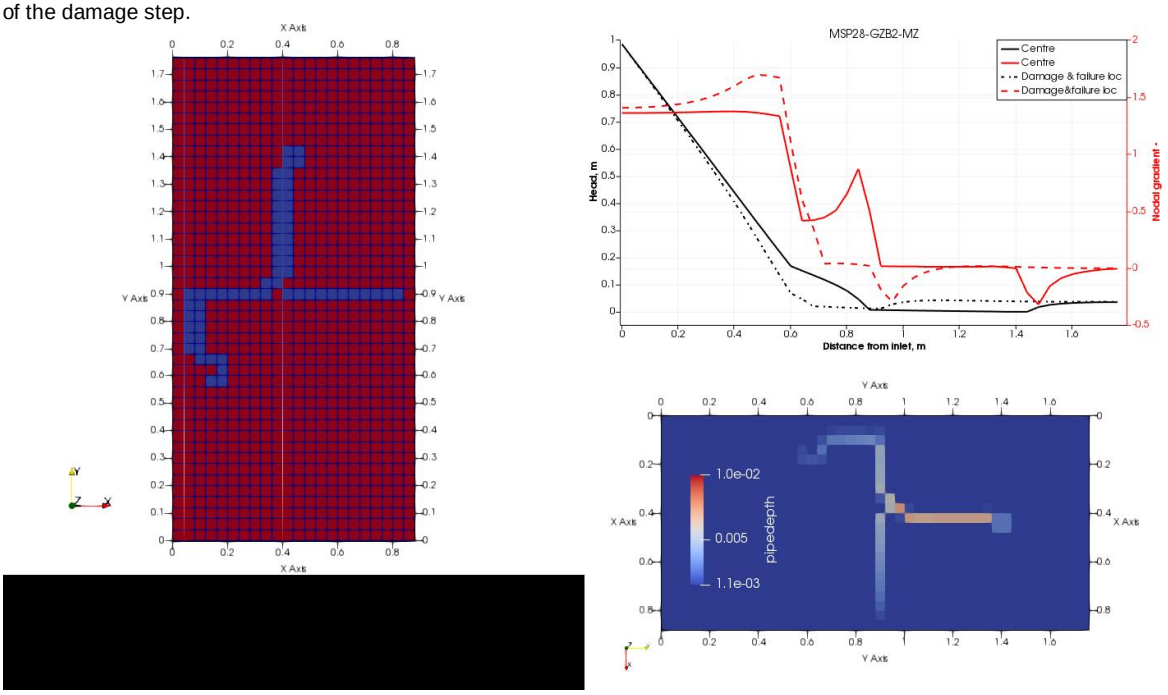


*Figure C.10 MSP_28 first step after pipe breaches through the barrier, the state of the simulation at the end of the damage step. Left hand side: indicates pipe progression (pipe is blue). Right hand side top: plots of heads and gradients along the y-axis at the top of the model at three locations: center of the model, the location where the pipe damages the barrier and the location where the pipe that causes failure occurs. Right hand side bottom: depth of the pipe*

# D Effect of scaling of primary erosion criterion

## D.1 Medium-scale simulation MSP_26

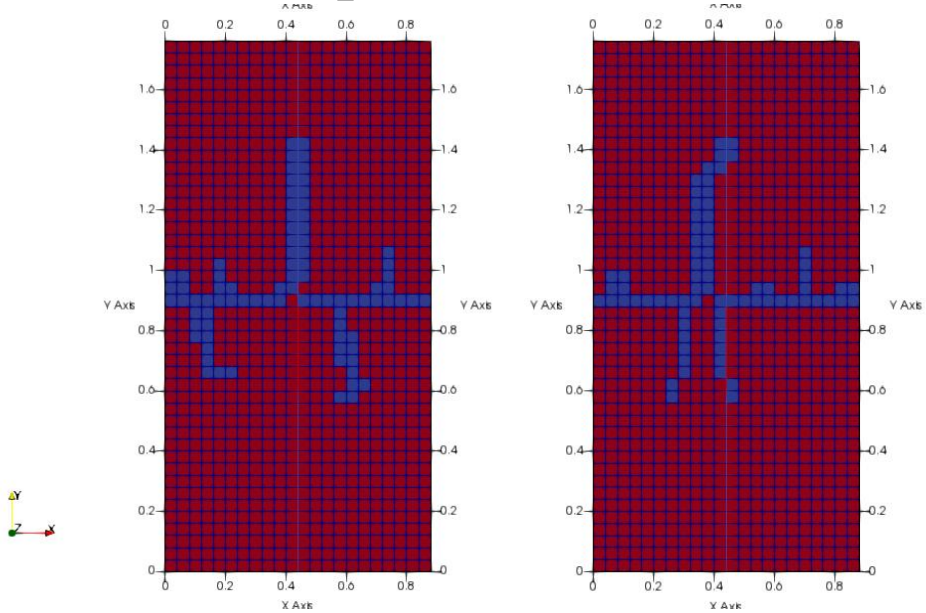


*Figure D.1 Basis simulation MSP_26 (left hand side) conversion of gradient over 10 cm to gradient over 4 cm with factor 1.6; simulation MSP_26_Scaling (left hand side) conversion of gradient over 10 cm to gradient over 4 cm with factor 1.1. Simulation at the point when the pipe has progressed 1 element beyond the upstream interface of the barrier. Red elements are soil, blue elements are pipe*

## D.2 Small-scale simulations

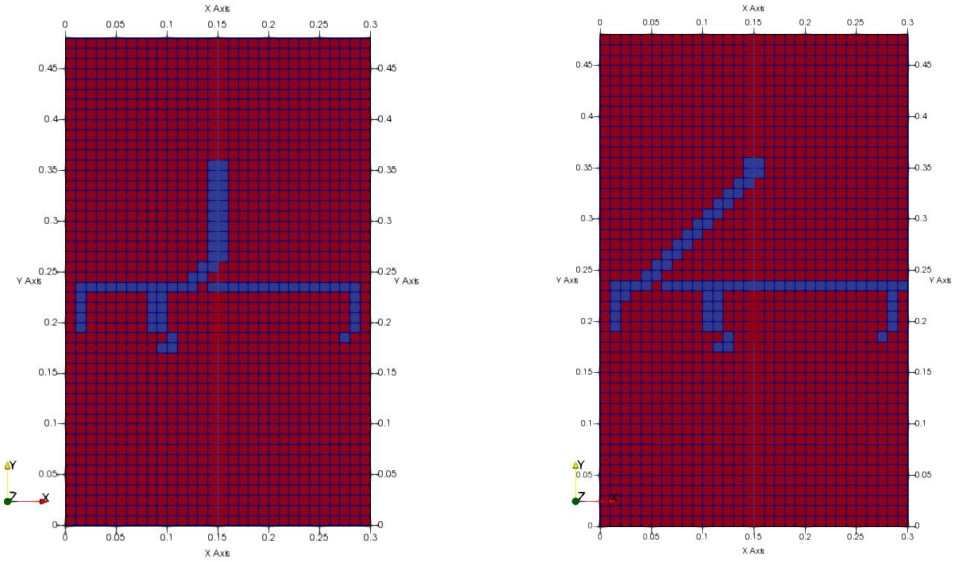


*Figure D.2 Basis simulation KSP_191 (left hand side) conversion of gradient over 10 cm to gradient over 1 cm with factor 3.1; simulation KSP_191_Scaling (left hand side) conversion of gradient over 10 cm with factor 2.2. Simulation at the point when the pipe has progressed 1 element beyond the upstream interface of the barrier. Red elements are soil, blue elements are pipe*

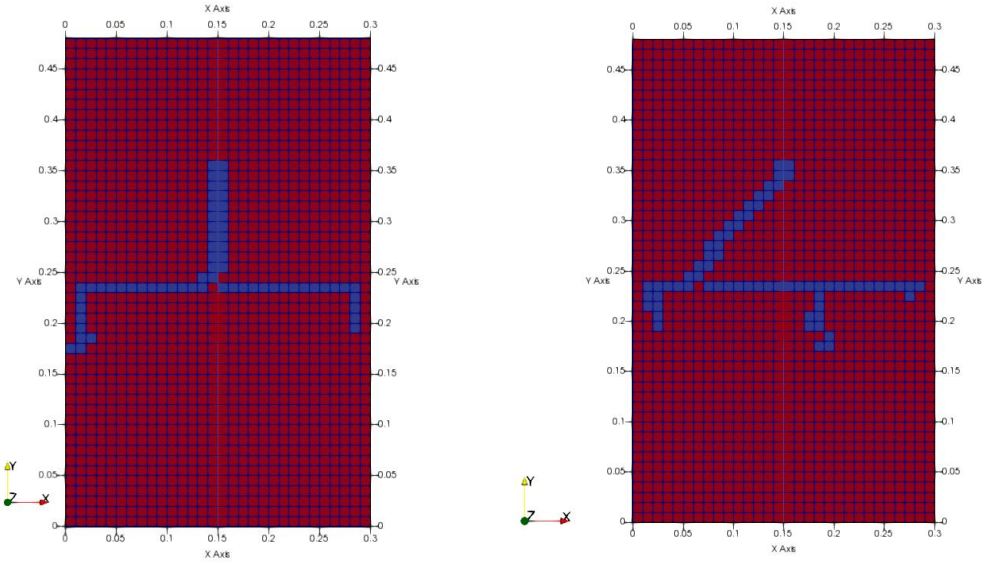


*Figure D.3 Basis simulation KSP_192 (left hand side) conversion of gradient over 10 cm to gradient over 1 cm with factor 3.1; simulation KSP_192_Scaling (left hand side) conversion of gradient over 10 cm with factor 2.2. Simulation at the point when the pipe has progressed 1 element beyond the upstream interface of the barrier. Red elements are soil, blue elements are pipe*

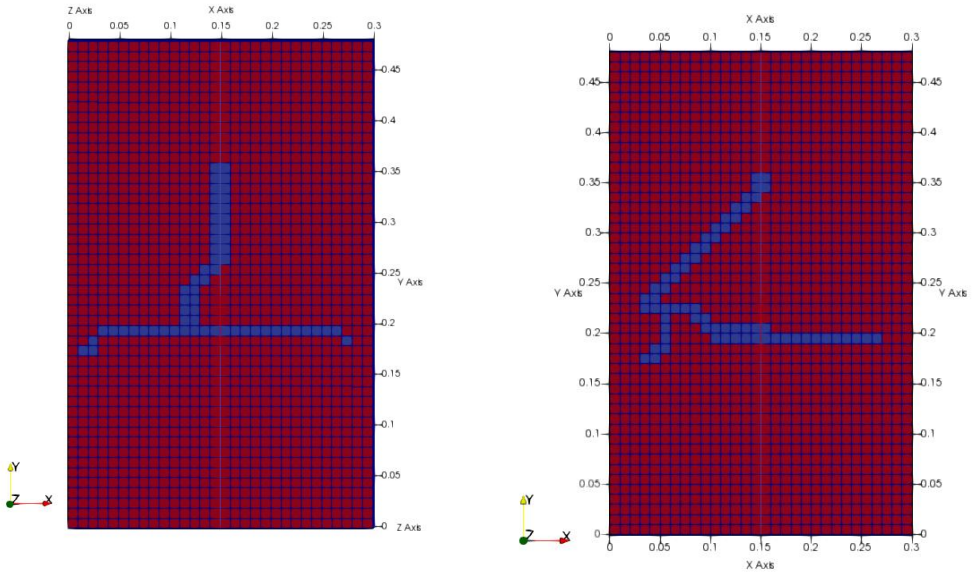


*Figure D.4 Basis simulation KSP_196 (left hand side) conversion of gradient over 10 cm to gradient over 1 cm with factor 3.1; simulation KSP_196_Scaling (left hand side) conversion of gradient over 10 cm with factor 2.2. Simulation at the point when the pipe has progressed 1 element beyond the upstream interface of the barrier. Red elements are soil, blue elements are pipe*

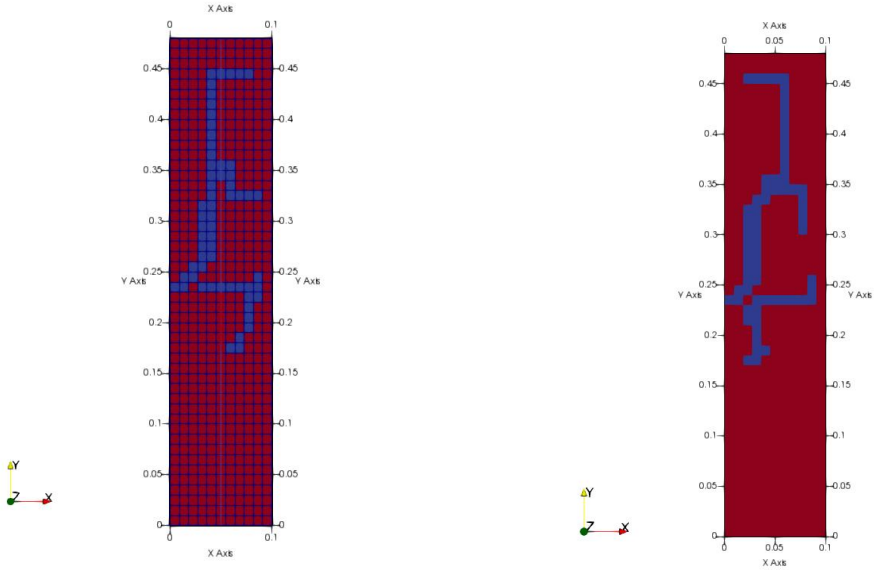


*Figure D.5 Basis simulation KSP_198 (left hand side) conversion of gradient over 10 cm to gradient over 1 cm with factor 3.1; simulation KSP_198_Scaling (left hand side) conversion of gradient over 10 cm with factor 2.2. Simulation at the point when the pipe has progressed 1 element beyond the upstream interface of the barrier. Red elements are soil, blue elements are pipe*

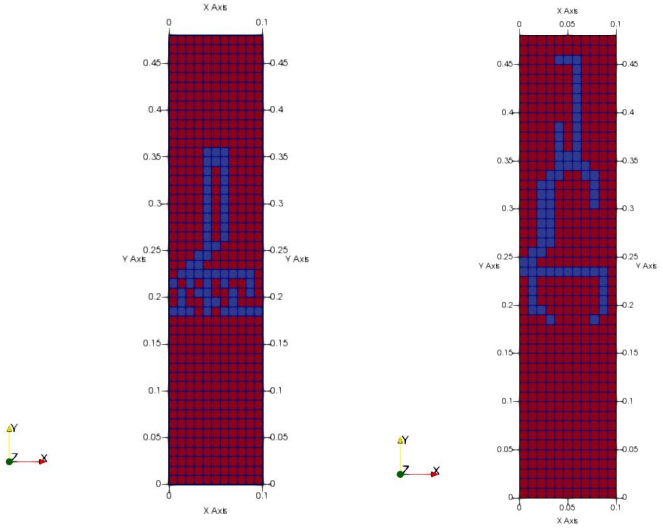


*Figure D.6 Basis simulation KSP_199 (left hand side) conversion of gradient over 10 cm to gradient over 1 cm with factor 3.1; simulation KSP_199_Scaling (left hand side) conversion of gradient over 10 cm with factor 2.2. Simulation at the point when the pipe has progressed 1 element beyond the upstream interface of the barrier for right hand side. Red elements are soil, blue elements are pipe*

# E Effect of number of pipe elements activated per step

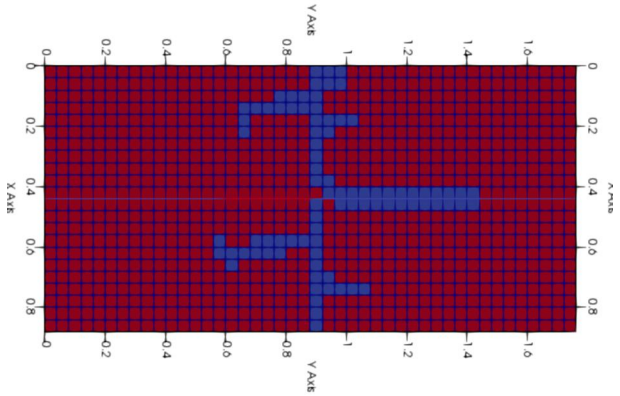

*Figure E.1 Basis simulation MSP_26. Simulation at the point when the pipe has progressed 1 element beyond the upstream interface of the barrier. Left side is upstream*

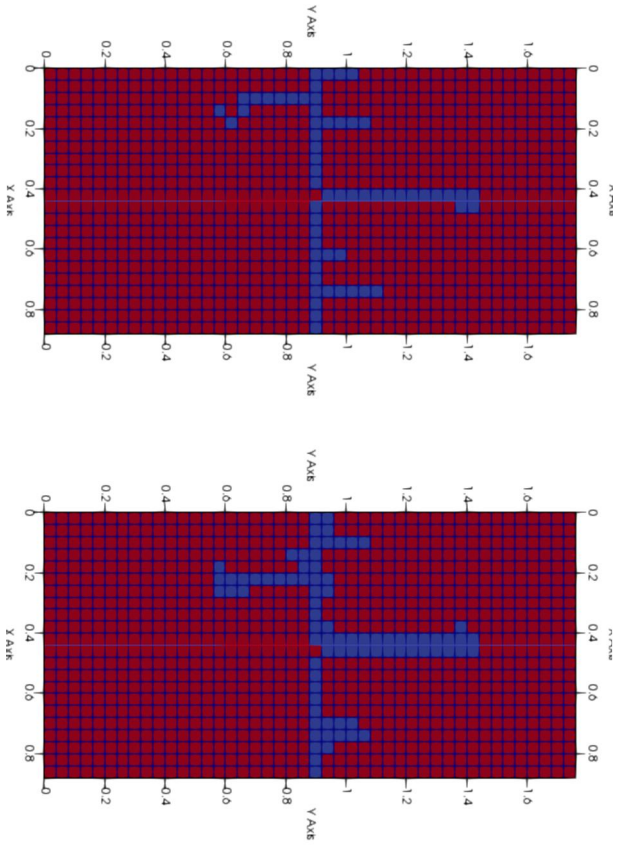

*Figure E.2 Top simulation with progression 1 element per step, bottom progression with 3 elements per step. Simulation at the point when the pipe has progressed 1 element beyond the upstream interface of the barrier. Left side is upstream*

# F Effect of barrier thickness

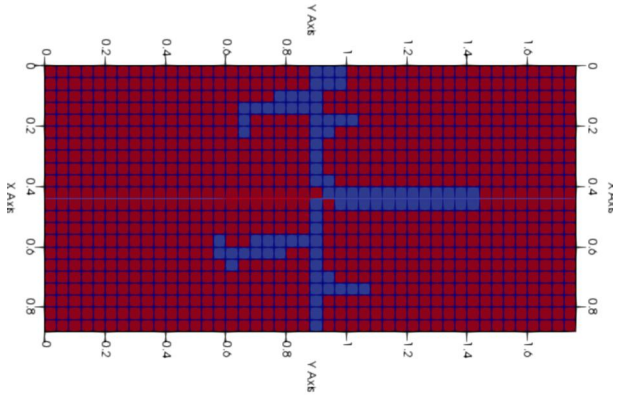

*Figure F.1 Basis simulation MSP_26. Simulation at the point when the pipe has progressed 1 element beyond the upstream interface of the barrier. Left side is upstream*

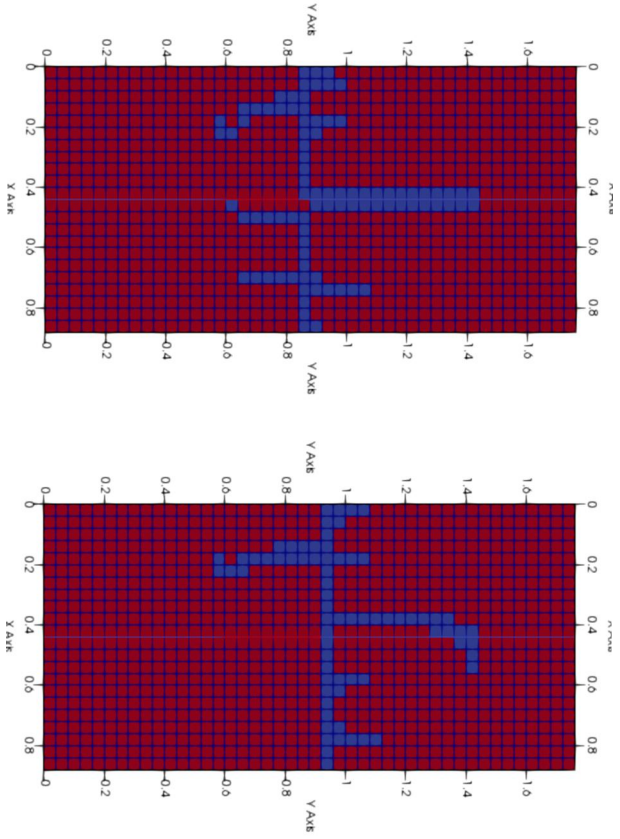

*Figure F.2 Top simulation MSP_26_B24 with barrier thickness 0.24 m, bottom simulation MSP_26_B32 barrier thickness 0.32 m. Simulation at the point when the pipe has progressed 1 element beyond the upstream interface of the barrier. Left side is upstream*

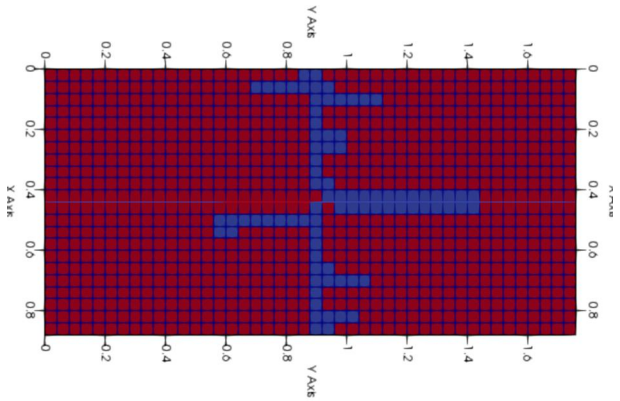

*Figure F.3 Basis simulation MSP_23. Simulation at the point when the pipe has progressed 1 element beyond the upstream interface of the barrier. Left side is upstream*

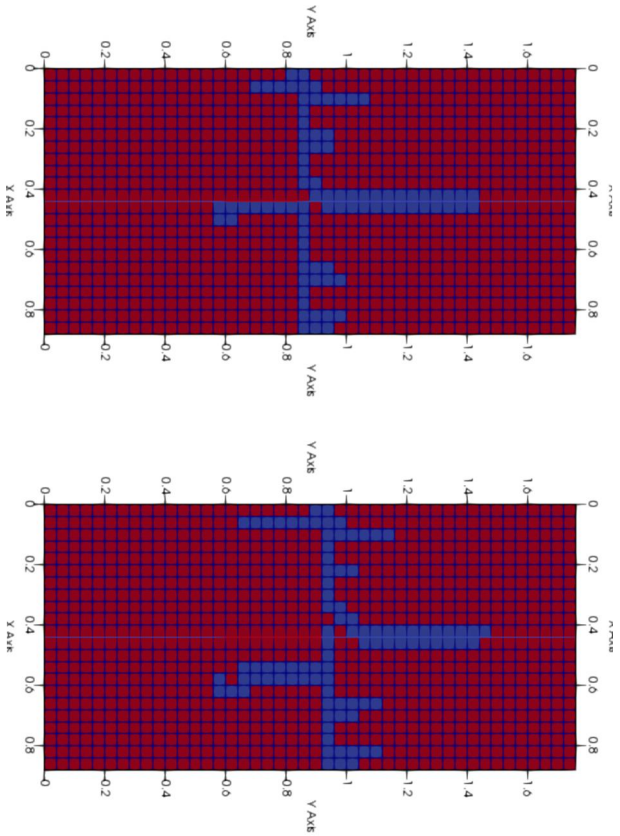

*Figure F.4 Top simulation MSP_23_B24 with barrier thickness 0.24 m, bottom simulation MSP_23_B32 barrier thickness 0.32 m. Simulation at the point when the pipe has progressed 1 element beyond the upstream interface of the barrier. Left side is upstream*

# G Discussion of pipe progression steps

## G.1 Progression parallel to the barrier interface in the background sand

Progression of the pipe parallel to the barrier in the background sand prior to damage of the barrier is observed in all experiments except MSP 28 (GZB 2 and Metselzand) (Deltares, 2018c). Possibly this is related to small-scale heterogeneity inside the sample in combination with a relatively high primary erosion criterion of the Metselzand. The other medium-scale experiments were performed by using Baskarp sand as background sand. However, in the small-scale experiments with Metselzand, progression of the pipe parallel to the barrier in the background sand was observed.

The simulations show progression of the pipe parallel to the barrier in the background sand in all simulations except small scale simulations KSP_196 and KSP_199.

- In simulation KSP_196, the primary erosion criterion in the barrier is lower than in the fine sand. This might be due to a too high primary erosion criterion for the background Metselzand, in combination with a too low primary erosion criterion in the barrier material GZB 3.
  The primary erosion criterion in the Metselzand was not measured in the set of cylinder experiments performed in April 2018. The value in the models is therefore based on the correlation with Cu. In June 2018, cylinder experiments were performed on Metselzand, and these could provide a better estimate of the primary erosion criterion of Metselzand. The primary erosion criterion of GZB 3 is currently based on only one cylinder experiment; an additional experiment was done in June 2018 which will allow for a check on the first result. Analysis of these new experiments should indicate whether the parameters that were used in the current simulation are appropriate.
  Additionally, in the current simulation the background fine sand has the hydraulic conductivity corresponding to the hydraulic conductivity of the fine sand upstream of the barrier. This might have caused a stronger convergence of flow to the top elements inside the barrier on the downstream interface of the barrier than was actually present in the experiments. That might possibly also contribute the pipe to immediately damaging the barrier rather than progressing along the barrier interface. However, it appears probable that the input critical primary erosion criteria for the barrier and background sand are the main causes for the observed progression.

  In simulation KSP_199 with the basis parameters, the pipe branches upon reaching the barrier with one branch entering the barrier and one branch progressing parallel to the barrier. The pipe inside the barrier also branches several times. The computed depth of the pipe in the barrier is $3\times d_{50}$, i.e. the initiation depth, indicating that this depth already satisfies the secondary erosion criterion. The shape of the pipe in the barrier, and the pipe depth is shown in Figure G.1.

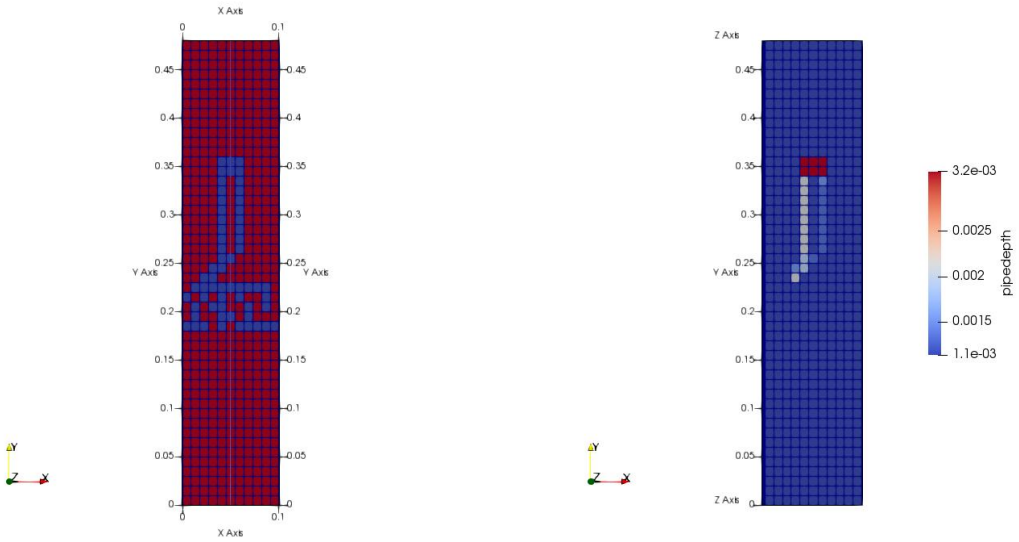


*Figure G.1 Simulation KSP_199. Left hand side shows the top view of the model, blue elements are pipe elements, and red elements are soil. Right hand side shows pipe depth, the pipe elements in the barrier have the minimum pipe depth of* $3 \times d_{50}$ *the color of the pipe elements indicates their depth as shown in the legend*

This growth pattern does not appear to be realistic and is likely an artefact of (1) the relatively coarse discretization and (2) the lack of pipe widening in the preliminary finite element model. Changing the number of pipe elements that could be switched on per progression step to 1 and to 3 gave similar results, however. The simulation in which the primary erosion criteria of the barrier and the fine sand were reduced to 70% of the basis values gave a regular pattern of pipe progression, where the pipe did progress parallel to the barrier interface prior to damaging the barrier.

## G.2 Number of pipes inside the barrier

Considering the number of pipes that enter the barrier, there is a clear difference between GZB 1 and GZB 2 in the medium-scale experiments (). For GZB 2 only one pipe enters the barrier, whereas multiple pipes enter the barrier in tests with GZB 1 (refer to figures in Appendix A).

In the basis simulations of GZB 1, there are two pipes that enter the barrier in MSP_23, and only one in the other simulations with GZB 1 (). In experiment MSP 23 there are indeed more pipes entering the barrier at damage than in the other experiments with this barrier (Deltares, 2018c). This is probably due to the higher hydraulic conductivity contrast, which concentrates flow to the edge of the barrier so that the primary erosion criterion is exceeded at multiple locations.

Considering that the modelled damage step is more similar to the experimentally observed long growth step, a comparison to the number of pipes that progress past half way through the barrier may be more appropriate. This is only one pipe for all experiments.

In the small-scale basis simulations, three and two pipes enter the barrier in simulations KSP_191 and KSP_192 respectively, and only one pipe in the other models (). In all small-scale experiments, multiple pipes enter the barrier ().

The sensitivity analysis using MSP_26 shows that the number of pipes that enters the barrier in the simulations is also affected by modelling parameters such as the barrier thickness (thickness 0.24 m = 3 pipes; thickness 0.28 = 2 pipes; thickness 0.32 m = 1 pipe), the number

of elements that are switched on per pipe iteration (2 elements = 2 pipes, 1 or 3 elements = 1 pipe) and hydraulic conductivity downstream (basis = 2 pipes, lower hydraulic conductivity = 1 pipe) (). Therefore, differences between the number of pipes inside the barrier in the simulations and the experiments may not be significant.

## G.3 Critical growth steps in medium-scale tests

In the medium-scale basis simulations, the pipe that enters the barrier at damage progresses 0.24 m, i.e. only one element short of the barrier interface (). This differs from the experiments where the pipe does not progress past half way through the barrier at damage. In the experiments, the pipe was observed to grow in steps. Pipe progression was not explicitly studied in the small-scale experiments, but this was a subject of investigation of the medium-scale tests. In those experiments several characteristic steps were identified in which the pipe showed significant progression these characteristics steps are:

- Damage: pipe(s) entering the barrier.
- Short growth: progression where the pipe(s) do not proceed past half way through the barrier.
- Medium growth: progression (after short growth) where the pipe(s) do not proceed past half way through the barrier.
- Long growth: progression where the pipe(s) do proceed past half way through the barrier and come to a stop.
- Failure: the pipe progressing through the upstream interface of the barrier.

Appendix A shows sketches of the pipe outline at the end of these growth steps in the experiments.

Considering the length of the pipe at the end of the growth step in the basis simulations (0.24 m for those simulations where the pipe growth stops inside the barrier and 0.28 m where the pipe immediately progresses through the upstream interface of the barrier), the modelled damage of the barrier would correspond better to the experimentally observed long growth. However, the sensitivity analyses on MSP_26 show that the distance that the pipe progresses into the model at damage is also affected by the mesh refinement, the pipe only progresses 0.18 m into the barrier with a 2 cm mesh in MSP_26_2. Also, the model with a lower primary erosion criterion shows a shorter progression distance, 0.12 m in MSP_26_Scaling ().

Considering the ratio between the modelled head drop at damage to the measured head drops at damage, short growth, and long growth, also indicates that the modelled damage corresponds best with experimental long growth . The ratio of the modelled head drop at damage over the experimental head drop at long growth is similar to the ratio of the modelled head drop at failure over the experimental head drop at failure.

Additional indication of the similarity between the long growth step and the modelled damage is the close match between the critical gradient that is obtained from the cylinder experiments and the modelled critical gradient for the long growth step in the simulations of the box experiments in Deltares (2018c) shown in Section 3.5.2. Simulations of the damage and short growth steps give significantly lower critical gradients (Deltares, 2018c).

If the critical gradient of the barrier materials is indeed that which is indicated by the cylinder experiments, and found in the long growth step, the question is what causes the observed damage and short growth in the medium scale experiments to occur at lower gradients. As the pipe has a finite depth in the experiments, there can be some crumbling of the barrier to

the pipe to establish a stable slope. However, attempts were made in the observations to establish damage as something ‘more’ than just crumbling. Small-scale heterogeneity of the hydraulic conductivity or strength inside the barrier might possibly also contribute to small pipes forming locally at gradients below the critical gradient.